Specificity in Glia-Neuron Interactions

Sneha Ray

A dissertation

submitted in partial fulfillment of the

requirements for the degree of

Doctor of Philosophy

University of Washington

2023

Reading Committee:

Aakanksha Singhvi, Chair

Jihong Bai

David Raible

Program Authorized to Offer Degree:

Neuroscience

University of Washington

Abstract

Specificity of Glia-Neuron Interactions

Sneha Ray

Chair of the Supervisory Committee:

Aakanksha Singhvi

Department of Biological Structure

Glia are important regulators of nervous system development and function. In both central and peripheral nervous systems, glia modulate neuron structure and function through a vast array of molecular mechanisms. One remaining question is whether a single glia regulates all its associated neurons in the same way. In this thesis, I answer this question using the cation chloride cotransporter KCC-3 in the amphid sheath (AMsh) glial cell of the model organism *C. elegans*. Briefly, I find that AMsh KCC-3 localizes to only one of the glia's associated neurons, the thermosensory AFD neuron to regulate its shape and function. This localization is directed through repulsion by the cilia of other amphid neurons, and through two regions of the KCC-3 protein. First, a central sequence guides KCC-3 to apical-like adneuronal membrane, and then a C-terminal sequence localizes KCC-3 to a microdomain. In addition, I also collate our current knowledge of how peripheral glia use ionic regulation to modulate sensation. Together, this dissertation provides evidence and mechanistic details of glia-neuron specificity.

DEDICATION & ACKNOWLEDGEMENTS

This thesis is dedicated to my family, friends, and mentors, whose support was crucial for the completion of this degree.

I want to first and foremost acknowledge my primary mentor Aakanksha, whose support has been instrumental in completing this project. Being one of your first students was such a privilege and I am so thankful for my place in your lab. Thank you for always treating me with kindness and patience and for all the time you devoted to my maturation as a scientist. I cannot thank you enough for the hours you put into helping me with experimental planning and troubleshooting, editing my writing, providing feedback on presentations, and time just chatting about science and careers and life. I could not have asked for a better graduate school advisor.

I also want to thank Drs. Jihong Bai, Cecilia Moens, Dave Raible, and Tom Reh for serving on my committee. Thank you for your feedback throughout the course of this project and always showing up to committee meetings engaged and curious about my science.

I want to thank everyone in the Singhvi lab, past and present, for making the lab feel so welcome. Thank you all for always being willing to help with experiments and provide feedback, and also for making the lab a fun place to work. I especially want to acknowledge all the research technicians, past and present, for keeping the lab running smoothly. Our work would not be possible without you. I also want to thank Sean Manning, Pralaksha Gurung, and Sasha Kravchuk for your close collaboration on this thesis.

I finally want to thank my friends and family, who's support has been indescribable. Thank you German and Pralaksha for keeping me sane inside and out of the lab. Thank you Isaac

for feeding me so much throughout the years. Trisha, Seattle would not be the same without you, and I'm so grateful for all the support you've provided me throughout the years. Thank you to all the friends I've made in this city and through graduate school for making the time fly by—I've loved getting the chance to know all of you. Finally, I want to thank my parents for always encouraging me to pursue my educational aspirations and for providing a safe homebase to return to. I couldn't have done this without you.

Table of Contents

Chapter 1

INTRODUCTION

Glia and neurons comprise the two major cell types of bilateral animals. When discovered, glia were thought to provide mere passive structural support for neurons, and were even referred to simply as "Nervenkitt", or nerve glue (Jäkel & Dimou, 2017). However, across both the central nervous system (CNS) and peripheral nervous system (PNS) in a wide variety of systems, glia today are appreciated as active players in nervous system development and function. In both the CNS and PNS, a single glia can contact multiple neurons. This raises an important yet unanswered question: does a single glia modulate all associated neurons the same way, or can glia target cues to particular associated neurons? Understanding the logic by which glia modulates associated neurons is a crucial facet of decoding how nervous systems function.

In my thesis, I use the glial cation chloride cotransporter KCC-3 in the *C. elegans* model system to address the question of glia-neuron specificity. This introduction is formatted to give readers context on the thesis project. Here, I first delve into existing literature of specificity in glia-neuron interactions and then provide background of both *C. elegans* glia and KCC-3. In Chapter 2, I include a published review on the role of ionic regulation by peripheral glia on sensory perception, across systems and modalities. In Chapter 3, I describe my thesis findings on how and why *C. elegans* glia specifically localize KCC-3 to a microdomain around only one associated neuron. Finally, in Chapter 4, I will discuss the importance and next stages of these findings.

A single glia interacts with many neurons

A single glia can actively modulate many different aspects of neuron development and function. One such area of regulation is at regions where neurons receive input from other cells or the environment, termed neuron receptive endings (NREs). During development, glia regulate synaptogenesis of both excitatory and inhibitory NREs, through both secreted molecules that aid synapse formation (thrombospondins, SPARC, hevin, etc) and pruning to remove excess NREs (Allen & Eroglu, 2017; Wilton, Dissing-Olesen, & Stevens, 2019). Functionally, glia express transporters for glutamate, dopamine, GABA, and histamine to rapidly remove these neurotransmitters from synaptic clefts to prevent "spill-over" into neighboring synapses (Eulenburg & Gomeza, 2010). Similarly, glia express a number of ionic channels and transporters, including cation chloride cotransporters (CCCs), inward rectifying potassium channels, and sodium-calcium exchangers (Djukic, Casper, Philpot, Chin, & McCarthy, 2007; Song, Luo, Sun, & Sun, 2020), to regulate the ionic balance around NREs. Finally, glia can release small compounds like ATP and D-serine to affect neuron communication (Barres, 2008). Thus, a single glial cell can use a vast array of molecules and processes to regulate an associated neuron.

Glia-neuron interactions becomes all the more complex when considering that an individual glia associates with many neurons in both the CNS and PNS. In the CNS, a single cortical astrocyte can ensheath multiple neuron cell bodies, 300-600 dendrites, and over 100,000 synapses (Chung, Welsh, Barres, & Stevens, 2015). A single CNS oligodendrocyte too can myelinate between 20-60 different axons (Duncan, Simkins, & Emery, 2021). In the PNS, a single glia-like retinal pigment epithelial cell regulates multiple different rod and cone photoreceptors, while Muller glia span the entire retina to interact with photoreceptors and

ganglion cells (Tworig & Feller, 2022). In the tongue, Type 1 glia-like support cells contact taste buds that express different receptors types (Rodriguez et al., 2021). Specificity of glia-neuron interactions in any of these examples has yet to be described.

Functional glial specificity

There has been some functional evidence of glia-neuron specificity. For one, glia display calcium transients that are constrained into smaller microdomains, that act independently of each other (Khakh & Sofroniew, 2015). Intriguingly, calcium microdomains appear to be physiologically distinct. For example, when an astrocyte is exposed to two different neuroactive substances, distinct sets of glial microdomains show activity, suggesting that these microdomains are composed of and reactive to different stimuli (Agarwal et al., 2017). In addition, in *C. elegans,* ablation of the amphid sheath (AMsh) glial cell of the major sensory organ results in non-uniform effects on associated sensory neurons (Bacaj, Tevlin, Lu, & Shaham, 2009). Finally, oligodendrocytes show distinct myelination patterns to distinct groups of neurons (Yang, Michel, Jokhi, Nedivi, & Arlotta, 2020).

Glial polarity

Thus far, there has not been molecular mechanistic evidence of glia-neuron specificity. However, glia and glia-like cells show evidence of polarity, suggesting an ability of glia to communicate with associated cells non-uniformly. CNS radial glia extend processes that attach to the ventricular and ependymal surfaces of the developing brain, and require extensive polarization for proper brain development (Chou, Li, & Wang, 2018). Astrocytes produce both numerous fine processes that interact with neighboring neurons and large processes that envelop

cerebral blood vessels (Etienne-Manneville, 2008). Reactive astrocytes, too, show dramatic polarization whereby they extend processes towards wounded brain regions (Ridet, Malhotra, Privat, & Gage, 1997). In the (PNS), Schwann cells are polarized such that apically polarized membranes are found adjacent to the axons, while basolateral markers face the basement membrane (Tricaud, 2018). *Drosophila* ensheathing glia, too, are polarized such that the basolateral plasma membrane abuts an extracellular matrix formed at the neuropil-cortex interface, while the apical plasma membrane faces the neuropil (Pogodalla et al., 2021). PNS NRE glia, including mammalian olfactory sustentacular cells, retinal pigment epithelia, and inner ear support cells, have apical membranes face the outer lumen (subretinal space, nasal cavity, scala media endolymph) and basolateral membranes face the basement membrane (Ray & Singhvi, 2021). Some of these cells, such as inner ear support cells, also establish planar cell polarity, providing another avenue of asymmetry within cells (Wan, Corfas, & Stone, 2013).

Glial microdomains

Glia also exhibit smaller molecular microdomains, suggesting an ability to compartmentalize molecules into even smaller areas. Astrocytes localize molecules like Ezrin and metabotropic glutamate receptors 3/5 specifically to their peripheral astrocyte processes (PAP), which preferentially associates with the synapse, and not broadly across astrocyte processes (Lavialle et al., 2011). Astrocytes also have mRNA and ribosomes in their PAPs, allowing for the possibility of specific mRNAs localized opposite specific NRE contacts (Sakers et al., 2017) In addition, the microvilli of Schwann cells provide for another specialized and unique microdomain, which specifically localizes Crb3 and KCC-3 (Tricaud, 2018). Finally, endfeet contact points with vasculature are also an isolated, molecularly unique microdomain. In

addition to Kir4.1 channels and aquaporin, this contact point contains a multiprotein complex including GlialCAM and MLC1 (Díaz-Castro, Robel, & Mishra, 2023). These examples suggest that glia have the ability to localize molecules into small domains, perhaps to specific associated NREs.

C. elegans as a model to understand glia-neuron specificity

Glia-neuron interactions are difficult to study in most systems due to the vast numbers of both neurons and glia and stochasticity in their development. As such, to assess glia-neuron specificity, I leverage the power of the model system *C. elegans*, which have a condensed nervous system of only 300 neurons and 56 glia with invariant neuron-glia contacts, allowing for reproducible inquiry of specific glia-neuron pairs (Singhvi, Shaham, & Rapti, 2023). In addition, this organism is optically transparent, allowing for *in vivo* cell biology and functional studies, has a fully mapped connectome, and has well-established robust behaviors of individual neurons. In this system, I focus on the amphid sheath (AMsh) glia, located in the head of the animal and part of the animal's major sense organ. This glial cell interacts with 12 unique sensory neurons only at their NREs. Of these 12 neurons, 8 extend ciliated NREs through a channel formed by the AMsh glia (channel NREs), three embed their ciliated NREs in the AMsh glia (wing NREs), and one is comprised of microvillar NREs (AFD NREs) (Singhvi et al., 2023). Channel and wing NREs all contact interconnected extracellular milieu, while AFD NREs contact an isolated extracellular pocket of its own in the AMsh glia.

A few features of AMsh glia make it a great model for glia-neuron specificity. AMsh glial ablation affects the shape of AWA wing, AWC wing, and AFD microvilli NREs, while leaving all other amphid NRE shape unaffected (Bacaj et al., 2009). AMsh ablation also affects

the function of all amphid neurons except the AWB wing neuron (Bacaj et al., 2009). These features suggest that AMsh glia regulates associated neurons in distinct manners. In addition, AMsh glia show glial calcium responses to multiple sensory inputs, including mechanical and olfactory stimuli (G. Ding et al., 2015; Duan et al., 2020). Finally, others have shown that AMsh glia regulate AMsh channel morphogenesis via opposing activities of DAF-6/Patched and LIT-1/NEMO-like kinase (Oikonomou et al., 2011; Perens & Shaham, 2005). Both of these localize to the channel and lack of these proteins lead to the inability of channel neurons to access the external environment. Thus, AMsh glia has non-uniform interactions with contacting neurons, speaking to a level of glia-neuron specificity.

We previously showed that AMsh glia affect AFD shape and function through multiple mechanisms (Martin, Bent, & Singhvi, 2022; Raiders et al., 2021; Singhvi & Shaham, 2019). One such mechanism is via the glial cation chloride cotransporter KCC-3, whose loss causes defects in AFD NRE shape, function, and associated thermotaxis behavior (Singhvi et al., 2016). In my work, I found that KCC-3 localizes to a microdomain in AMsh glia to just AFD NREs. Thus, understanding AMsh glial KCC-3 localization is a fantastic model to decipher mechanisms of glia-neuron specificity.

KCC-3 and cation chloride co-transporters

KCC-3/SLC12A6 belongs to a family of transporters called cation-chloride cotransporters (CCCs). CCCs can be broken up into two groups: Na^+-dependent transporters (NKCCs) and Na^+-independent transporters (KCCs). KCC-3 falls into the latter of these clades, along with closely related isoforms KCC-1, KCC-2, and KCC-4. The main function of KCC proteins is to utilize K^+ gradients to transport Cl^- ions across the plasma membrane in a 1:1 ratio.

KCCs are were first widely studied in red blood cells to understand their role in cell volume regulation (Garneau et al., 2017). In recent years, however, neurobiologists have shown increased interest in KCC biology, especially in nervous system development, function, and their role in neurological disorders.

While other CCC proteins are implicated in disease, only mutations in KCC-3 cause a human Mendelian monogenic disease, called agenesis of the corpus callosum with peripheral neuropathy (ACCPN), or Andermann syndrome (Kaila, Price, Payne, Puskarjov, & Voipio, 2014). This disorder is characterized by progressive sensory neuropathy, mental retardation, dysmorphic features, and is ultimately fatal. Further, KCC-3-dependent chloride transport is involved in the production of cerebrospinal fluid and critical in the inner ear system for audition (Zhang et al., 2020). Expression-wise, KCC-3 is detected in all adult CNS regions of mice. Some studies have found KCC-3 mainly in the myelinated tracts of the spinal cord and brain (Pearson, Lu, Mount, & Delpire, 2001), while others failed to note KCC-3 in CNS white matter (Boettger et al., 2003; Howard et al., 2002). KCC-3 is also found peripherally, in Schwann cell microvilli and in Deiter's and inner phalangeal cells of the inner ear (Sun, Lin, Tzeng, Delpire, & Shen, 2010).

In which cell types does KCC-3 cause disease phenotypes? Whole animal knockout of KCC-3 causes axonal swelling, hypomyelination, demyelination, and fiber degeneration in sciatic nerves (Boettger et al., 2003; Howard et al., 2002). In addition, adult KCC-3 mutant mice also show reduced exploratory behavior, progressive degeneration of inner ear cells leading to deafness, and inability of cerebellar Purkinje cells to regulate their volume (Boettger et al., 2003; Howard et al., 2002). Two separate groups constructed conditional KCC-3 knockout mice to address which cells require KCC-3. CRE recombinase-mediated KCC-3 deletion under the

synapsin promoter (all neurons) showed significant motor function impairment and a reduction in corpus callosum volume (Shekarabi et al., 2012). CRE recombinase-mediated KCC-3 deletion under a parvalbumin promoter (sensory neurons and CNS interneurons) showed neurodegeneration and locomotor defects (J. Ding & Delpire, 2014). CRE recombinase-mediated KCC-3 deletion under a desert hedgehog promoter (Schwann cells) showed an absence of neurodegeneration (J. Ding & Delpire, 2014). Together, this suggests development of neurodegeneration seen in whole animal *kcc-3* mutants arise largely from neurons, particularly parvalbumin+ neurons, with minimal participation of Schwann cells. However, of note, many phenotypes, such corpus callosum length and locomotor behavior, was less severe in the neuron knockouts compared to global knockouts, suggesting contributing roles of other cells. In addition, pan-neuronal knockout of KCC-3 did not cause defects in hearing, as seen in global knockouts (Shekarabi et al., 2012), suggesting a strong role of glial and other non-neuronal KCC-3 in mediating audition.

The crystal structure of KCC-3 was recently uncovered (Chi et al., 2020). Similar to other KCCs, KCC-3 has a central core of 12 transmembrane segments (TM), intracellular termini, and a large extracellular loop between TM5 and TM6, which houses the putative N-linked glycosylation sites. KCC-3 exists as a homo-oligomer, with both TM and C-terminal domains playing a role in dimerization, and can also be coprecipitated with KCC-1, KCC-2, KCC4, or NKCC-1 (Chi et al., 2020; Kahle et al., 2015). All CCC family members are highly conserved, especially in their central transmembrane core and C-terminus.

KCC-3 is functionally inhibited under isosmotic conditions and requires hypotonic-induced cell swelling for transporter activation. Mechanistically, phosphorylation of two threonine residues in the KCC-3 C-terminus, termed site 1 (Thr991) and site 2 (Thr 1048) are

prime regulators of KCC-3 volume sensation (Kahle et al., 2015). Hypotonic conditions rapidly dephosphorylate these sites, causing activation of KCC-3. Knockdown of With No Lysine (WNK)-1 suppresses phosphorylation of these sites, and overexpression of WNK isoforms inhibits KCC-3. The WNK substrate SPAK/OSR1 kinase, in the presence of the Cab39/MO25 regulatory subunit, directly phosphorylates site 2 and physically interacts with the N-terminus of KCC-3 in yeast two-hybrid screens (Alessi et al., 2014; de los Heros et al., 2014). Thus, WNK and SPAK/OSR1 kinases are prime regulators of KCC-3 activity. In addition, the C-terminus of KCC-3 also directly interacts with brain-specific creatine kinase (CK-B), and inhibition of CK-B reduces KCC-3 activity in a *Xenopus* oocyte functional assay (Adè Le Salin-Cantegrel et al., 2008). Interestingly, most pathogenic KCC-3 mutations disrupt the C-terminus, in agreement with the above (Kahle et al., 2015). Finally, an R207C KCC-3 mutation significantly decreases plasma membrane localization of KCC-3 and causes misfolded KCC-3 to accumulate in the endoplasmic reticulum (Adèle Salin-Cantegrel et al., 2011).

Homologs of KCC-1, KCC-2, and KCC-3, as well as NKCC-1, exist in *C. elegans*, although they are largely unstudied. As mentioned above, we find that AMsh glial KCC-3 regulates the shape and function of the AFD thermosensory neuron (Singhvi et al., 2016). Current work in our lab and others suggest that KCC-3 is expressed only in sheath glia in *C. elegans* (Purice et al., 2023; Tanis, Bellemer, Moresco, Forbush, & Koelle, 2009). Prior work by the Koelle lab also showed that KCC-2 is required for the development of inhibitory neurotransmission and synapse structure (Tanis et al., 2009). *C. elegans* only have one conserved WNK kinase, WNK-1, and a homologue of SPAK and OSR-1, GCK-3. These have yet to be connected to CCCs in *C. elegans*; however WNK-1/GCK-3 have been linked to tube formation

by modulating a CLH-3, ClC chloride channel (Falin, Miyazaki, & Strange, 2011). Thus, KCCs and their regulation are vastly understudied in *C. elegans*.

Chapter 2

CHARGING UP THE PERIPHERY: GLIAL IONIC REGULATION IN SENSORY PERCEPTION

Sneha Ray[1,2] and Aakanksha Singhvi[1, 2, 3, 4]*

(This is published work, DOI: https://doi.org/10.3389/fcell.2021.687732)

[1]Division of Basic Sciences, Fred Hutchinson Cancer Research Center, Seattle, WA

[2]Graduate program in Neuroscience, University of Washington -Seattle WA

[3]Department of Biological Structure, University of Washington School of Medicine, WA

*To whom correspondence should be addressed:

Email: asinghvi@fredhutch.org | Tel (206) 667-3606 | Fax (206) 667-5939

KEYWORDS: sense-organs, peripheral glia, sensory perception, ions, non-myelinating

Thesis: Sense-organ glia contribute to sensory processing by regulating the ionic milieu around sensory cells

ABSTRACT

The peripheral nervous system (PNS) receives diverse sensory stimuli from the environment and transmits this information to the central nervous system (CNS) for subsequent processing. Thus, proper functions of cells in peripheral sense organs are a critical gate-keeper to generating appropriate animal sensory behaviors, and indeed their dysfunction tracks sensory deficits, sensorineural disorders, and aging. Like the CNS, the PNS comprises two major cell types, neurons (or sensory cells) and glia (or glia-like supporting neuroepithelial cells). One classic function of PNS glia is to modulate the ionic concentration around associated sensory cells. Here, we review current knowledge of how non-myelinating support cell glia of the PNS regulate the ionic milieu around sensory cell endings across species and systems. Molecular studies reviewed here suggest that, rather than being a passive homeostatic response, glial ionic regulation may in fact actively modulate sensory perception, implying that PNS glia may be active contributors to sensorineural information processing. This is reminiscent of emerging studies suggesting analogous roles for CNS glia in modulating neural circuit processing. We therefore suggest that deeper molecular mechanistic investigations into critical PNS glial functions like ionic regulation are essential to comprehensively understand sensorineural health, disease, and aging.

INTRODUCTION

Glia and neurons comprise the two major cell types of the nervous system of bilaterian animals. Glia of both the central and peripheral nervous systems (CNS and PNS, respectively) are found in close physical and molecular association with cognate neurons or sensory cells. However, despite the near coincident discovery of glia and neurons, the functions of glia remain relatively unknown compared to the depth of our knowledge of neuronal cell biology and physiology. As glia are non-excitable (unlike neurons), analyses of their properties have been historically inaccessible through classical electrophysiological techniques. Recent technological advances in molecular genetics, however, have renewed focus on glia in neuroscience research. In the CNS, glia roles include dictating pioneer axon trajectories, pruning synaptic structures, stabilizing/eliminating synapses, and ionic regulation (see reviews: Chung et al. 2013; Allen and Eroglu 2017; Chotard and Salecker 2004). The resulting molecular insights into glia biology have led to a growing appreciation that glia are not passive support cells in the nervous system, but active modulators of neural functions in development, health, and disease.

Glia associate with neurons at multiple sub-cellular points of contact, including at neuron receptive-endings (NREs). NREs are specialized sub-cellular structures on individual sensory cells or neurons dedicated to receiving input from either the environment or other neurons (Shaham, 2010; Singhvi & Shaham, 2019). In the CNS, this refers to dendritic spines at synapses, where a neuron receives neurotransmitter input from its pre-synaptic neuron partner. While not identical, NREs across the CNS bear significant functional, anatomical and/or molecular similarity. In contrast to this, each peripheral sense-organ has NREs exquisitely tuned to the sensory modality it transduces. Therefore, PNS NREs vary drastically by sense organ, both anatomically and physiologically. Examples of PNS NREs in mammals include cilia of olfactory

neurons, gustatory hairs of taste buds, and microvillar stereocilia of inner hairs cells in the ear (Figure 1).

Nervous system glia come in different subtypes within the CNS and PNS, many of which contact cognate NREs. In mammals, glia of the PNS and CNS have distinct developmental origins, with PNS glia arising from the neural crest, and CNS glia arising from the neural tube (oligodendrocytes, astrocytes) or myeloid lineages (microglia). Presumably tracking PNS-NRE anatomical diversity, PNS glia that associate with these are similarly diverse across sensory modalities. Examples of these in mammals include sustentacular cells of the olfactory epithelia and Deiter's cells in the inner ear (Figure 1). In invertebrates, glia arise from neuroectodermal lineages. Their sense-organs (called "sensilla") house glia and neurons with NRE cell-biological and anatomical organization equally tailored for the modality sensed (Figure 2).

One classic function of many glial sub-types is to modulate the NRE's ionic micro-environment. In the mammalian CNS, astrocyte glia regulate extracellular levels of various ions such as potassium (K^+), sodium (Na^+), and chloride (Cl^-), at dendritic spine NREs. Ion buffering at these sites impacts neural circuit dynamics (Olsen et al., 2015; M. Simard & Nedergaard, 2004). Impairments in ion regulation by CNS glia are implicated in various neurodevelopmental and degenerative disorders including Huntington's disease, autism and epilepsy (Song et al., 2020; Tong et al., 2014; Verkhratsky, 2019). In striking functional analogy, shared across modalities and with CNS glia, multiple PNS glia sub-types across species also regulate the ionic micro-environment around sensory NREs. As reviewed below, PNS sense organ glia can modulate extracellular levels of K^+, Na^+, Cl^-, as well as calcium (Ca^{2+}) ions. This can have functional consequences on sensory cell development and activity, sensory perception and animal behavior. As may be expected then, mutations in PNS glial ion channels and transporters

that execute this function are implicated in many sensory disorders such as deafness and blindness.

Here, we review how PNS glia have been shown to regulate the neural ionic micro-environment around NREs, across sensory modalities as well as species. This summary focuses extensively on modulation of three ions (K^+, Na^+, and Cl^-) in PNS NRE extracellular space and readers are referred elsewhere for detailed discussion of Ca^{2+} dynamics in PNS neural cells (Anselmi et al., 2008; Hegg, Irwin, & Lucero, 2009; Newman & Zahs, 1998) . We collate this in the context of sense-organ neuroanatomy and discuss how ionic modulation by PNS glia can impact sensory NRE shape, neural activity, and sensory processing. Finally, we highlight gaps in knowledge in each modality, and conclude with evaluating evolutionary conservation across species and systems. We suggest that instead of a passive support function, glial ionic regulation of sensory cell/NRE milieu can be viewed as an active modifier of animal sensory perception.

REGULATION OF SENSORY CELL IONIC MILIEU BY PNS GLIA

OLFACTION

Olfaction is the perception of volatile external chemical stimuli through either the nose (vertebrates) or chemosensory sensilla (invertebrates). In both groups, glia-like support cells adjacent to primary chemosensory sensory NREs have been shown to influence sensation by regulating local levels of K^+, Na^+, and Cl^-. Besides ionic regulation, additional functions ascribed to chemosensory sense-organ glia include metabolic support of ORNs and odorant modification, buffering, and clearance (Heydel et al., 2013; Larter, Sun, & Carlson, 2016).

Mammals: Mammals transduce the percept of volatile chemicals through specialized odorant receptors on the ciliary NREs of olfactory receptor neurons (ORNs) in the main olfactory nasal epithelium (Buck, 2004). Embedded along with ORNs within this epithelium are support glia called sustentacular cells (SCs; Figure 1A). SC glia form a tightly packed columnar monolayer on the apical surface of the olfactory epithelium. They have microvilli that access the lumen of the nasal cavity where ORNs detect odorants through either ciliated or microvilli NREs (Chen, Kachramanoglou, Li, Andrews, & Choi, 2014; Elsaesser & Paysan, 2007). The mammalian vomeronasal organ, which detects pheromones, has a similar anatomy. There are different types of ORNs (ciliary, microvilli) bearing distinct olfactory receptors. To our knowledge, it remains to be determined if all support glia across the olfactory epithelia are molecularly and functionally analogous or distinct.

SC glia in mice generate voltage gated Na^+ and K^+ currents, and have outwardly rectifying "leak" conductance (Vogalis, Hegg, & Lucero, 2005). Voltage gated Na^+ channels are inactive at SC resting potentials, and their functions in sensory perception await inquiry. The voltage-gated K^+ current is largely generated by charybdotoxin-sensitive calcium (Ca^{2+})-activated BK channels. These channels are active at rest and densely localized on the apical surfaces of SC glia. The polarized localization of these channels suggests vectoral transport of K^+ ions in SC glia; however, the existence of such directional flow has yet to be established. The leak conductance in SC glia is equally permeable to Cs^+, K^+, and Na^+ and also likely passes anions such as Cl^- and F^-. Such broad permeability suggests that the leak current is generated in part by the opening of gap junction channels. In support of this model, application of the connexon-blocker 18beta-GA causes a ~3-4x increase in the resting membrane potential of

sustentacular cells in the neonate (Vogalis et al., 2005). How electrical coupling between groups of SC glia impacts neuron activity or sensory animal behaviors remains unknown.

The vomeronasal organ (VNO) detects mammalian pheromones. Ion substitution patch-clamp studies in neonate mice found that VNO-SC membranes have high resting permeabilities to K^+, Na^+ and Cl^- (Ghiaroni, Fieni, Tirindelli, Pietra, & Bigiani, 2003). Since pheromone-laden fluids like rodent urine have high concentrations of K^+, Na^+, and Cl^-, this suggests two plausible mechanisms by which SCs could modify pheromone-sensing. First, spatial buffering of K^+, Na^+, and Cl^- ions by support cells could alter VNO sensory neuron membrane excitability. Second, by modifying pheromone fluid ionic balance. In turn, such regulation could impact the biophysical properties of the pheromone molecules themselves or their binding to cognate receptors.

Neonatal VNO SCs also display voltage-gated K^+ (outward) and Na^+ (inward) currents (Ghiaroni et al., 2003). The uniformity of voltage gated currents across cells indicates that VNO support cells may be a homogeneous population. Voltage gated K^+ currents in VNO-SCs are similar to delayed rectifier types (K_{DR}) described in other glia, with some key pharmacological and electrophysiological differences. While K_{DR} channels in astrocytes and Schwann cells are only moderately sensitive to TEA, VNO-SC K_{DR} channels show high sensitivity to TEA. Further, K_{DR} channels in astrocytes are equally sensitive to TEA and 4-AP, while VNO support cell K_{DR} channels display a lower sensitivity to 4-AP compared to TEA. VNO support cell K^+ currents are also unusually noisy, compared to K_{DR} currents in other cells, and not Ca^{2+}-dependent, unlike charybdotoxin-sensitive BK channels in olfactory SCs. Na^+ channels in VNO support cells are electro-physiologically and pharmacologically similar to Na^+ channels of CNS protoplasmic astrocytes, as both have steady-state inactivation properties and low sensitivity to TTX (Ghiaroni et al., 2003). The exact identity and functional importance of VNO-SC K^+

channels and Na^+ channels have yet to be established. Spatial buffering, or the redistribution of K^+ ions in the extracellular space, may involve both resting and voltage-gated K^+ channels. Such ionic adjustment of the VNO lumen can impact VNO sensory neuron resting membrane potential and consequent activity. Importantly, investigations in mature VNO support cells are necessary to discriminate between developmental and adult ionic modulation.

Drosophila: Flies use special innervated hairs, or sensilla, to sense external chemicals. Each sensillum houses one or more sensory neuron(s), along with stereotyped glia-like support cells called shaft glia (trichogen), sheath glia (thecogen), and one or two socket glia (tormogen) (Hartenstein, 1988) (Figure 2Bi). The role of these glia in ionic regulation is not well-defined.

C. elegans: The invertebrate model, *C. elegans*, has 50 ectoderm-derived glia and 6 mesoderm-lineage glia-like cells. All 50 ectoderm-lineage glia physically approximate sensory neurons within sensilla and can be sub-typed as sheath or socket glia, similar to *Drosophila*. The *C. elegans* chemosensory system relies on three sense-organs: the amphid, inner labial organ, and phasmid, with the first two located in the animal nose tip and the last in the tail. Of these, the amphid sensillum is the primary and best studied sense-organ of the animal. This sensory structure consists of the amphid sheath glia (AMsh) and amphid socket glial cell (AMso), which both associate with 12 sensory NREs, including those of 11 chemosensory neurons (Perkins, Hedgecock, Thomson, & Culotti, 1986; Singhvi & Shaham, 2019; Ward, Thomson, White, & Brenner, 1975) (Figure 2A). Glial roles in the phasmid and
inner labial organ still await investigation.

AMsh glia modulate NRE shape and/or functions of its associated chemosensory neurons

(Bacaj, Tevlin, Lu, & Shaham, 2008; Singhvi et al., 2016; Y. Wang, D'Urso, & Bianchi, 2012; Ying Wang et al., 2008). However, the specific glia-neuron interactions underlying this are largely unknown, barring a few molecules. In the context of ionic regulation, AMsh glia expression of the Degenerin/epithelial (DEG/ENaC) Na^+-selective channel ACD-1 has been shown to support function of the odor-sensing AWC neuron. Wildtype animals display chemotaxis towards and changes in AWC intracellular Ca^{2+} levels upon exposure to the AWC-sensed odorant isoamyl alcohol (IAA). Animals with a loss-of-function allele of AMsh *acd-1* or a hypomorphic allele of neuronal *tax-2,* a subunit of the cGMP-gated channel required for chemosensation, show intact chemotaxis and appropriate AWC Ca^{2+} responses to IAA. Double mutations in both AMsh *acd-1* and neuronal *tax-2,* however, impairs IAA chemotaxis and AWC Ca^{2+} responses to low levels of IAA. Knockout of AMsh *acd-1* further exacerbates AWC chemotaxis defects caused by mutations in the G_i protein ODR-3 and the guanylate cyclase protein DAF-11, which are proposed to regulate the activity of TAX-2 channels. Interestingly, exogenous depolarization of AWC neurons in *acd-1; tax-2* double mutants rescue these sensory deficits to IAA. These studies suggest that glial Na^+ transport may contribute either directly or indirectly to chemosensation, possibly by regulating basal neuron excitability. This effect of AMsh ACD-1 also appears to be odor specific, as *acd-1* knockout does not exacerbate chemotaxis defects of hypo-morphic *tax-2* mutants to octanol or trimethylthiazole.

AMsh glia also expresses the Cl^- channel CLH-1, which is permeable to Cl^- and HCO_3^-. This channel has been shown to regulate AMsh intracellular pH via HCO_3^- flux through CLH-1. Interestingly, glial ACD-1 currents are strongly inhibited by both extra- and intracellular acidification, suggesting that pH modulation by CLH-1 may play a role in chemosensation. (Grant, Matthewman, & Bianchi, 2015). The direct role of this channel on sensation, however,

has yet to be investigated.

Other: The olfactory epithelium of frogs and salamanders bear similar anatomy to that in mammals (see Figure 1A), and SCs in both organisms are thought to play a role in K^+ buffering. Patch clamp studies in frog and salamander olfactory SCs describe high K^+ permeabilities. In the frog, SC K^+ currents are mediated by Ca^{2+}-activated BK channels, similar to mammalian olfactory SCs, suggesting evolutionary conservation. Frog and salamander SCs further exhibit membrane depolarization after odorant stimulation, likely due to the influx of excess extracellular K^+ following ORN activation (Trotier, 1998; Trotier & MacLeod, 1986). Whole cell recordings with a gap junction blocker in frog SCs reveals electrical coupling between olfactory support cells, which could facilitate the clearance of K^+ ions released by ORNs (Trotier, 1998). Electrophysiological studies suggest that K^+ buffering in salamander SCs occurs in hundreds of milliseconds, which parallels the timescale of mouse ORN activation (Trotier & MacLeod, 1986). This suggests that SCs are well poised to regulate ORN sensitivity to odors in real time. Whether and how K^+ buffering in frog or salamander SCs affects chemosensation, however, has yet to be formally investigated.

GUSTATION (TASTE)

Taste is the percept of nonvolatile external stimuli including ions. Roles of glia in gustation are poorly understood across systems.

Mammals: Taste sensation in mammals begins in taste buds, onion bulb-like structures in the tongue (Figure 1B). Each taste bud consists of 50-100 elongated neuroepithelial cells that are

sub-categorized as Types 1-3. Type 2 and Type 3 cells are considered taste receptor cells that sample tastants through primary cilia NREs that house taste receptors (Roper & Chaudhari, 2017; Yarmolinsky, Zuker, & Ryba, 2009) . Type 1 cells, on the other hand, exhibit glia-like functions both chemically and structurally. Similar to CNS glia, Type I cells express transporters that are required to eliminate extracellular neurotransmitters, including the glutamate-aspartate transporter GLAST. Further, similar to the close interactions of CNS glia and neurons, Type I cells have cytoplasmic extensions that ensheath other taste bud cells (Bartel, Sullivan, Lavoie, Sévigny, & Finger, 2006; Lawton, Furness, Lindemann, & Hackney, 2000; Roper & Chaudhari, 2017). Few other details of these PNS glia or their molecular diversity across taste buds are known.

Type I taste bud glia-like cells display a small voltage-dependent outward K^+ current and express the inward-rectified K^+ channel ROMK (Dvoryanchikov, Sinclair, Perea-Martinez, Wang, & Chaudhari, 2009; Medler, Margolskee, & Kinnamon, 2003; Romanov & Kolesnikov, 2006). This suggests that these cells may spatially buffer K^+ in the taste bud, which could alter Type II and Type III taste cell excitability. They are also the only taste bud cells to express amiloride-sensitive ENaC Na^+ channels. Behavioral studies in rodents show that amiloride decreases taste perception of NaCl, suggesting that amiloride-sensitive ENaC channels play a crucial role in taste transduction of salt. Type I cell expression of these channels implicates a role of these glia-like cells in salt detection (Vandenbeuch, Clapp, & Kinnamon, 2008). Further studies are required to illuminate the precise role of glial ENaC Na^+ channels in salt sensing.

C. elegans: In addition to olfaction, the AMsh glial DEG/ENaC Na^+ channel ACD-1 is also required to sense water-soluble tastants, such as NaCl, acidic solutions, and lysine acetate.

Similar to IAA chemosensation (see above), AMsh *acd-1* knockout exacerbates the reduced chemotaxis of hypomorphic *tax-2* mutants to NaCl. Acid avoidance and chemotaxis to the amino acid lysine requires the neuronal DEG/ENaC channel DEG-1. AMsh *acd-1* knockout further exacerbates the impaired acid avoidance and lysine chemotaxis of *deg-1* mutants. Similar to olfaction, these findings suggest that AMsh ACD-1 plays a role in setting chemosensory neuron excitability. As the AMsh HCO_3^- channel CLH-1 may affect ACD-1 activity (see above), glial regulation of HCO_3^- may additionally play a role in taste sensation (Y. Wang et al., 2012; Ying Wang et al., 2008). The precise mechanistic role of ACD-1 and CLH-1 in sensing water-soluble tastants awaits further investigation.

AUDITORY AND VESTIBULAR SENSATION

The auditory system is exteroceptive and mediates sound perception, while the vestibular system is proprioceptive and concerned with maintaining body equilibrium and orientation in space. Since these systems are anatomically and functionally related, they are discussed together here. Glia-like support cells adjacent to peripheral auditory and vestibular sensory structures influence sensation by regulating local levels of K^+, Na^+, and Cl^-. Besides ion regulation, auditory/vestibular support cells modulate the extracellular matrix to support sensory epithelial integrity, form new hair cells upon injury, and engulf synaptic terminals.

Mammals: Hearing and balance in mammals is mediated by modified epithelial cells called hair cells in the cochlea and vestibular system of the ear, respectively. Cochlear hair cells are activated by sound waves, and vestibular hair cells by head movements and gravitational force (Corey, 2009; T. Reichenbach & Hudspeth, 2014). The cochlea is anatomically divided into

three compartments, the scala media, scala tympani and scala vestibuli. The developing cochlea also contains a transient epithelial structure called Kolliker's organ, which comprises columnar-shaped supporting cells that differentiate into auditory sensory cells. Each adult hair cell NRE comprises ~100 actin-based stereocilia (microvilli) and a single cilium termed the kinocilium. Cochlear hair cells are surrounded by various glial cell-types that are location-specific, such as inner phalangeal cells, Deiter's cells, and cells of Hensen's (Figure 1C). In contrast, the vestibular system anatomically has a more homogeneous group of support cells (Wan et al., 2013).

The neural physiology of hair cells differs from that of most nervous system cells. While most neurons fire action potentials by influx of $Na^{+,}$ hair cells rely on K^+ entry for neuronal activation. This requires K^+ depolarization, which in turn requires that hair cell NREs are bathed in the high K^+/low Na^+ ionic environment of the scala media endolymph. Endolymph ion composition uniquely resembles intracellular fluid, while the low K^+/high Na^+ perilymph of the scala tympani and scala vestibuli are typical of extracellular spaces. Support cells help keep endolymph and perilymph compositions distinct by serving as a neuroepithelial barrier between their respective compartments. To do so, support cells make extensive bicellular and tricellular tight junctions (TJs) with hair cells. Mutations in junctional proteins concentrated at support cell-hair cell TJs, including claudin 14, tricellulin, and angulin-2/ILDR1, cause deafness (Kitajiri & Katsuno, 2016; Riazuddin et al., 2006). (Wilcox et al., 2001). Therefore, the composition of this endolymph, and thereby auditory perception, requires the surrounding glia.

Upon sensory transduction, K^+ flows passively into hair cells from the endolymph and exits through basolateral KCNQ4 channels into the perilymph. Radiotracer and molecular genetic studies show that endolymph fluid derives from the surrounding perilymph, rather than

the blood. This suggests that K^+ is recycled from the perilymph back to the endolymph. Two support-cell dependent pathways, the lateral and medial transport routes (see below), are thought to mediate K^+ recycling. Mutations in support cell proteins involved in K^+ recycling lead to hearing loss, highlighting the importance of this process to auditory perception (Zdebik, Wangemann, & Jentsch, 2009).

The lateral transport route is the canonical pathway underlying K^+ recycling from the perilymph to the endolymph. The stria vascularis of the cochlea or dark cells of the vestibular system secrete K^+ into the endolymph. Three non-exclusive theoretical models describe how perilymph K^+ gets to the stria vascularis. We summarize these briefly here, and refer readers to (Zdebik et al., 2009) for a deeper review. *Model A:* glia-like Deiter's and inner phalangeal cells uptake K^+ from the basal poles of hair cells using K^+/Cl^- co-transporters (KCCs) and relay K^+ back to the stria vascularis through a system of gap junctions and transporters. Consistent with this, Deiter's glia-like cells express the K/Cl co-transporters KCC-4 and KCC-3, and inner phalangeal support cells express KCC-3 (Boettger et al., 2003). Knockout of either *kcc-3* or *kcc4* results in progressive hearing loss (Boettger et al., 2003). In agreement with their role in support glia, auditory defects are observed in ubiquitous *kcc-3* knockout animals, but not in neuron-specific *kcc-3* knockout animals (Shekarabi et al., 2012). As further support for this model, audio-vestibular support cells are electrically coupled by gap junctions made predominantly of connexin-26 (Cx26) and connexin-30 (Cx30) subunits (Hama & Saito, 1977; Kikuchi, Adams, Paul, & Kimura, 1994; Nadol, Mulroy, Goodenough, & Weiss, 1976). (H. B. Zhao, Kikuchi, Ngezahayo, & White, 2006). Cx26 and Cx30 are mutated in hereditary forms of deafness, and knockout mouse models replicate this phenotype. Interestingly, targeted ablation of Cx26 in support cells and flanking epithelial cells alone can cause hearing impairment (Cohen-Salmon et

al., 2002; Stong, Chang, Ahmad, & Lin, 2006). *Model B:* Glial support cells use KCCs to relay K^+ from the basal poles of hair cells to the scala tympani. From here, K+ travels through the open perilymph space to the stria vascularis for secretion into the endolymph. This model is consistent with the *kcc-3* and *kcc-4* gene expression and mutant studies above. In further support, the perilymph of the scala tympani contains standing currents that are altered upon acoustic stimulation (Zidanic & Brownell, 1990). To note, however, standing currents can also exist if K^+ is directly shuttled into the scala tympani without support cells. *Model C:* t K^+ enters glial support cells through P2X purinergic signaling and is shuttled through gap junctions or via the perilymph back to the stria vasicularis. Consistent with this, sub/micromolar levels of ATP evoke a K^+ dependent inward current in cochlear glia, including Deiters, Pillar, Hensen, and Claudius cells. This current tracks [ATP] and is abolished in the absence of ATP or with P2X receptor antagonists (Zhu & Zhao, 2010). It is feasible that support glia gap junctions move the ATP driving K^+ intake (Hong Bo Zhao, Yu, & Fleming, 2005).

In the putative medial K^+ recycling pathway, K^+ effluxed from inner hair cells travels through border cells and inner ear epithelial cells to return directly to the scala media. This is also supported by structural and immunohistochemical evidence. Namely, border and epithelial cells have morphological and histochemical features similar to Hensen and Claudius cells of the lateral transport route (Spicer & Schulte, 1998). These cells also have gap junctions that might allow transcellular transport of K^+ ions (Spicer & Schulte, 1998). However, direct evidence of this route has yet to be demonstrated. If the medial route is a canonical K^+ recycling pathway, this would suggest that border support cells of the inner ear mediate K^+ levels in the auditory NRE extracellular milieu, with possibly consequences on hearing.

Maintenance of high K^+ in the endolymph necessitates a counterbalance of Na^+ absorption. Na^+ ion imbalance in the endolymph causes blebbing of the inner hair cell NREs (Kim & Marcus, 2011) . This is enabled by activity of proteins like Na^+/K^+ ATPase, expressed by both Dieter's cells and the inner phalangeal cells of the organ of Corti . Mutations in this ATPase pump are associated with Meniere's disease, an inner ear condition characterized by dizzy spells (vertigo) and hearing loss (Stephenson et al., 2021). Caudius' and Deiter's support cell glia also express all three subunits of ENaC channels (Gründer, Müller, & Peter Ruppersberg, 2001). Interestingly, mutations in the transmembrane serine protease TMPRSS3, thought to regulate ENac channels, is implicated in non-syndromic autosomal recessive deafness (DFNA8/10) (Guipponi et al., 2002). How glia regulate Na^+ levels is not well-elucidated.

A recent study also finds that purinergic-signaling driven regulation of Cl^- by support cell glia impacts cochlear development. Support cells in the transient Kolliker's organ of the developing mammalian cochlea spontaneously release ATP, likely through connexin hemichannels, stimulating purinergic P2RY1 support cell auto-receptors (Tritsch et al 2007). Activation of purinergic auto-receptors opens support cell TMEM16 Ca^{2+}-activated Cl^- channels, triggering osmotic cell shrinkage, Cl^- efflux, and forcing concurrent K^+ efflux (Wang et al 2015; Babola et al 2020). This K^+ efflux from support cells causes transient depolarization of IHCs near ATP release sites and triggers action potential bursts in primary auditory neurons. Osmotic shrinkage of support cells also increases the extracellular space and speed of K^+ redistribution. Thus, by modulating Cl^- flux, support cells can both initiate spontaneous hair cell activity and regulate hair cell excitability by controlling the volume of the extracellular space.

Drosophila: Fly hearing is mediated by sensilla in the chordotonal Johnston's organ (JO) in the antenna of the animal (Figure 2Bii) ,which detect air vibrations. The JO is comprised of an array of ~250 auditory units called scolopidia that house two to three sensory neurons with cilia NREs, and several glial "support cells". The principle support cell, scolopale, encloses the neuronal dendrite NRE in fluid-filled lumen called the scolopale space (Figure 1Cii). Similar to the vertebrate cochlear endolymph, this fluid is believed to rich in K^+ ions, although the composition has not yet been analyzed (Eberl & Boekhoff-Falk, 2007).

In the JO, the ATP$\propto$ Na^+/K^+ ATPase subunit is enriched in scolopale cells, and knockdown in the entire JO or specifically in scolopale cells results in animal deafness. The Na^+/K^+ ATPase extrudes Na^+ out and K^+ in in a 3:2 ratio. Knockdown of the nrv2 β Na^+/K^+ ATPase subunit, expressed specifically in scolopale cells in the JO, similarly results in almost complete deafness (Roy, Sivan-Loukianova, and Eberl 2013). Thus, K^+ ion regulation by scolopale support cell glia may be crucial for proper auditory transduction and setting sensory neuron excitability, although this is not formally demonstrated.

Other: In the zebrafish *Danio rerio*, mechanosensitive hair cells of the lateral line sense movement, vibration, and water pressure. This is critical for the animals to orient, school socially, and detect predators. Lateral line hair cells bear morphologic and genetic resemblance to those of the vertebrate inner ear, and also have NREs composed of stereocilia and a kinocilium that mediate hair cell activation (Nicolson, 2017; Pinto-Teixeira et al., 2015). Hair cells are organized into a collection of neuromasts spaced along the body of the animal. Each neuromast consists of roughly 60 cells organized in a circular epithelium: 16-20 mechanosensory hair cells and ~30 glia-like sustentacular cells intermingle at the center of the organ, while ~10

glia-like mantle cells occupy the periphery (Figure 2C). Within the neuromast, support cell gap junctions maintain low K^+ levels in associated hair cells, likely through K^+ buffering. Pharmacologically blocking gap junctions in support cells drastically reduces presynaptic Ca^{2+} activity in hair cells, with impact on sensory stimuli encoding (Q. Zhang et al., 2018). Molecular mechanisms regulating this function are not well-elucidated.

SOMATOSENSATION

Somatosensation includes processing of information received at the skin/cuticle, and includes sub-modalities such as mechanoreception, thermosensation, and nociception. Together, these enable the animal to sense touch, pressure, stretch, heat, cold, and pain (Abraira & Ginty, 2013). The role of glia on somatosensation remains largely a mystery.

Mammals: A subset of somatosensory NREs in the vertebrate skin are encapsulated by lamellae of modified glial Schwann cells (Figure 1D). These structures include Meissner's corpuscles (which sense pressure), Pacinian corpuscles (which sense vibration), and Ruffini's corpuscles (which sense skin stretch). Both physiological and biophysical studies suggest that this lamellar encapsulation contributes to somatosensory perception (Cobo, García-Piqueras, Cobo, & Vega, 2021).

Ion channels are present in the modified Schwann cells of somatosensory receptors. Histological studies have shown that the DEG/ENaC Na^+ channel ASIC2 and subunit ENaCbeta are present in lamellar cells of Pacinian corpuscles and terminal Schwann cells of Ruffini corpuscles, respectively (Calavia et al., 2010; Hitomi et al., 2009; Montaño et al., 2009). Since

DEG/ENaC channels have been implicated in touch sensation in many systems (Ben-Shahar, 2011), this raises the possibility that Schwann cells associated with these encapsulated receptors may play a mechanosensory role, but this has not yet been explored. In addition, voltage-gated Na^+ channels have also been identified by immunocytochemistry in Pacinian corpuscle lamellae, suggesting that these may also contribute to mechano-transduction (Pawson, Slepecky, & Bolanowski, 2000). Similarly, immunohistochemistry also reveals the presence of the polymodal Ca^{2+} permeant channel TRPV4 (a known mechano-sensor itself) in the lamellar cells of human Meissner corpuscles (Alonso-González et al., 2017). However, the precise contribution of TRPV4 channels and lamellar glia in pressure sensation has not yet been established.

C. elegans: The OLQ and IL1 glial sheath and socket cells, which associate with OLQ and IL1 mechanosensory neurons, express the DEG/ENaC subunits DELM-1 and DELM-2. These ion channels act cell-autonomously in the OLQ and IL1 glial socket cells to drive sensitivity to mechanical stimulus and nose touch and foraging behaviors. Indeed, animals lacking DELM-1 exhibit defects in setting basal OLQ and IL1 neuron excitability (Han et al., 2013). This shows direct evidence of glial ion channels mediating mechano-sensation.

C. elegans thermosensation is mediated by the temperature-sensing AFD neuron. AMsh glia directly regulate thermosensation by modulating the microvilli NRE shape of AFD. One mechanism by which AMsh glia control AFD microvilli NRE shape is using the glial K/Cl transporter, KCC-3, which localizes specifically around the AFD NREs. Molecularly, Cl^- extruded by the AMsh glia directly inhibits the GCY-8 receptor guanylyl cyclase located on AFD NREs. cGMP generated by GCY-8 antagonizes the actin regulator WSP-1/NWASP which drives actin assembly and polymerization (Singhvi et al., 2016). Thus, inhibition of GCY-8 by

AMsh glial KCC-3 reduces AFD cGMP levels, allowing WSP-1/NWASP to properly shape AFD NRE microvilli. *kcc-3* mutants have short AFD microvilli and, consequently, an inability to perform wildtype thermotaxis behaviors. These findings describe a precise molecular mechanism by which ionic regulation by glia mediates animal sensation. Whether other glial ion channels and transporters also controls thermosensation remains uninvestigated.

Further, recent work from our laboratory has found that AMsh glia also track AFD activity to engulf fragments of AFD NRE dynamically (Raiders, Black, et al., 2021). Altering this glial pruning activity can alter NRE shape and associated animal behaviors post embryonic development, similar to ionic modulation by glial KCC-3. How glial ionic regulators like KCC-3 cooperate with other glial regulatory pathways like pruning of NREs is not clear in any setting.

Other animals: In the spider (*Cupiennius salei*) mechanosensory organ, Na^+ channels are expressed at similar levels in both neurons and their surrounding glial cells, as quantified by immunofluorescence (Seyfarth, Sanders, & French, 1995). These glia may regulate Na^+ levels in mechanosensory organs to regulate sensation.

VISION

Vision is the transduction of light stimuli through photosensitive cells. Glia-like support cells adjacent to light-sensing NREs have been shown regulate local levels of K^+, Na^+, and Cl^- ions to affect vision. Besides ionic regulation, additional functions of sense-organ glia include regeneration of visual pigments retinal and phagocytosis of photoreceptor NREs.

Mammals: The mammalian retina develops from the neural tube rather than the neural crest, making vision the only vertebrate sensory modality that is technically CNS and not PNS. However, because the retina is a sense organ, we include the role of glial ionic modulation in mammalian visual sensation for completeness.

Mammals sense light using photoreceptor cells called rods and cones, whose "outer-segment" NREs are modified cilia. Retinal pigment epithelia (RPE), a polarized monolayer of glia-like support cells, form the outermost layer of the retina and physically approximate photoreceptor NREs. Microvilli extend from the apical surface of RPE cells to envelop the outer segments of both rods and cones. (Reichenbach and Bringmann 2020) (Figure 1E). RPE glia-like cells transport ions and water from the apical subretinal space (proximal to photoreceptor NRE) to the basolateral vasculature, or choroid. Tight junctions between RPE ensure a barrier between these spaces. Below we discuss ions individually for simplicity, but also note that each ionic current is also influenced by the concentration and conductance of other ions.

Na^+*:* Unlike most epithelia, RPE localize Na^+/K^+ ATPases to their apical membranes for transepithelial transport. This establishes a Na^+ gradient that facilitates bicarbonate uptake via a Na^+-bicarbonate transporter, and uptake of K^+ and Cl^- through the NKCC cotransporter (Strauss, 2005). Further, unstimulated photoreceptors passively intake Na^+ ions through open cyclic-nucleotide gated channels. This "dark current" establishes the depolarized resting potential needed for vision. Apically localized RPE Na^+/K^+ ATPase in the RPE help set the sub-retinal Na^+ concentration needed to drive these currents, a critical requisite for visual perception (R. Sparrrow et al., 2010).

K^+: K^+ enters RPE apically through either the Na^+/K+ ATPase or NKCC. From the RPE, K^+ ions can leave the cell through either the apical or basolateral membranes. In dark, photoreceptors intake Na^+ and extrude K^+ (see above). The consequent high K^+ levels in subretinal space promote K^+ uptake apically and release to the basolateral choroid. Higher basolateral K^+ conductance allows for net K^+ transport from photoreceptor space to basolateral vasculature. The channels/transporters driving basolateral conductance await molecular identification, but candidates include the large-conductance Ca^{2+}-dependent K^+ channels and the M-type K^+ channel (Strauss, 2005). Upon light-stimulation, photoreceptor dark current drops, which reduces subretinal K^+ levels. This hyperpolarizes the apical RPE membrane, which activates apical Kir7.1 inward rectifying K^+ channels. Activation of Kir7.1 channels drive K^+ efflux out of the apical membrane, which replenish subretinal K^+ levels. Such RPE K^+ buffering crucial for the fast-occurring changes during visual transduction and maintaining photoreceptor excitability for repeated activation (R. Sparrrow et al., 2010; Strauss, 2005). While mechanisms by which RPE regulate Kir7.1 remains unclear, this likely impacts visual function.

Cl^-*:* In addition to K^+, the apical NKCC cotransporter also facilitates entry of Cl^- into the RPE. Intracellular Cl^- exits the cell through basolateral Ca^{2+}-dependent Cl^- channels including CLC-2, and the cystic fibrosis transmembrane conductance regulator (CFTR) (Strauss, 2005). Transgenic mice lacking ClC-2 channels show no RPE transepithelial potential and exhibit retinal degeneration comparable to retinitis pigmentosa (Bösl et al., 2001). Best's vitelliform macular degeneration, in which RPE degeneration causes retinal degeneration, is also associated with defective Cl^- transport. The leading diagnostic in this case is a reduction in the light peak-to-dark ratio in an electro-oculogram and extracellular fluid filled lesions, both indicative of decreased

RPE basolateral Cl^- transport (Xiao, Hartzell, & Yu, 2010). However, mechanistic insights into these regulators in health or disease remains poorly understood.

Reduced RPE transepithelial ion transport is associated with impaired visual function. For example, macular edema is the buildup of fluid in the center of the retina, likely caused by damage to the RPE/endothelium mediated blood/retina barrier. It is successfully treated with carbonic anhydrase inhibitors. These reduce RPE intracellular bicarbonate concentration by reducing uptake of Cl^- by the basolateral Cl^-/bicarbonate exchanger and driving its release baso-laterally instead. This Cl^- extrusion drives water transport into the choroid, eliminating the edematous fluid. Thus, ionic transport by RPE cells is critical for retinal health.

Drosophila: The Drosophila compound eye consists of units called ommatidia. Each ommatidium houses 8 core photoreceptor neurons (R-cells) that sense light using microvilli NREs called rhabdomeres. These R-cell bundles are additionally surrounded by 4 support cells, called cone cells, and 2 pigment cells (Figure 2Bii). Recent molecular studies suggest that cone cells express sense-organ glial signature genes such as *pax-2, prox-1, and olig-1*; and may serve glial functions like energy support and sustaining photoreceptor neurotransmission, in the fly retina (Chotard and Salecker 2007; Charlton-Perkins et al. 2017). Dark adapted flies exhibit strong photoreceptor depolarization in response to light, as measured by electroretinograms. Genetic knockdown of the ATP-alpha, nrv2, or nrv3 subunit of the Na^+/K^+ pump in cone cells significantly reduced photoreceptor responses to light. Knock-down of cone cell inward rectifying Irk2 K^+ channel similarly reduced photoreceptor responses (Charlton-Perkins et al 2017). Thus, ion regulation by retinal glia are crucial for proper vision.

Other animals: Outer pigment cells, the principle glia in the honey-bee (*Apis mellifera)* drone retina, spatially buffer K^+ in the extracellular space around photoreceptors, based on electrophysiological studies (Coles, 1989). How this impacts animal vision is not yet established.

CONCLUDING REMARKS

ANALOGY IN GLIAL IONIC REGULATION ACROSS SENSORY MODALITIES

One important glial function is regulation of ionic milieu around neurons (Olsen et al., 2015). It is evident that glia across sensory modalities, and species, deploy analogous machinery to regulate associated sensory cells/neurons. For example, many PNS glia across sensory systems and species use cation chloride cotransporters (CCCs), DEG/EnaC channels, inward rectifying channels and Na^+/K^+ ATPases to regulate K^+, Na^+, and Cl^- (above) and (Figure 3). However, PNS glia ionic regulation of NREs is an emerging field with many remaining unknowns. For example, the entire repertoire of ion channels and transporters and their subcellular localization is not described for any PNS glia. How any one glia regulates its ionic transporters/channels, and how this modifies sensorineural activity is not well-elucidated. Moreover, how these ionic regulators interact with each other is also poorly understood. Finally, it is not even clear if all PNS glia within a sense organ are functionally and molecularly identical, even in regulating NRE ionic microenvironment. Thus, studies of such cross-utilized molecules in one modality may also inform on its function in another sensory context or species.

ANALOGY IN GLIAL IONIC REGULATION ACROSS CNS AND PNS

Based on the literature, we also propose that studies of glial ionic regulation in the PNS may inform CNS-centric biology in two ways. One, we note that many neurological disorders also

have a sensory component. For example, anosmia can precede motor deficits in Parkinson's disease patients, and Autism patients exhibit significant sensory impairments (Doty, 2012; Marco, Hinkley, Hill, & Nagarajan, 2011). How these causally link across the PNS and CNS is not well-defined, and further investigation of sensory impairments in animal models where these ionic regulators are implicated may be insightful into early stages of disease-progression as well as diagnostics.

Two, comparative analyses of glial functions across CNS/PNS suggests that, despite deriving from distinct embryonic developmental cell lineages, glia across systems and species show partial functional and mechanistic analogy in the molecular strategies with which they regulate ionic milieu of associated neurons. Thus, CCC channels are implicated not only in many sensory systems (Figure 3A), but also in CNS disorders like Epilepsy, Hydrocephalus, Autism, Anderman syndrome and Ischemic stroke (Alexandre P Garneau et al., 2017; Huang et al., 2019; Jin et al., 2019). Similarly, DEG/ENac channels express not across sensory systems, but are also implicated in forming hybrid channels with related ASIC channels to drive amiloride-sensitive currents and migration in human glioma cells (Kapoor et al., 2011; X. Sun et al., 2013). Inward rectifying potassium channels also not only regulate sensory glia biology (Figure 3C) but are also a prominent feature of mature post-mitotic astrocytes. They are implicated in many diseases including epilepsy, multiple sclerosis, glial malignancy (Olsen et al., 2015; Seifert, Henneberger, & Steinhäuser, 2018). Lastly, while our compilation highlights a theme of sensory glia utilizing Na^+/K^+ ATPase (Figure 3D), these also are not a PNS-specific glia feature. They, along with many of the other channels above, are critical regulators of cerebral edema, and implicated in diseases like Alzheimer's disease (Ugbode et al., 2017).

Furthermore, we note that this analogy in CNS and sense-organ glia functions persists beyond glial ionic regulation. For example, mammalian CNS astrocytes secrete thrombospondin (TSP)-1 and 2 to promote synaptogenesis (Christopherson et al., 2005). Analogously, the *C. elegans* sense-organ amphid sheath glia secretes the TSP-1 domain containing protein FIG-1 to modulate sensory neuron properties (Bacaj, Tevlin, et al., 2008). Vertebrate astrocytes use the MEGF10 and MERTK phagocytic pathway to mediate synapse elimination (Won Suk Chung et al., 2013), while *Drosophila* astrocytes similarly deploy the MEGF10 ortholog Draper to clear synaptic and neuronal debris following injury (Hilu-Dadia & Kurant, 2020; MacDonald et al., 2006; Raiders, Han, et al., 2021) and *C. elegans* peripheral sense organ glia use a similar (albeit not identical) machinery to regulate sensory neuron shape and animal behavior (Raiders, Black, et al., 2021).

We therefore propose that investigations into PNS glia biology may be broadly relevant. Comparative studies across CNS/ PNS, and species, may inform on novel insights into ontogenic and evolutionarily conserved molecular mechanisms by which glia sensorineural health and disease.

Figures

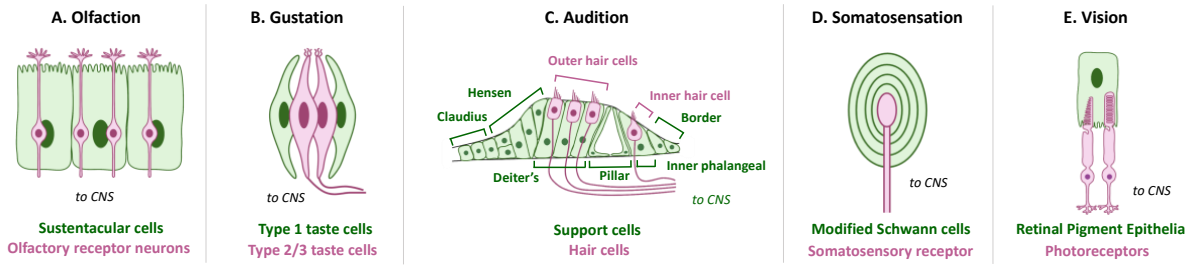

FIGURE 1: Glia-like support cells at mammalian peripheral sense organs across modalities

(A) Olfaction: Sustentacular cells appose olfactory receptor neurons at its dendrite and ensheathing glia contact its axons. **(B)** Gustation: Type I glia-like cells contact Type II receptor cells, and Type III in vertebrate taste buds. **(C)** Audition: Deiter's support cells interact with outer hair cells, and inner phalangeal support cells interact with the inner hair cell. Also shown are Hensen's support cells. **(D)** Somatosensation: Somatosensory receptors are surrounded by modified Schwann glia cell lamellae in Pacinian corpuscles. **(E)** Vision: Glia-like retinal pigment epithelia contact photoreceptor NREs while Muller glia span the entire length of the retina except the NREs.

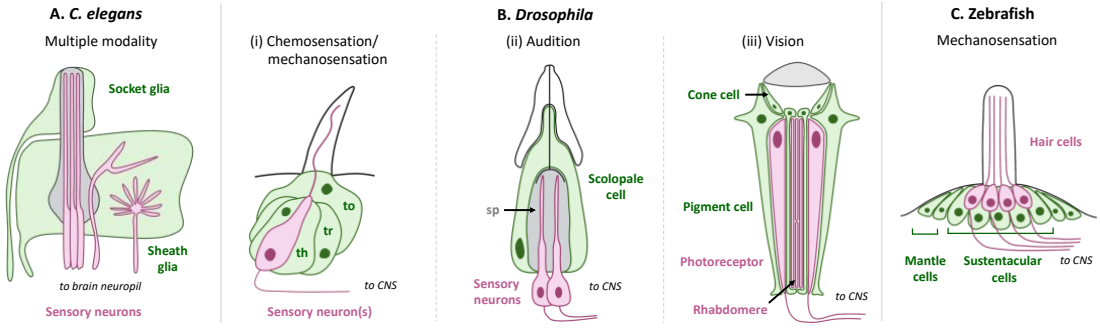

FIGURE 2: PNS glia across modalities in sense-organs of non-mammal model systems

(A) *C. elegans* sense- organs comprise socket and sheath glia that ensheath sensory neurons. **(B)** Support cells in *Drosophila*. (i) Chemosensation/mechanosensation: Thecogen (sheath glia); tr: trichogen (shaft glia); th: to: tormogen (socket glia) associate with neurons in sensory hairs called sensilla. (ii) Audition: Sensory neurons in Johnston's organ are surrounded by the scolopale space regulated by glia-like scolopale cells. (iii) Vision: Drosophila photoreceptor cells are surrounded by two types of glia: pigment cells and cone cells. **(C)** Zebrafish hair cells in the lateral line are organized into neuromasts. Each neuromast houses hair cells intermingled with sustentacular cells at the center, and mantle cells at the periphery.

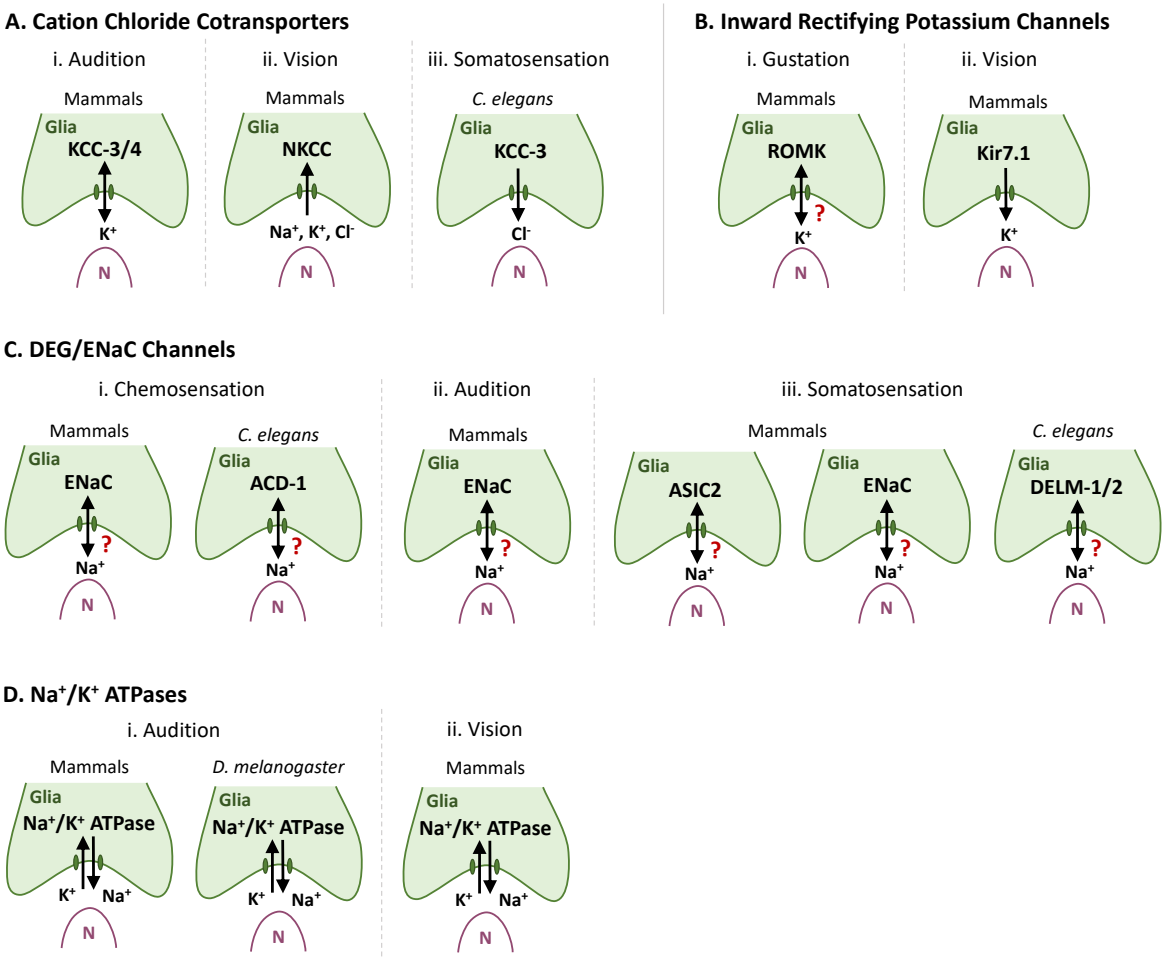

FIGURE 3: Glial ionic regulators regulate sensory neuron shape and functions across sensory modalities and species. (A) Cation chloride cotransporters. (i) Glial KCC-3 regulates thermosensory NRE shape and animal behavior in *C. elegans.* (ii) Glial Ncc69 regulates synaptic transmission and vision in *Drosophila.* Mammalian RPE express NKCC to modulate the ionic milieu in the subretinal space; how this protein specifically affects vision is unknown. (iii) Glial KCC-3/ KCC-4 in inner ear support cells regulate auditory transduction and their loss leads to hair cell degeneration and deafness. **(B)** DEG/ENaC channels. (i) *C. elegans* glial DELM-1/DELM-2 channels set basal sensory neuron excitability and drive sensitivity to mechanical stimuli. The glial DEG/ENaC channel ACD-1 regulates *C. elegans* acid avoidance behavior, and

chemotaxis to the amino acid lysine. ENaC channels are also expressed in vertebrate glia-like Type I taste cells and support glia of the inner ear. **(C)** Inward rectifying K^+ channels. (i) Type I taste cells express the ROMK channel, possibly to buffer extracellular K^+. (ii) Mammals express Kir7.1 channels in RPE cells and Kir4.1 channels in Muller glia. Both are implicated in spatial buffering of K+ for continued neuron excitability.

ACKNOWLEDGEMENTS

We thank members of the Singhvi laboratory for discussions and comments on the manuscript.

Funding: This work is supported by a Simons Foundation/SFARI grant (488574), a Glenn Foundation for Medical Research and AFAR Junior Faculty Award and National Institutes of Health/NINDS R01 NS114222 grant to AS.

Author Contributions: SR and AS conceptualized and co-wrote the manuscript.

Competing Interests: The authors declare no competing interests.

Chapter 3

Microdomain localization of glial KCC-3 by neuron cilia impacts multisensory processing

Sneha Ray[1, 2], Pralaksha Gurung[1, 2], R. Sean Manning[1], Alexandra Kravchuk[1, 3], Aakanksha Singhvi[1, 4,*]

(A version of this is published, DOI: https://doi.org/10.1101/2023.03.18.533255)

[1]Division of Basic Sciences, Fred Hutchinson Cancer Research Center, Seattle, WA 98109

[2]Neuroscience Graduate Program, University of Washington, Seattle, WA

[3]University of Washington School of Medicine, WA 98195

[4]Department of Biological Structure, University of Washington School of Medicine, WA 98195

*To whom correspondence should be addressed:

Email: asinghvi@fredhutch.org | Tel (206) 667-3606 | Fax (206) 667-5939

ABSTRACT

Most glia interact with multiple neurons, but it is unknown if their interactions with each neuron is distinct. Our interrogation of this at single-cell resolution reveals that a single glia exhibits specificity in its interactions with different contacting neurons. Briefly, *C. elegans* AMsh glia have polarized membranes, with apical-like domains contacting neuron endings. Within these, AMsh glia localize KCC-3/K-Cl transporter to a microdomain exclusively around the thermosensory AFD neuron to regulate its shape and function. For this, KCC-3 is transported first to neuron-proximal regions in the glia. Cilia of neighboring non-AFD chemosensory neurons then constrain KCC-3 to a microdomain at AFD-contacting membranes. Aberrant KCC-3 localization impacts both AFD and non-AFD neurons and associated sensory behaviors. Thus, polarized microdomain localization of a glial cue to one neuron contact dictates multi-modal processing across neurons. As glia across species compartmentalize cues like KCC-3, we posit that their microdomain localization may be a conserved mechanism by which glia modulate information processing across circuits.

Key Words: glia, sensory processing, KCC-3, glial polarity, glial microdomain

INTRODUCTION

In centralized nervous systems, glia physically contact neurons to regulate neuron shape, function, and animal behavior (Barres, 2008; von Bartheld, Bahney, & Herculano-Houzel, 2016). Across both central and peripheral nervous systems (CNS and PNS, respectively), a single glia contacts multiple neurons (Allen & Eroglu, 2017). This raises a fundamental logic question: does one glia modulate all its contacting neurons similarly or through distinct mechanisms? If differently, are different glia-neuron interactions interdependent or independently controlled within each glia? Decoding the specificity logic of glia-neuron interactions is key to understanding the organizational principle of the nervous system.

This is relevant for both CNS and PNS/sensory biology. In the CNS, each astrocyte glia can interact with an estimate >1,000 neurons, and ~100,000 NREs (Won-suk Suk Chung et al., 2015), and can regulate excitatory and inhibitory neurons differently through different molecular regulators (Allen & Eroglu, 2017; Eroglu et al., 2009; Stogsdill et al., 2017). Similarly, in sense-organs like retina, different glia contact multiple neurons, including rod and cone photoreceptors (RPE glia-like cells) as well as interneurons (Muller glia) (R. Sparrrow et al., 2010). Further, in the tongue, Type I support cells contact different taste receptor cell-types (Rodriguez et al., 2021). In any instance, molecular specificity of glia-neuron interactions remains to be explored at single-cell detail.

Various functional studies have suggested that there is likely specificity in glia-neuron interactions. In murine astrocytes, intracellular calcium (Ca^{2+}) dynamics vary with different neuron circuit activities, suggesting that glia functionally differentiate between different neuron input (Khakh &

Sofroniew, 2015). In *C. elegans*, ablation of a single glial cell has differential effects on different neurons (Bacaj et al., 2009). Finally, in adaptive experience-dependent myelin remodeling, mouse oligodendrocytes exhibit bias toward specific neuron classes (Yang, Michel, Jokhi, Nedivi, & Arlotta, 2020).

While it is molecularly enigmatic if/how glia interact with different neurons, there is evidence at least that they interact non-uniformly with different contacting cell types through molecular asymmetry of contacting membranes. An emergent theme for this across glia is that polarity markers that are associated with canonical apical domains in polarized cells (e.g. PIP2, apical $ß_H$-spectrin) localize to neuron-proximal (i.e. adneuronal) contacting membranes, and basolateral-domain polarity markers to membranes that appose basal lamina/ECM or endothelia (i.e. abneuronal) (Belin, Zuloaga, & Poitelon, 2017). This has been explicitly demonstrated for PNS Schwann cells and retinal RPE glia-like cells in mammals and ensheathing cells of the *Drosophila* CNS (Pogodalla et al., 2021). Further, while mammalian CNS astrocytes do not have explicitly apical-basal polarity, they localize basolateral domain-associated AQP4/Aquaporins to endothelia-contacting end-feet, and Ezrin, mGluR3/5, and GLT-1 to perisynaptic astrocytic processes at neuron-contact sites (Murphy-royal et al 2015). Whether this ability of glia, to create molecularly polarized membranes around different cell types, also extends to interactions with different neurons within the neuron-proximal membrane remains to be determined.

To molecularly interrogate specificity in glia-neuron interactions at single-cell resolution, we exploited a single glia cell in *C. elegans*, the amphid sheath (AMsh) glia, as a powerful and genetically tractable experimental platform (Singhvi & Shaham, 2019). This glia resides in the

animal's major sense organ at the anterior nose-tip and offers four unique advantages to probing glia-neuron interactions definitively at single-cell and -gene resolution rapidly (Oikonomou & Shaham, 2011; Singhvi & Shaham, 2019; Singhvi et al., 2023). One, each bilateral AMsh glia associates with twelve sensory neurons at their neuron receptive ending (NRE), where they receive sensory input (Perkins et al., 1986; Ward et al., 1975). Two, the identity, cell biology, and function of each NRE is invariant across animals. This allows for reproducible inquiry into each of their individually distinct properties. Three, each NRE transduces a distinct sensory modality and animal behavior, each of which can be individually quantified *in vivo*. Finally, the animal's optical transparency allows facile cell biology and functional studies in behaving animal nervous systems.

Of the twelve NREs contacting AMsh glia, 8 extend ciliated NREs through an autotypic channel formed by AMsh glia (channel NREs), three are ramified cilia (wing NREs) and one is microvillar (AFD NRE) (Figure 1A) (Perens & Shaham, 2005; Perkins et al., 1986) (Singhvi & Shaham, 2019). Of these, AFD is the animal's primary thermosensor, with the transduction machinery located at the AFD NRE (Goodman & Sengupta, 2018; Kimura, Miyawaki, Matsumoto, & Mori, 2004). We previously showed that AMsh glia regulate AFD NRE shape and functions dynamically through life through multiple regulatory modules (Raiders, Han, et al., 2021; Singhvi et al., 2016; Wallace et al., 2016). One glial regulatory cue identified was the potassium chloride cotransporter, KCC-3, whose loss causes defects in AFD NRE shape, function, and associated animal thermosensory behavior (Singhvi et al., 2016; Yoshida et al., 2016).

Here, we report that AMsh glia indeed regulate associated NREs differently, and uncover the underlying molecular mechanism. Briefly, glial KCC-3 affects shape of only AFD NRE but not

other glia-associated NREs. To enable this, glial KCC-3 localizes to a microdomain within the glia's neuron-proximal membrane specifically at AFD NRE contacts. This microdomain localization requires both cell-intrinsic and neuron cilia cues. Glia-intrinsic mechanisms and KCC-3 N-terminal sequence regulate localization to neuron-proximal glial regions. Refinement to AFD specific microdomain requires KCC-3 C-terminal regions, and cilia NREs of at least two non-AFD neurons, the olfactory AWC and gustatory ASE neuron. Finally, we find that glial KCC-3 localization to AFD NRE also impacts AWC neuron activity response properties, as well as associated animal behavior. Thus, compartmentalization of a glial cue to the thermosensory neuron AFD informs fidelity of the animal's sensory perception across modalities.

RESULTS

AMsh glia localize KCC-3/K-Cl transporter to a microdomain around only AFD neurons

We previously reported that AMsh glia uses the cation chloride cotransporter KCC-3 to regulate AFD NRE shape and animal thermosensory behavior (Singhvi et al., 2016). Intriguingly, a translational *kcc-3*:GFP reporter does not localize uniformly on AMsh glia membranes (Figure S1A). To validate this, we engineered a transgenic animal where the AMsh glia was labeled with cytosolic CFP and KCC-3 expressed under the AMsh + PHsh $P_{F53F4.13}$ promoter was tagged with mScarlet. Analyses of this strain using widefield and 3D-SIM super-resolution microscopy confirmed that KCC-3 localizes to the anterior region of AMsh glia, where the glia contacts associated NREs, including the AFD NRE (Figure 1A-C''). Further, even within the anterior region, KCC-3 does not localize uniformly but is constrained to a sub-domain (Figure 1B-B', 1D-D"). We call this subcellular KCC-3 localization a "glial molecular microdomain".

The pattern of KCC-3 enrichment was architecturally reminiscent of the shape of AFD NRE microvilli (Figure 1D). We therefore generated animal strains that co-labeled fluorescent reporter-tagged KCC-3 with reporters marking individual AMsh glia-associated neurons. Strikingly, we found that KCC-3 localizes to glial membranes proximal to AFD NRE microvilli, but not to any other glia-associated NREs (Figure 1E-G'', S1B-C''). Thus, AMsh glia differentiate between and restrict KCC-3 to a subset of individual neuron contact sites. This identifies KCC-3 localization as a facile molecular tool to probe glia-neuron interaction specificity.

In addition to the microdomain, we noted that KCC-3 localization terminates sharply in the proximal glial process ~50um away from the animal nose tip (Figure 1C, white arrowhead). For reasons explained below, we refer to this boundary as the "glial adneuronal boundary", or GAB.

KCC-3 exhibits microdomain localization across glia and is age-dependent

Examination of *kcc-3:GFP* through development showed that KCC-3 anterior localization and GAB restriction are apparent in developing 3-fold stage embryos, shortly after most glia are born (Figure S2F-G, S1A). Since KCC-3 expresses in most sheath glia (Purice et al., 2023; Tanis et al., 2009), we asked if this restricted localization pattern was reflective of all glia. To test this, we expressed KCC-3:mScarlet in two individual glia, the CEPsh (in animal head) and PHsh (in animal tail) glia, under cell-specific promoters. Both glia restricted KCC-3 localization to anterior process ends around neuron contact sites, like AMsh glia. Temporally, we also examined if this localization maintains through animal life in AMsh glia. Longitudinal examination of AMsh glial KCC-3 showed that microdomain integrity was apparent from the earliest stage examined (L2 larva, once

$P_{F53F4.13}$ turns on) onward and is compromised with animal age (Figure 2G-K). Curiously, KCC-3 maintains GAB restriction throughout (Figure 2G-J).

KCC-3 localizes to an apical-like adneuronal microdomain in AMsh glia

It has been proposed that glial membranes have apical-basal polarity like epithelia (Low et al., 2019). In epithelia, tight junctions segregate apical and basolateral domains (Shin, Fogg, & Margolis, 2006). We therefore asked if glial neuron-proximal membranes that contain KCC-3 are true apical membranes bound by tight junctions.

First, we re-engineered versions of previously reported SAX-7/L1CAM-based polarity markers in AMsh glia under $P_{F53F4.13}$ (Low et al., 2019; Martin et al., 2022). Full-length, fluorescently tagged SAX-7 (BasoRed) localized to the outer membrane of the glial cell, including its cell body and process, where AMsh glia contacts epithelia (Figure S2A). In contrast, a fragment of SAX-7 (ApiGreen) that localizes to apical epithelial domains in canonical epithelia (Low et al., 2019), exhibited two features of note. One, it localized to the anterior region of the glia, as reported. Two, like KCC-3, its expression terminated at the GAB (Figure S2B). Simultaneous co-labeling of apical and basolateral markers showed that apical membrane markers localize to neuron-proximal (adneuronal) sites, while basolateral domains face overlying epithelia (abneuronal) (Figure 2A-D) (Movie 1).

We considered the caveat that these SAX-7/L1CAM based markers may inadvertently alter glial cell biology due to overexpression of a cell adhesion molecule. As such, we generated a second marker of apical membranes in AMsh glia by expressing fluorescently tagged PH-PLCδ:GFP

(Mahon, 2011) under $P_{F53F4.13}$. We found that PH-PLCδ:GFP expression is similar to the SAX-7-based ApiGreen construct in labeling both the adneuronal membrane and terminating at the GAB (Figure S2C, white arrowhead denotes GAB). Thus, glial adneuronal membranes are molecularly analogous to epithelial apical membranes.

Because both KCC-3 and apical PH-PLCδ:GFP ends expression at the GAB, we hypothesized KCC-3 localizes to a microdomain within glial apical-like adneuronal membranes. To confirm this, we overlaid AMsh glial apical and basolateral membrane reporters individually with fluorescently labeled KCC-3. KCC-3 indeed colocalizes with the apical but not basolateral membrane marker (Figure 2C-D"). Further, the GAB of KCC-3 and AMsh apical markers overlaid perfectly (Figure 2E-E", white arrowhead). Finally, KCC-3 expression was restricted to a subset of membranes labeled with the apical marker, consistent with it being excluded from non-AFD contact sites (Figure 2E-E", yellow arrows). Thus, AMsh glial KCC-3 localizes to a microdomain within apical-like adneuronal membranes at AFD NRE contact sites. In further corroboration, mutations in *unc*-23/hBAG2, which induces expansion of apical-marker labeled glial adneuronal membranes (Martin et al., 2022), also caused expansion of KCC-3 microdomain, as expected (Figure S2E).

If AMsh glia has true apical-basal polarity, tight junctions should demarcate the boundary of the apical domain, as for epithelia apical domains (Shin, Fogg, & Margolis, 2006). To probe this, we generated transgenic animals that co-expressed fluorescently tagged KCC-3 with either of two junctional markers, AJM-1/AJM and DLG-1/DiscsLarge (McMahon, Legouis, Vonesch, & Labouesse, 2001). We found that neither junctional proteins marked the edge of KCC-3 expression

in glia (Figure 2F-F'', Figure S2D-D''). AJM-1 did label AMsh glia-NRE contacts in circular pattern, as previously reported (Low et al., 2019; Martin et al., 2022). Curiously, though, the junctional protein DLG-1 was absent at these sites (Figure S2D-D''). This discrepancy leads us to infer that while apical proteins mark adneuronal glial membranes, they may be maintained by mechanisms distinct from tight junction-based epithelial apical-basal polarity.

AMsh glia makes distinct microdomains at different neuron contact sites

AMsh glia associate with 12 NREs, 8 of which traverse a channel made by the glia. This channel contains glial DAF-6/Patched, CHE-14/SSD/Dispatched, VAP-1/CRISP2, and LIT-1/Nemo-like kinase (Oikonomou et al., 2011; Perens & Shaham, 2005). Co-labeling of VAP-1:sfGFP and KCC-3:mScarlet revealed that they localize to distinct, non-overlapping glial domains (Figure 3A-B''). Interestingly, neither of these localize to glial membranes contacting AWC NRE (Figure 3B-C''). This reveals that AMsh glia make at least three distinct molecular microdomains around different neuron contact-sites: around channel NREs (VAP-1 positive, KCC-3 negative), around AFD NRE (VAP-1 negative, KCC-3 positive), and around AWC NRE (VAP-1 negative, KCC-3 negative). Thus, making molecular microdomains is a general feature of AMsh glia.

We next wondered whether the KCC-3 and channel microdomains affect the localization of one another. To probe this, we asked if mutations in channel domain proteins alter KCC-3 localization and *vice versa.* We found that KCC-3 localization was largely intact in animals mutant for *daf-6, che-14,* and *lit-1* (Figure 3D, 3G). Further, while SNX-1/Retromer antagonizes DAF-6 to regulate channel architecture (Oikonomou, Perens, Lu, & Shaham, 2012), it is dispensable for KCC-3 localization. Consistent with this, loss of *kcc-3* only marginally impacted VAP-1 localization, and

retained normal LIT-1:GFP localization (Figure 3E-F', 3H). We therefore infer that the different microdomains on AMsh are not maintained by each other but likely compartmentalized by independent mechanisms.

Glial KCC-3 microdomain does not require canonical KCC regulators

How does KCC-3 localize properly? We asked if known regulators of cation-chloride transporter (N/KCC) family proteins are involved. WNK and GCK/Ste20 kinases SPAK/PASK and OSR, are major regulators of N/KCC transporters across species (Alessi et al., 2014; Blaesse, Airaksinen, Rivera, & Kaila, 2009; Hisamoto et al., 2008; Kaila et al., 2014; Payne, Rivera, Voipio, & Kaila, 2003). The *C. elegans* genome encodes a single WNK ortholog (WNK-1) (Hisamoto et al., 2008). Neither loss of function *wnk-1(tm487)* mutation nor *wnk-1* RNAi altered AMsh glial KCC-3 microdomain localization (Figure S3A-B). Consistent with this, *in silico* analyses revealed that *C. elegans* KCC-3 coding sequence lacks conserved WNK or GCK kinase phosphorylation sites or binding motifs (Figure S3C-E). Further, loss of ARGK-1/creatine kinase, reported to co-localize with KCC-3 in cell culture models (Burgess, Shah, Hough, & Hynynen, 2016; Adèle Salin-Cantegrel et al., 2011), also did not disrupt KCC-3 localization (Fig. S3A). Thus, microdomain localization of KCC-3 in AMsh glia is independent of previously identified CCC regulators.

Different protein regions regulate KCC-3 targeting to distinct membrane regions

We next decided to *ab initio* define protein domains in KCC-3 that guide localization to a microdomain. For this, we exploited the interspersed sequence similarity of KCC-3 coding regions with that of the related KCC-1 and KCC-2 (Figure 4A). *In silico* analysis showed that dissimilarity between KCC-1/KCC-2 and KCC-3 coding sequences was restricted to N-terminal intracellular

domain (1-90 AA), the large extracellular loop (LEL) between TM5 and TM6 (265-397 AA), and an 81 amino acid (AA) region of the C-terminal (915-996 AA) (Figure 4B). We fluorescently tagged *C. elegans* K/Cl homologs KCC-1 and KCC-2 and found that they localize to basolateral abneuronal membranes in AMsh glia (Figure 4C-F). Thus, sequences dissimilar between KCC-1/KCC-2 and KCC-3 drive both adneuronal and microdomain localization of KCC-3. We then generated KCC-2/3 chimeras at the dissimilar sequences and asked how these localize within AMsh glia.

First, we swapped the N-terminal 90 AA sequence of KCC-3 with the 84 AA equivalent aligned sequence of KCC-2 (Figure S4E, Chimera A). This was sufficient to localize the chimera to basolateral membranes (Figure 4I, 4K). Narrowing this further, swapping the first 55 AA sequence of KCC-3 with 41 AA equivalent aligned sequence of KCC-2 also drove the chimera to basolateral membranes (Figure 4K, Figure S4E, Chimera B). Swapping the first 20 AA sequence of KCC-3 with the 20 AA equivalent aligned sequence of KCC-2 (Figure S4C, Chimera D), however, localized the chimera to the apical-like adneuronal microdomain, as wildtype KCC-3 (Figure 4G, S4D). To test necessity, we also swapped the first 41 AA of KCC-2 with the 55 AA equivalent aligned sequence of KCC-3 (Figure S4E, Chimera C), and found it no longer restricts KCC-2 to basolateral membranes (Figure S4B). Further attempts to identify sequence motifs within 20-41 AA by either site-directed mutagenesis of predicted phosphorylation or dileucine sites, or deletions (Figure S4C-D) were not successful, hinting at redundant targeting motifs. Nonetheless, these results show that the 19 AA N-terminal sequence (AA 20-41) of KCC-2 is necessary and sufficient to localize KCC-2 to abneuronal/basolateral membranes.

Similarly, other chimeras led us to also identify an 87 AA microdomain-targeting sequence. A chimera that swapped the last 155 AA (915-1070 AA) of KCC-3 with the equivalent 171 AA (890-1061 AA) of KCC-2 (Figure S4G, Chimera G) localized apically, but not to a microdomain (Figure 5H, 5K). However, swapping the last 68 AA (1002-1070) AA of KCC-3 with the equivalent 66 AA (995-1061 AA) of KCC-2 (Figure S4G, Chimera H), localized the chimera to a microdomain (Figure 4K). Thus, the 87 AA C-terminal sequence (915-1002 AA) of KCC-3, highly dissimilar with KCC-1/2 (Figure S4G), directs KCC-3 to a microdomain.

Two observations suggest that KCC-3 further has adneuronal/apical-targeting motifs distinct from the two motifs identified above. One, Chimera C lacks a GAB unlike KCC-3, an expression pattern that we call "other" (neither apical-like nor basolateral; Figure 4K, S4A). Two, a swap of 671 AA (399-1070 AA) of KCC-3 with the equivalent 681 AA (380-1061) of KCC-2, also exhibits the "other" expression pattern (Figure 4K, Chimera F). We found above that KCC-3 sequences until 915 AA localize to adneuronal/apical membranes (Chimera G). Thus, regions between 390-915AA on KCC-3 drive adneuronal/apical localization. Consistent with this, double-swap of both N-and C- terminal domains of KCC-3 alone to KCC-2 (without the 390-915 AA KCC-3 region) also only exhibits "other" localization (Figure 4K, Chimera I). Thus, sequences in 390-915 AA likely contain adneuronal/apical targeting motifs that are needed for further microdomain enrichment.

Lastly, K/Cl proteins exist as oligomers through a C-terminal dimerization domain (C. F. Simard et al., 2007). We therefore considered if adneuronal or microdomain localization of C-terminal Chimeras F and G respectively was, in fact, driven by endogenous wild-type KCC-3-dependent trafficking. To test this caveat, we examined localization of these chimeras in *kcc-3(ok228)* null

mutant animals and found that they behaved similarly (Figure 4J). If at all, endogenous protein out-competes (not enables) chimera localization. Thus, dimerization does not account for KCC-3's ad-neuronal/apical and microdomain localization.

There were a few constructs that failed to show any expression in AMsh glia. Human and mouse KCC-3 did not show expression in *C. elegans*, when expressed in either WT or *kcc-3* mutant backgrounds. A chimera with the first 33AA of KCC-3 as KCC-2 also did not show expression. Finally, a chimera with the large extracellular loop of KCC-3 as KCC-2 also did not show expression. This was true over multiple extrachromosomal arrays. These are curious as overall structure of the KCC protein was intact.

All together, these structure-function studies reveal that KCC-3 localization requires three sequence features (a) lack of N-terminal basolateral targeting sequences, (b) presence of apical-targeting sequences (390-915 AA), and (c) presence of microdomain-targeting sequences at the proximal C-terminal (910-1002 AA). Further, this localization occurs in a two-step process, with apical targeting a prerequisite to microdomain enrichment.

Glial KCC-3 localization is independent of AFD neuron shape or function

The structure-function studies above revealed a two-step mode of KCC-3 localization; however, the identified sequences did not reveal any conserved motifs. So, we undertook an orthogonal strategy and asked if microdomain localization is entirely cell-autonomous or requires neuron function. This was partly guided by two observations: one, that *daf-6* mutants partially affect KCC-

3 microdomain localization, and two, DAF-6 localization at channel microdomain requires neuron cilia (Perens & Shaham, 2005).

We first asked if AFD NRE shape is required recruit glial KCC-3 to contacting membranes. The AFD NRE is a composite of ~40-50 microvilli and one pseudocilium (Figure 5A) (Goodman & Sengupta, 2018; Raiders, Black, et al., 2021). We found that KCC-3 localization was unaltered in *ttx-1* mutants, which lack AFD NRE microvilli, suggesting that microvilli are not required (Figure 5B) (Satterlee et al., 2001). We then examined KCC-3 localization in animals mutant for the ciliary protein DYF-11/IFTB/TRAF3IP1, whose loss leads to truncated cilia (Perkins et al., 1986; Swoboda, Adler, & Thomas, 2000). Strikingly, in *dyf-11* mutants, while glial KCC-3 maintained the GAB demarcation, it was no longer constrained to an apical microdomain but instead spread to the entirety of the AMsh glial anterior region (Fig. 5B, 5C-C"). This pattern was strikingly reminiscent to apical region enriched Chimera G. Thus, neuron cilia restrict KCC-3 to a microdomain.

AFD NRE cilia house sensory transduction channels at their base (Goodman & Sengupta, 2018). As such, we tested if *dyf-11*mutant effects were due to altered AFD NRE activity. For this, we examined KCC-3 localization in animals mutant for the sole CNG channel β-subunit required for AFD activity, TAX-2 (Coburn & Bargmann, 1996) or animals with a gain-of-function *gcy-8(ns335)* mutation, which have constitutively activated levels of the sensory transduction second-messenger, cGMP (Singhvi et al., 2016). Surprisingly, neither had any impact on KCC-3 localization (Figure 5B). Furthermore, cultivation temperature (AFD's sensory input) also did not

impact KCC-3 localization (Figure S5A). Thus, neuron cilia structure, but not activity, drives KCC-3 microdomain localization.

Because DYF-11 is expressed in all ciliated neurons, we asked if DYF-11 function in AFD NRE itself is necessary for KCC-3 microdomain localization (Kunitomo & Iino, 2008). To do so, we ablated the AFD neuron in two temporally distinct ways (Figure 5D). First, we genetically ablated AFD by expressing the pro-apoptotic factor EGL-1 under an AFD specific-promoter (P_{srtx-1}) (Nehme & Conradt, 2009; Singhvi et al., 2016) . P_{srtx-1} promoter is expressed shortly after the birth of AFD in the 3-fold stage embryo, indicating that it is competent to induce embryonic cell-loss (Figure S5B-B''). Independently, we performed targeted laser microdissection to ablate AFD neurons in L1 larvae (Sulston, 1983). In either ablation method, successful AFD ablation was confirmed by disappearance of P_{srtx-1}:GFP (Figure S5D). Surprisingly, glial KCC-3 maintained localization to an apical microdomain in both scenarios (Figure 5E, S5C). Consistent with this, a rescuing DYF-11 cDNA expressed only in AFD neurons was unable to rescue KCC-3 localization defects of *dyf-11* mutants (Figure 5H-I). Thus, while neuron cilia guide KCC-3 to a microdomain around AFD NRE, the AFD itself is dispensable for this compartmentalization.

Ciliary transport drives glial KCC-3 microdomain localization

The findings above led us to wonder if the KCC-3 localization defects were DYF-11-specific, or due to a general loss of cilia. We performed a candidate screen of other regulators of cilia biogenesis and transport machinery (Dwyer, Adler, Crump, L'Etoile, & Bargmann, 2001; Lechtreck, 2015) (Figure S5E). Briefly, mutations in the cilia biogenesis regulator DAF-19/RFX transcription factor, OSM-3/Kinesin II, CHE-11/IFT-A component, DYF-11/IFT-B component,

OSM-6/IFT-B component, BBS-8/BBsome or UNC-101/AP1, all led to aberrant expansion of glial KCC-3 beyond its microdomain, while keeping the GAB intact (Figure 5F). We note that except for UNC-101/AP1, enrichment around AFD NRE persisted in all other mutants (Figure S5F).

Finally, we considered the confound that global cilia NRE loss may indirectly affect AMsh glia shape, leading to apparent KCC-3 mislocalization. However, AMsh morphology in *daf-19* and *dyf-11* mutant animals appeared grossly normal, although the AMsh glia anterior regions appeared marginally smaller in *daf-19* mutants (Figure S5G-I). This is consistent with prior EM studies on these mutants (Bacaj, Lu, & Shaham, 2008; Perkins et al., 1986). Taken together then, we conclude that KCC-3 localization to AFD NRE requires shape and IFT transport of non-AFD cilia.

Cilia of two neurons minimally drive glial KCC-3 microdomain localization

Next, we asked where ciliary IFT transport is required. All non-AFD NREs contacted by AMsh glia are cilia-based (Figure 5A), and anatomically segregate into two classes, wing and channel NREs (Figure 1B). To parse DYF-11 site of action, we performed both candidate screening and cell-specific rescue studies. First, we examined KCC-3 localization in mutants for the OIG-8/Ig domain protein, which regulates elaboration of wing NRE cilia (Howell & Hobert, 2017), and CHE-12/HEAT domain protein, known to affect only channel neurons (Bacaj, Lu, et al., 2008). *oig-8* mutants exhibit KCC-3 localization defects similar to cilia mutants, although with significantly less penetrance, while *che-12* mutants had no effect on KCC-3 localization (Figure 5F). This suggests that KCC-3 localization is driven primarily by wing neurons.

We then asked if fate specification of wing neuron subtypes is relevant. For this, we examined KCC-3 localization in animals bearing mutations in wing or channel neuron identity determinants: ODR-7/NHR (AWA), CEH-37/Otx homeodomain (AWB), CEH-36/Otx (AWC), and CHE-1/GLASS Zn finger (ASE) (Lanjuin, VanHoven, Bargmann, Thompson, & Sengupta, 2003; Piali Sengupta, Colbert, & Bargmann, 1994; Uchida, Nakano, Koga, & Ohshima, 2003). These genes act with DAF-19/RFX to specify the different NRE cilia shape for each neuron (Figure S5J) (Lanjuin & Sengupta 2004). To note, in these mutants, specific NRE cilia are altered or misspecified, but are not missing. Curiously, none of these mutants perturbed KCC-3 localization (Figure 5G), suggesting that specific ciliary identity of at least these four neurons does not guide KCC-3 to a microdomain. We then ablated each of the three wing neurons (AWA/B/C) individually and found that this did not alter KCC-3 localization either (Figure 5G). Thus, identity or presence of a single wing neuron does not regulate KCC-3 localization.

We therefore hypothesized that multiple neuron cilia redundantly localizes KCC-3. To define the minimal set, we undertook cell-specific rescue experiments in *dyf-11* mutant animals, which show a complete loss of KCC-3 microdomain localization. We reintroduced DYF-11 under promoters that express in different combinations of neurons and asked which rescued KCC-3 microdomain localization. (Fig. 5H-I). DYF-11 expressed under its native $P_{dyf\text{-}11}$, $P_{gpa\text{-}3}$, or $P_{tax\text{-}4}$ promoters, which express in all, 9, and 10 amphid neurons respectively, rescues KCC-3 localization (Figure 5H-I). Thus, DYF-11 rescuing cDNA is functional when expressed broadly. We next tested smaller non-overlapping subsets of amphid neurons. $P_{R102.2}$ (all channel neurons and AFD only) and $P_{flp\text{-}19} + P_{odr\text{-}1}$ (all wing neurons only) both exhibited equivalent rescue, suggesting that the localization cue(s) is broadly expressed. Finally, expression under either combination of two

neurons by P_{odr-1} (AWC and AWB), or P_{ceh-36} (AWC+ASE) was able to rescue. This was specific since expression in two other neurons by P_{odr-4} (2 channel neurons) did not rescue (Figure 5H-I). Taken together, we conclude that AWC+X is the minimal 2-neuron combination to guide KCC-3 localization.

Similar to the chimera experiments, there were a few DYF-11 constructs that showed minimal or odd expression patterns. $P_{R13H4.1}$ and P_{che-1} showed only minimal punctate DYF-11 expression. In addition, P_{DCS-1} altered AWC morphology. As such, these constructs were left out of the analysis.

AFD NRE shape requires AMsh glial KCC-3 microdomain enrichment around itself

Why do AMsh glia localize KCC-3 to a microdomain around AFD NRE, and why does AWC+X regulate this? First, we asked if KCC-3 localization impacts AFD NRE shape, by assessing if mislocalized chimeras can rescue AFD NRE shape of *kcc-3* mutants (Figure 6A-A') (Singhvi et al., 2016). While expression of full-length KCC-3 in a *kcc-3* background rescues AFD shape, the basolaterally localized Chimera B fails to rescue AFD shape (Fig. 6B). In contrast, the apical-localized Chimera G which retains some microdomain enrichment, could rescue *kcc-3(ok228)* mutant AFD NRE defects (Figure 6B), albeit less efficiently. In corollary, a mutation in *unc-101,* that completely loses AFD NRE microdomain enrichment, has defects in AFD NRE shape similar to *kcc-3(ok228)* mutant animals (Figure S6E). Taken together, we conclude that KCC-3 enrichment around AFD NRE is required for its shape regulation, but AFD is not impacted if KCC-3 additionally expands to other adneuronal membrane regions. Consistent with this, mutations in *dyf-11* and *osm-6* mutant animals, where AMsh glial KCC-3 enriches around AFD NRE while also

expanding aberrantly to other NREs (Figure 3E), do not exhibit defects in AFD NRE shape (Singhvi et al 2016).

AWC neuron activity requires AMsh glial KCC-3 microdomain around AFD NRE

We next asked if KCC-3 mislocalization to other NREs causes deleterious consequence to their shape or function (Figure 1E-G'', S1B-C''). We found that loss of *kcc-3* does not impact shape of any NRE tested (wing: AWA/B/C, channel: ASE) (Figure 6C-C', 6D, S6A-D'). Further, overexpressing Chimera G, which expresses in adneuronal/apical membranes outside the KCC-3 microdomain, also does not affect AWA NRE shape (Figure 6C", 6D).

In contrast, we found that KCC-3 regulates sensory behaviors mediated by non-AFD neurons. While ASE-dependent salt chemotaxis was unaffected, we found that *kcc-3* mutant animals show impaired AWA and AWC neuron-driven animal behaviors (Figure S7C). Specifically, *kcc-3* mutant animals fail to chemotax towards attractive odorants sensed by AWA (methyl pyrazine and diacetyl) and AWC (isoamyl alcohol and benzaldehyde) (Figure 5E, S7A-B). These deficits were comparable to the strong behavior impairments seen in either AMsh glia-ablated or *dyf-11* cilia-deficient animals (Figure S7D-E) (Bacaj, Lu, et al., 2008; Bacaj et al., 2009).

These defects are likely not secondary to impaired downstream interneurons shared with AFD, because *ttx-1* mutants, with defective AFD NRE shape and function, does not cause defects in AWA- or AWC behaviors. They are also not due to KCC-3 in interneuron-associated CEPsh glia, because expression of KCC-3 in AMsh glia rescued chemotaxis defects of *kcc-3* mutants animals completely for AWC. It also partially but significantly rescued AWA-driven behaviors. Thus,

KCC-3 in AMsh glia, which is around AFD, also modulates AWC and AWA functions.

To confirm this striking cross-modal deficit, we also directly assessed AWC neuron functions by monitoring intracellular Ca^{2+} dynamics via functional GCaMP imaging of AWC neurons in wildtype and *kcc-3* mutant animals (Chalasani et al., 2007). We found that AWC neurons had significantly dampened responses to both isoamyl alcohol presentation as well as withdrawal in *kcc-3* mutant animals compared to wildtype animals (Figure 6G-I). Furthermore, in animals expressing apical Chimera F in *kcc-3(ok228)* mutant background (KCC-3 is aberrantly in glial regions around AWC), we found that AWC now exhibits strikingly variable Ca^{2+} responses to isoamyl alcohol (Figure 6G-I, S6E-G). Finally, consistent with this, Chimera F was unable to rescue AWC-driven behavior deficits of *kcc-3(ok228)* mutant animals (Figure 6F), even though it could rescue AFD NRE shape defects (Figure 6B). Thus, proper localization of AMsh glial KCC-3 to a microdomain around AFD NRE regulates shape of AFD NRE as well as function of AWC NRE, with consequences on both thermosensory and chemosensory animal behaviors (Figure 7).

DISCUSSION

In this study, we show that a single glia can differently regulate associated neurons, uncover the underlying cell biological mechanism, and identify consequence of misregulating this specificity. Briefly, using the localization of glial KCC-3 around a single neuron contact site (AFD NREs) as a powerful and tractable molecular tool, we first uncover that AMsh glia have polarized membranes decorated by apical-basal polarity markers and demarcated by a sharp transition boundary (GAB), but with features that distinguish this from classical epithelial polarity.

Furthermore, within the apical-like adneuronal membrane, AMsh glia partitions multiple and distinct molecular microdomains around individual NRE-contact sites. Focusing on one microdomain cue, the K/Cl transporter KCC-3, our studies reveal a two-step model for KCC-3 localization. First, it localizes apically, and is then repelled by non-AFD NRE cilia, rendering it localized to AFD NRE (Figure 7). This mechanism is distinct from previously reported regulation of the disease-relevant K/Cl family transporters. Finally, and surprisingly, microdomain localization of KCC-3 to AFD NRE not only regulates AFD sensory perception, but also function of non-AFD neurons. That microdomain localization of one glial cue around one NRE influences cross-neuron sensory processing leads us to posit that such sub-cellular organization may be a mechanism by which glia modulate information across contacting circuits.

Glial cell polarity

Our findings extend prior studies to show that AMsh exhibit apical-basal polarity (Low et al., 2019). Specifically, while adneuronal membranes localize apical markers and ab-neuronal membranes localize basolateral markers, two features distinguish glial cell polarity from epithelial polarity. One, the apical-like domain is not bound by the tight-junction proteins AJM-1 and DLG-1. In fact, it is curious that AMsh glia localize AJM-1 to non-GAB domains without DLG-1, which in epithelia is known to recruit AJM-1 to junctions (Köppen et al., 2001; Segbert, Johnson, Theres, Van Fürden, & Bossinger, 2004). Two, this domain is instead demarcated by the GAB boundary, which overlays perfectly for all apically restricted molecules (PH-PLCδ, KCC-3, SAX-7). We propose, therefore, that instead of epithelia, this glia cell biology is rather conceptually analogous to that of neurons (Leterrier, 2018). Thus, the GAB may be a sorting center like the neuronal Axon Initial Segment (AIS) that delimits diffusion of membrane proteins across different polarized cell

domains (axons and dendrites). It will be interesting to dissect in future studies how the GAB develops or maintains.

Neuron cilia regulation of glial cues

Most mammalian cells have a primary, non-motile cilia. In neurons and glia, their presence and functions are only recently being appreciated (Green & Mykytyn, 2014; Ki, Jeong, & Lee, 2021; Piali Sengupta, 2017). We find here that non-AFD NRE cilia localize a glial membrane cue to a microdomain, through a signal transported by IFTA/B complex. While the molecular identity of this cue remains to be identified, we suggest that this may be independent of at least extra-cellular vesicle release (Razzauti & Laurent, 2021). This is because loss of *daf-19* impacts KCC-3 localization but not extracellular vesicle release. To our knowledge, a role for neuron cilia in guiding glial properties, and thereby distal neuron functions, has not yet been reported.

Glial regulation of K/Cl transporters

KCC-3 is a SLC12A6/K-Cl electroneutral cotransporter implicated in neurological diseases including autism, epilepsy, and schizophrenia (Boettger et al., 2003; Delpire & Kahle, 2017; Alexandre P Garneau et al., 2017; Shekarabi et al., 2012). In *C. elegans* KCC-3 acts in AMsh glia to regulate AFD thermosensory neuron shape and function (Singhvi et al., 2016). We find that it does so specifically by restricted localization to AFD's contact site on AMsh glia.

Not only do multiple *C. elegans* glia restrict KCC-3 localization, we also note that glia across species localize KCC-3 to molecular microdomains. Thus, in rodents, Schwann cell peripheral glia localize KCC-3 to apical microvilli around nodes (Y. T. Sun et al., 2010). In mammals, inner

ear Deiter cells (glia-like support cells) localize KCC-3 to basal poles of hair cells (Boettger et al., 2003; Ray & Singhvi, 2021). This is likely a specific regulation of KCC-3 in glia, as we find that KCC-2 does not exhibit this localization when mis-expressed in glia (Figure 3A-D). This exquisitely specific localization is also independent of the canonical K/Cl regulators, which were identified primarily in KCC-2 studies, and depends on motifs that have not been previously characterized. Thus, glial regulation of KCC-3 is mechanistically distinct from how other cell-types including neurons regulate KCC-1/2, highlighting the relevance of cell-specific context molecular studies. Defining how glia regulate KCC-3, then, will be broadly relevant to understanding neural functions and KCC-3 associated neurological diseases.

Glial microdomains and cross-modal information processing

AMsh glia maintain at least three distinct molecular microdomains of regulatory cues on their adneuronal membrane, at contact sites of different NRE. Strikingly, for KCC-3, its microdomain localization at one NRE can also impact distal NRE function. This sets up a powerful cellular and molecular platform for future inquiry on how glia generate microdomains, how these microdomains interact, and how they influence neurons they do not even physically appose. Nonetheless, this finding raises the tantalizing notion that glia may be well-positioned to mediate cross-circuit information integration and processing.

Independent studies have suggested that glia can directly tune synapses and animal-behavior through neurotransmitter release (X. Zhang et al., 2021) and exhibit functional Ca^{2+} microdomain responses to sensory cues and neuron activity (Agarwal et al., 2017; Khakh & Sofroniew, 2015). While the correlation between functional and molecular microdomain is

unclear, these and our studies lead us to the speculative notion that glia may actively participate in integrating information processing across neural circuits more than was previously appreciated.

ACKNOWLEDGEMENTS

We thank the Singhvi lab and Jihong Bai for discussions and comments on the manuscript; lab members Cecilia Martin, James Bent, Alex Neitz, and Olivia Okamoto for gift of reagents. We thank Shai Shaham, Max Heiman and Jihong Bai for sharing reagents, and Bai lab for generous support on the calcium imaging studies. SR was funded by a T32 training grant (5T32NS099578-03). This work was funded by Simons Foundation/SFARI grant (488574), Esther A. & Joseph Klingenstein Fund and the Simons Foundation Award in Neuroscience (488574) and NIH/NINDS funding (NS114222) to AS. This work was performed while AS was a Glenn Foundation for Medical Research and AFAR Junior Faculty Grant Awardee. This work is also supported by a Brain Research Foundation Grant to AS. AS sincerely thanks philanthropic supporters to her laboratory including Stephanus and Van Sloun Foundations. Some work was performed at the Fred Hutch Shared Resources Core Facilities. We sincerely apologize if we missed citing works due to our oversight or space considerations.

AUTHOR CONTRIBUTIONS

SR and AS designed all studies, analyzed data and co-wrote the manuscript. SR performed all experiments and was assisted by RSM and AK in construction of some strains and plasmids. PG performed the functional Ca2+ imaging and analyzed the data with SR and AS.

Figure 1

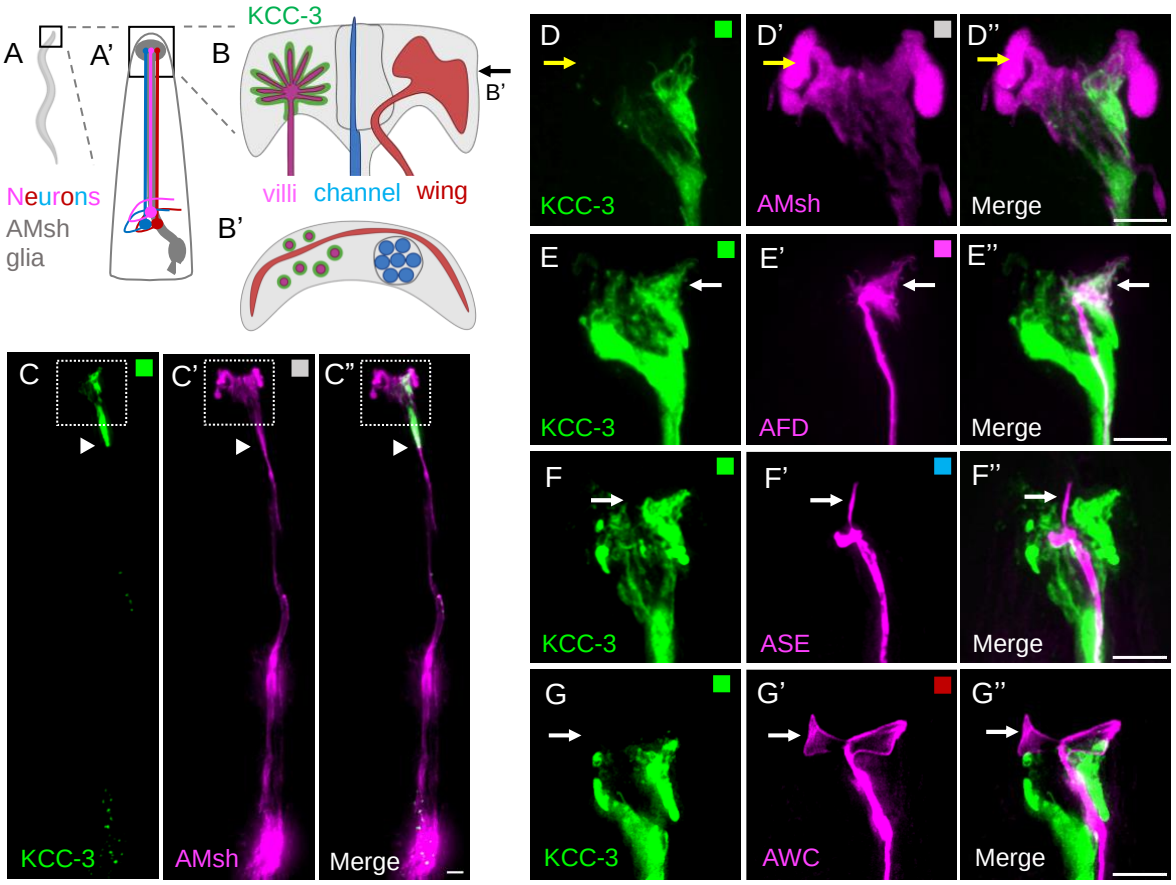

Figure 1. KCC-3 localizes specifically around AFD NRE

(A-A') Schematic of a whole *C. elegans* (left) with boxed region zoomed in showing schematic of AMsh glia (grey) and three contacting neurons (magenta, red, blue). (**B-B'**) Schematic of AMsh glial contact sites with villi/AFD (magenta), channel (blue), and embedded wing (red) neurons as side profile (B) and top-down orthogonal view (B') at the plane denoted by the arrow line in B. Only one of the bilateral glia-neuron pair is shown. **(C-C")** Fluorescent images of KCC-3 labeled with a fused mScarlet tag (C; pseudo-colored green), the whole AMsh glia labeled with cytosolic CFP (C', pseudo-colored magenta), and merge (C"). White arrowhead denotes glial apical boundary (GAB) discussed in Figure 2 (8/8 animals). D-G" zoom in on the white dotted box. (**D-D"**) Fluorescent images of KCC-3 (D, pseudo-colored green), AMsh glia (D', pseudo-colored

magenta), and merge (D") showing restricted microdomain localization of KCC-3 in the glia (38/38 animals). Yellow arrow denotes region of AMsh glia that lacks KCC-3. (**E-E''**) Fluorescent images of KCC-3 (E, pseudo-colored green), AFD neuron (E', pseudo-colored magenta), and merge (E") showing KCC-3 localization to AFD NREs (white arrow; 30/30 animals). (**F-F"**) Fluorescent images of KCC-3 (F, pseudo-colored green), ASE neuron (F', pseudo-colored magenta), and merge (F") showing that KCC-3 does not localize to ASE NREs (white arrow; 15/15 animals). (**G-G"**) Fluorescent images of KCC-3 (F, pseudo-colored green), AWC neuron (F', pseudo-colored magenta), and merge (F") showing that KCC-3 does not localize to AWC NREs (white arrow; 20/20 animals). Colored boxes in in E-G' correspond to neuron colors in B. Scale bar 5µm throughout.

Figure 2

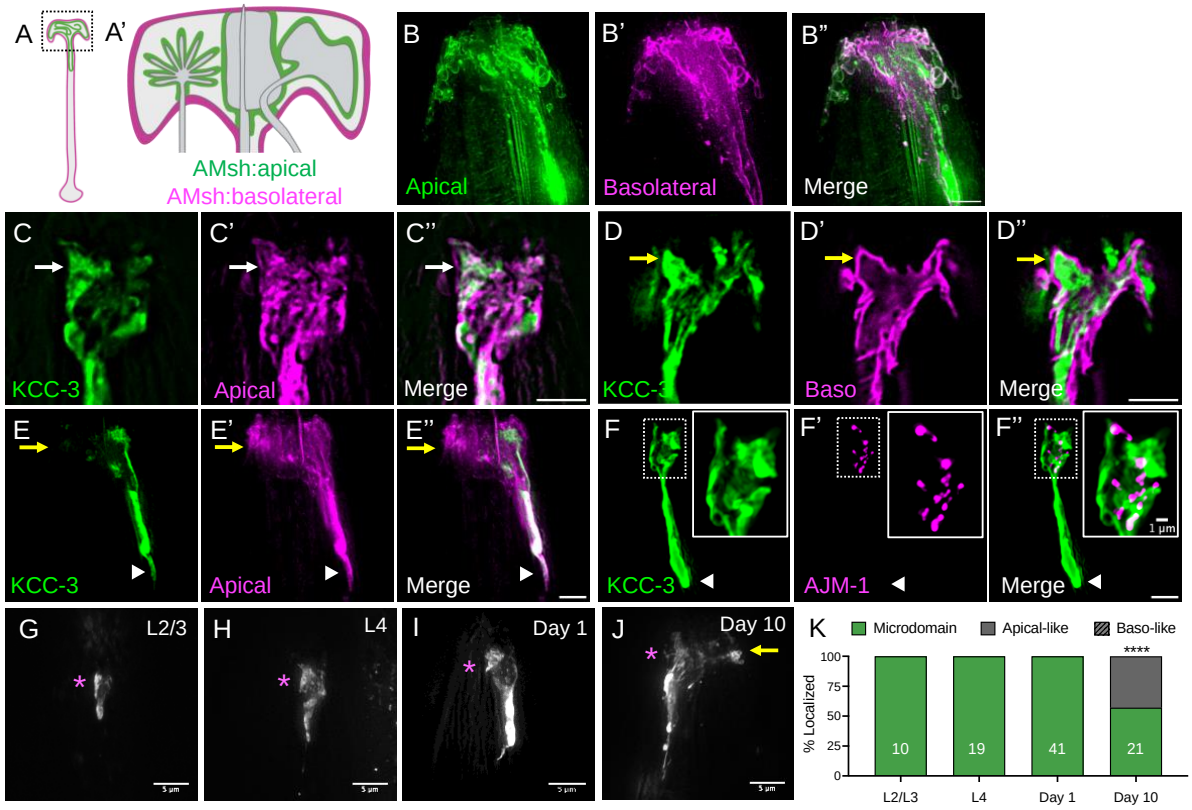

Figure 2: KCC-3 localizes to a glial apical microdomain in age-dependent manner.

(**A-A'**) Schematic of AMsh glia with apical and basolateral membranes marked. The entire glia is labeled in A, while A' shows a zoomed in schema of the black dotted box in A. (**B-B"**) Fluorescence images of truncated SAX-7 labeling AMsh apical membranes (B, pseudo-colored green), full-length SAX-7 labeling AMsh basolateral membranes (B', pseudo-colored magenta), and merge (B"). 10/10 animals show basolateral membranes on the outer glial membranes, and apical membranes contained within. (**C-C"**) Fluorescence images of AMsh KCC-3 (C, pseudo-colored green), truncated SAX-7 labeling AMsh apical membranes (C', pseudo-colored magenta), and merge (C"). White arrow denotes overlay between KCC-3 and the AMsh apical marker (5/5 animals). **(D-D")** Fluorescence images of P_{KCC-3}:KCC-3 (D, pseudo-colored green), full-length SAX-7 labeling AMsh basolateral membranes (D', pseudo-colored magenta), and

merge (D"). KCC-3 present outside of AMsh basolateral membranes are derived from other glia. Yellow arrow denotes lack of colocalization between KCC-3 and AMsh basolateral membranes (4/4 animals). **(E-E")** Fluorescence images of AMsh KCC-3 (E, pseudo-colored green), truncated SAX-7 labeling AMsh apical membranes (E', pseudo-colored magenta), and merge (E"). White arrowhead denotes colocalization of KCC-3 and the AMsh apical marker at the glial apical boundary (GAB; 3/3 animals). (**F-F'**). Fluorescence images of AMsh KCC-3 (F, pseudo-colored green), tagged tight junction protein AJM-1 (F', pseudo-colored magenta), and merge (F"). White arrowhead denotes GAB. Note the lack of AJM-1 protein at the GAB (7/7 animals). Inset is zoom in of white dotted box. (**G-J**). Fluorescence images of AMsh KCC-3, expressed under P_{AMsh}-specific promoter across age, from L2/L3 larvae to Day 10 adults. White arrowhead denotes GAB. Magenta asterisk denotes region of AFD enrichment. Yellow arrow denotes expansion of KCC-3 beyond microdomain. (**K**) Quantification of KCC-3 localization with age. N= number of animals on graph. **** $p < 0.0001$, compared to Day 1 adults (Fisher's exact test). Scale bar 5µm throughout unless otherwise noted.

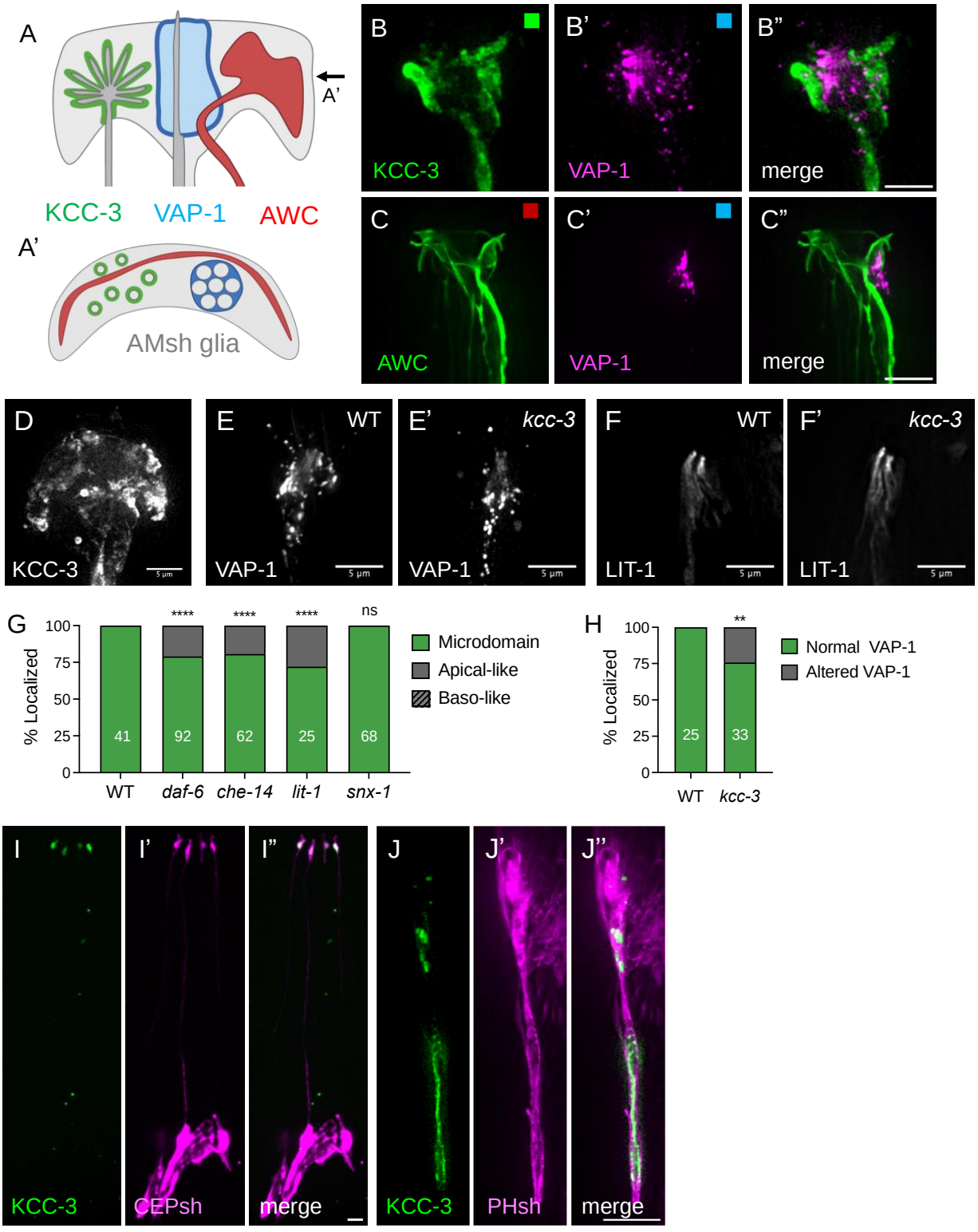
A
A'
KCC-3
VAP-1
AWC
A'
AMsh glia
B
KCC-3
B'
VAP-1
B"
merge
C
AWC
C'
VAP-1
C"
merge
D
KCC-3
E
WT
VAP-1
E'
kcc-3
VAP-1
F
WT
LIT-1
F'
kcc-3
LIT-1
5 µm
G
% Localized
100
75
50
25
0
41
92
62
25
68
****
****
****
ns
WT
daf-6
che-14
lit-1
snx-1
Microdomain
Apical-like
Baso-like
H
% Localized
100
75
50
25
0
25
33
**
WT
kcc-3
Normal VAP-1
Altered VAP-1
I
KCC-3
I'
CEPsh
I"
merge
J
KCC-3
J'
PHsh
J"
merge

Figure 3: Microdomains as a general feature of glia

(A-A') Schematic of multiple microdomains in AMsh glia, with KCC-3 in green, channel microdomain component VAP-1 in blue, and wing neuron AWC as side profile (A) and top-down orthogonal view (A') at the plane denoted by the arrow line in A. **(B-B'')** Fluorescence images of KCC-3 (B, pseudo-colored green), VAP-1 (B', pseudo-colored magenta), and merge (B"). **(C-C'')** Fluorescence images of AWC (C, pseudo-colored green), VAP-1 (C', pseudo-colored magenta), and merge (C"). **(D)** Fluorescent image of KCC-3 in *lit-1* mutants. **(E-E')** Fluorescent images of VAP-1 in wildtype (E) and *kcc-3* mutant (E') backgrounds. **(F-F')** Fluorescent images of LIT-1-1 in wildtype (F) and *kcc-3* mutant (F') backgrounds. **(G)** Quantification of KCC-3 localization in *daf-6, che-14, lit-1,* and *snx-1* mutants. **(H)** Quantification of VAP-1 localization in WT and *kcc-3* mutant. **(I-I'')** Fluorescent images of KCC-3 expressed under the CEPsh-specific HLH-17 promoter (I, pseudo-colored green), CEPsh glia (I', pseudo-colored magenta), and overlay (I"). **(J-J")** Fluorescent images of KCC-3 expressed under the AMsh/PHsh-specific F53F14.13 promoter (J, pseudo-colored green), PHsh glia (J', pseudo-colored magenta), and overlay (J"). ** $p<0.01$, **** $p < 0.0001$. Fisher's exact test. All scale bars at 5µm.

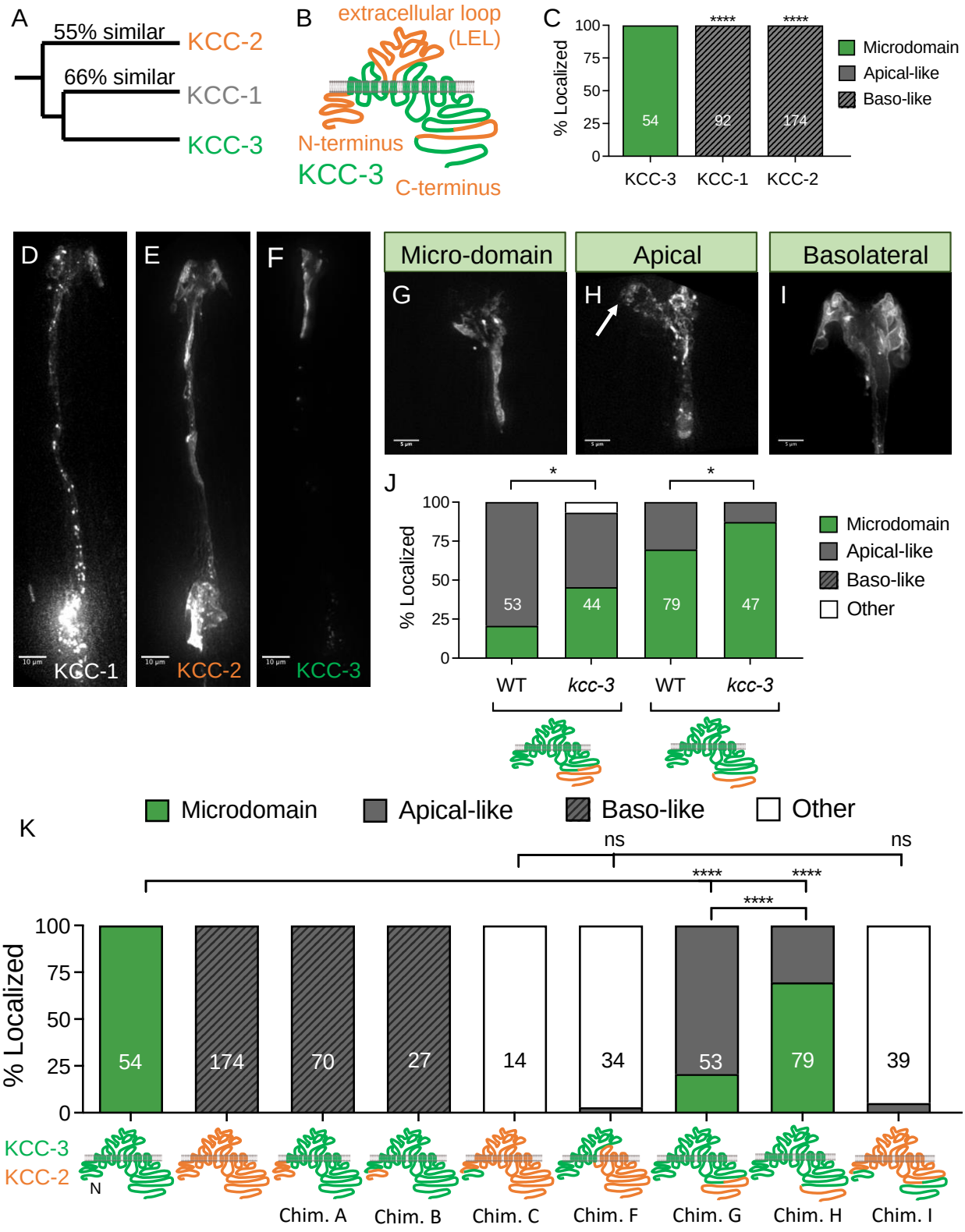
A
55% similar
KCC-2
66% similar
KCC-1
KCC-3
B
extracellular loop (LEL)
N-terminus
KCC-3
C-terminus
C
% Localized
100
75
50
25
0
****
****
54
92
174
KCC-3
KCC-1
KCC-2
Microdomain
Apical-like
Baso-like
D
E
F
KCC-1
KCC-2
KCC-3
Micro-domain
Apical
Basolateral
G
H
I
J
% Localized
*
*
53
44
79
47
WT
kcc-3
WT
kcc-3
Microdomain
Apical-like
Baso-like
Other
K
Microdomain
Apical-like
Baso-like
Other
ns
ns
****
****
****
% Localized
54
174
70
27
14
34
53
79
39
KCC-3
KCC-2
N
Chim. A
Chim. B
Chim. C
Chim. F
Chim. G
Chim. H
Chim. I

Figure 4: Glial KCC-3 localizes in a two-step process through two protein regions

(A) Phylogenetic tree denoting the relationship and sequence similarity of the three *C. elegans* KCC proteins. **(B)** Regions of high sequence dissimilarity between KCC-3 and KCC-1/2 from *in silico* sequence alignment studies, with orange denoting regions of high sequence dissimilarity. **(C)** Quantification of KCC-1 and KCC-2 localization when expressed in AMsh glia, compared to KCC-3. **(D-F)** Fluorescent images of KCC-1 (C), KCC-2 (D), and KCC-3 (E). Scale bar, 10 µm. **(G-I)** Fluorescent images of KCC localization patterns seen in KCC chimeras. White arrow points to apical expression beyond microdomain. Scale bar, 5 µm. **(J)** Quantification of localization patterns seen in KCC chimeras in WT and *kcc-3* mutant backgrounds. (**K)** Quantification of localization patterns seen in KCC chimeras. * $p < 0.05$, **** $p < 0.0001$, Fisher's exact test.

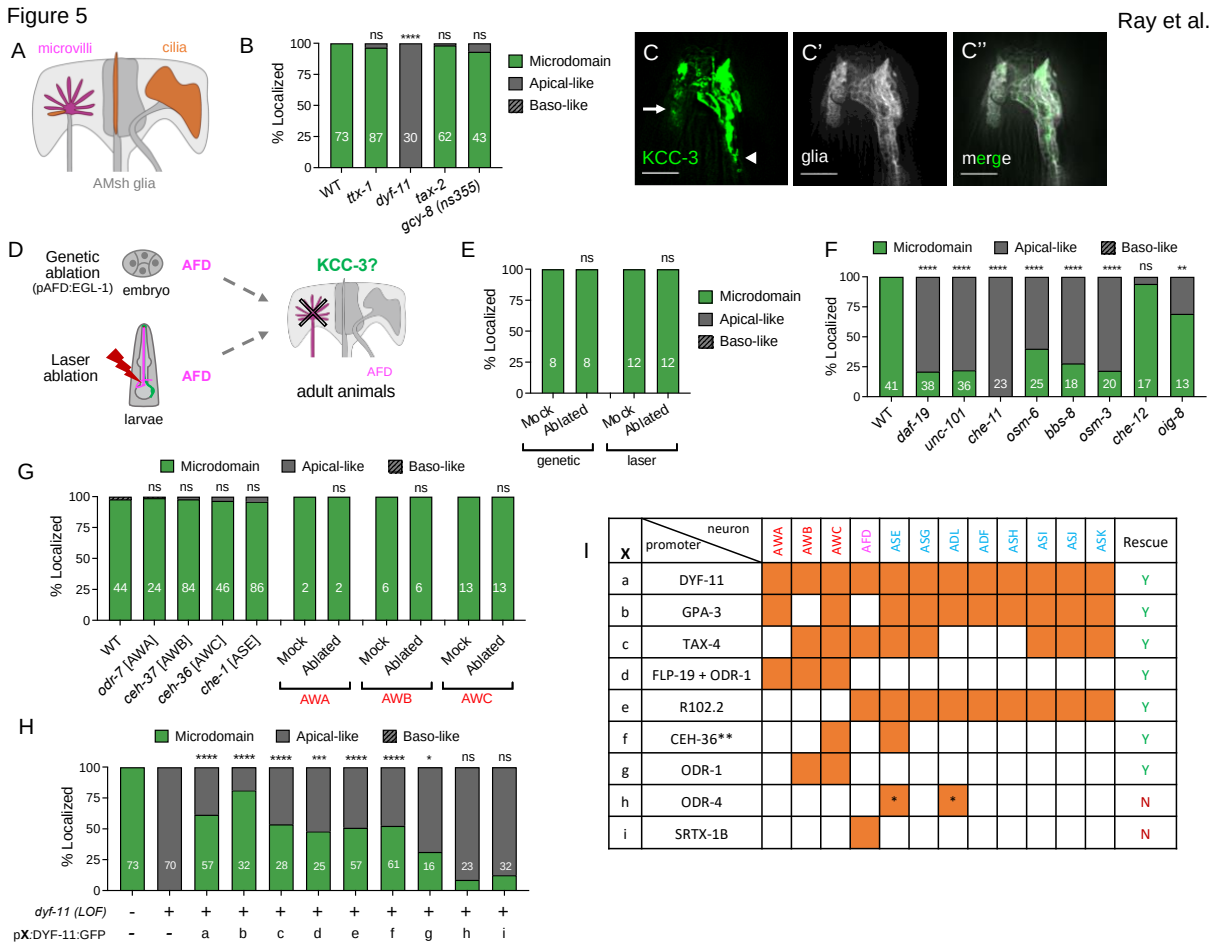

Figure 5: Glial KCC-3 localization is regulated by distal non-AFD NRE cilia

(A) Schematic showing distribution of microvilli and cilia structures in amphid NREs. AFD NREs contain microvilli and a pseudocilium, while all other amphid NREs are ciliated. **(B)** Quantification of KCC-3 localization in *tax-2*, *dyf-11*, *ttx-1*, and *gcy-8(ns355)* mutants compared to WT. **(C-C'')** Fluorescence images of KCC-3 (E), AMsh glia (E'), and merge (E") in *dyf-11* cilia mutant animals. Scale bar, 5 µm. **(D)** Schematic of genetic and laser ablation protocols to assess KCC-3 localization without AFD. **(E)** Quantification of KCC-3 localization in adults after genetic and laser ablation, compared to mock animals. **(F)** KCC-3 localization in *dyf-11* cilia mutants. **(G)** Quantification of KCC-3 localization in amphid neuron identity mutants (*odr-7*, *ceh-37*, *ceh-36*, *che-1*) and after wing neuron (AWA, AWB, AWC) laser ablation. **(H-I)**

Quantification of KCC-3 localization in DYF-11 rescue experiments (H). X refers to promoter(s) used for rescue experiments. Identity of X and the neurons the promoter(s) express in are expanded on in I. Orange denotes expression in associated neuron. ODR-4 expresses in an ASX and ADX neuron but the exact identity of these neurons are unclear. The CEH-36 rescue construct also has ODR-10 and R13H4.1, but only CEH-36 showed expression. For all graphs, * $p < 0.05$, ** $p < 0.01$, *** $p < 0.001$, **** $p < 0.0001$. Fisher's exact test to WT.

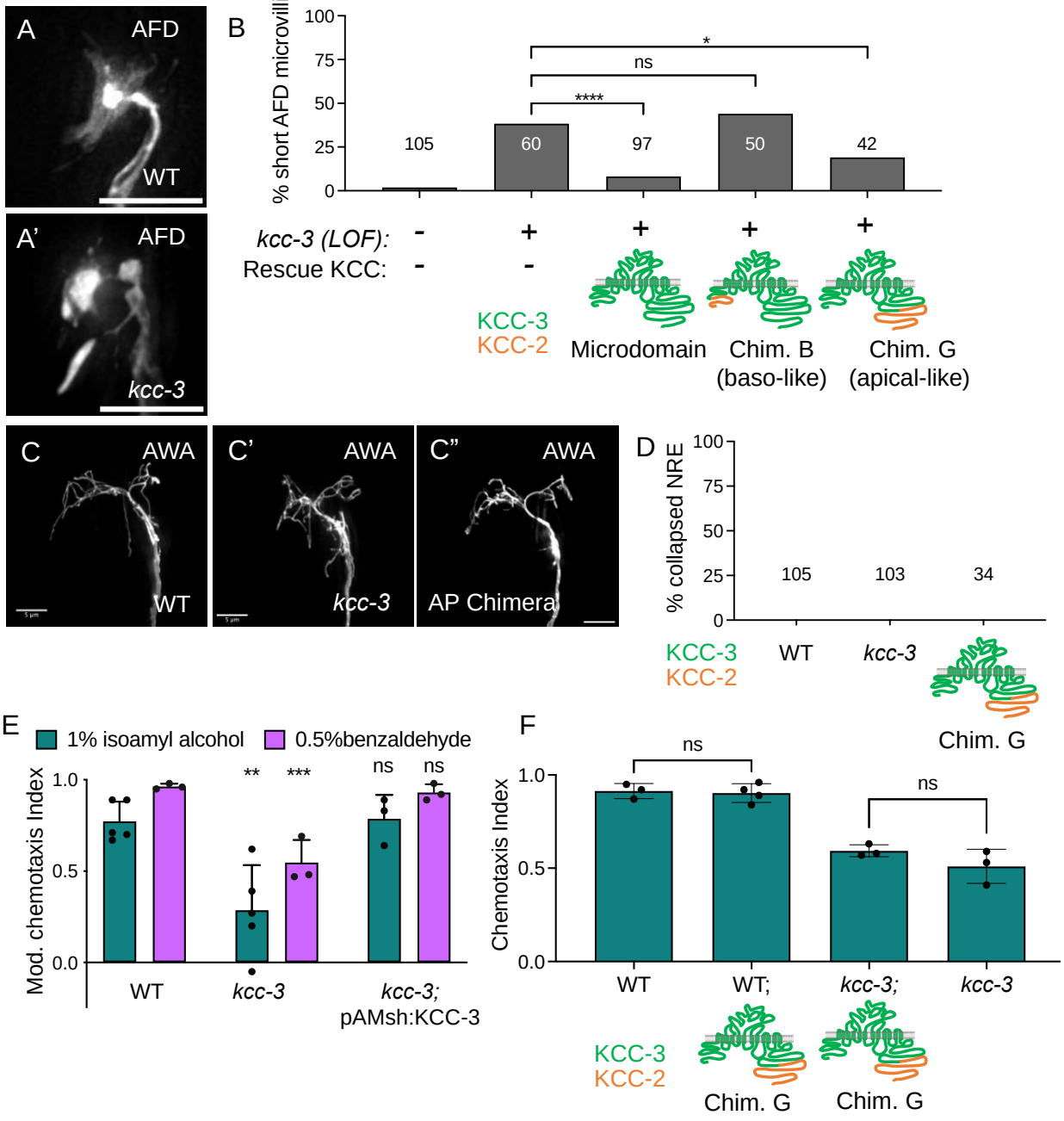

Figure 6: Microdomain localization of KCC-3 regulates both AFD and non-AFD neuron shape and associated animal behavior

(A-A') Fluorescent images of AFD NRE in both wildtype (A) and *kcc-3(ok228)* mutants (A').

(B) Quantification of AFD NRE shape rescue with WT KCC-3, basolaterally localized KCC-

2/KCC-3 chimera, and an apically localized KCC-2/KCC-3 chimera. **(C-C")** Fluorescent images of AWA in WT animals (C), *kcc-3* mutant animals (C'), and animals that express the apically localized KCC-3 chimera (C", AP chimera). **(D)** Quantification of AWA shape in WT animals, *kcc-3* mutant animals, and animals that express the apically localized KCC-3 chimera. **(E)** Behavioral quantification for AWC-sensed odorants 1% isoamyl alcohol and 0.5% benzadehyde. Significance compared to WT. One-way ANOVA with Tukey's post-hoc test. **(F)** Behavioral quantification for AWC-sensed odorants 1% isoamyl alcohol with the AP chimera. One-way ANOVA with Tukey's post-hoc test. All scale bars 5µm. * $p < 0.05$, ** $p < 0.01$, **** $p < 0.0001$.

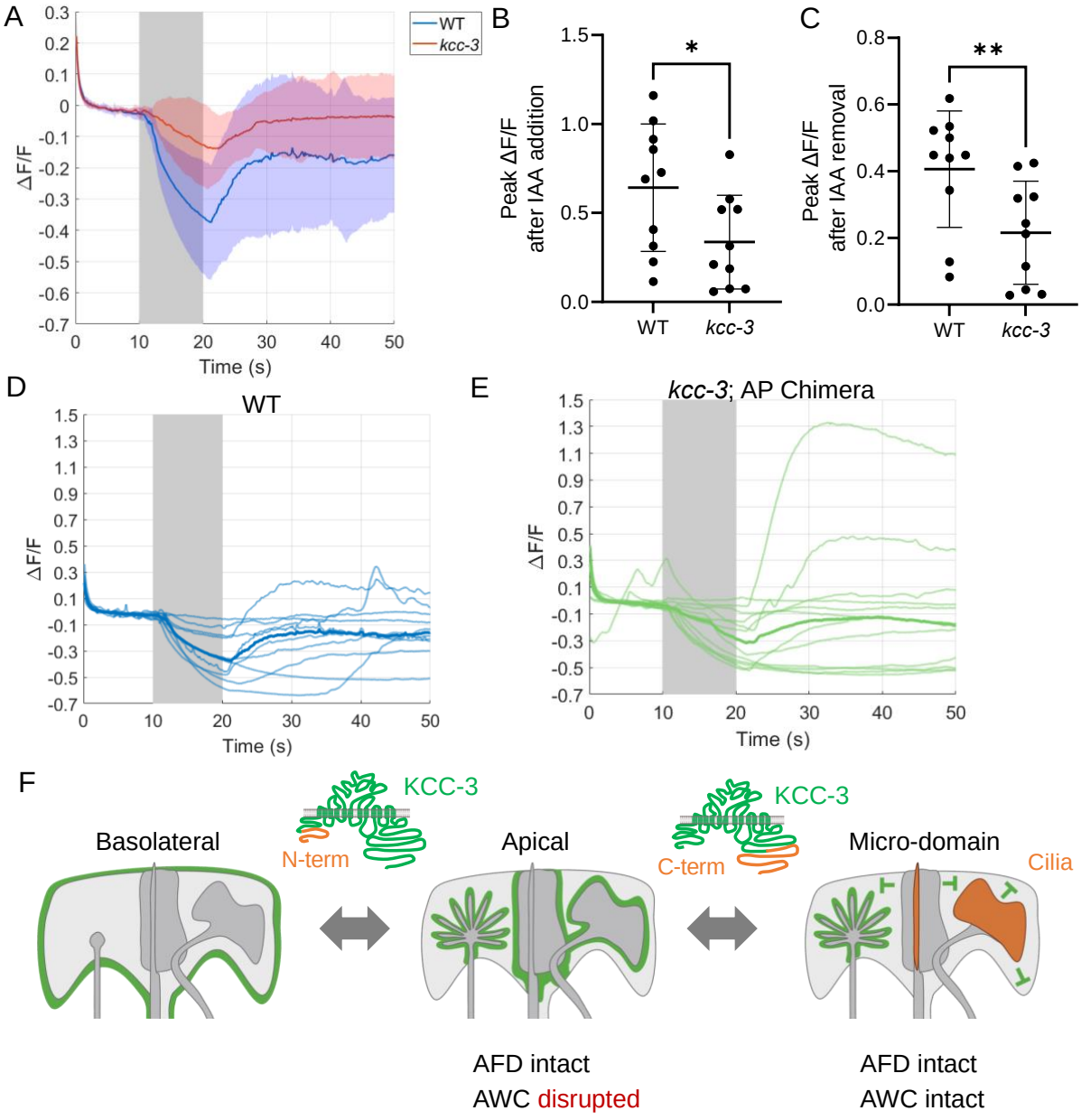

Figure 7: Schematic of KCC-3 localization in AMsh glia

(A) Averaged nascent calcium transients in animals with the addition of 0.01% isoamyl alcohol (IAA) in AWC neuron expressing GCaMP6s. Solid lines represent the average across 10-12 different animals WT (blue), kcc-3 (red) background, kcc-3 background overexpressing

expressing the KCC-3 chimera mislocalized in AMsh apical membrane (green). **(B)** Peak calcium responses when animal presented with stimulus (One-way ANOVA Bonferroni's multiple comparison test: WT v kcc-3 = 0.2414, WT v kcc-3; AP =<0.0011, kcc-3 v kcc-3; AP = <0.0001). **(C)** Peak calcium responses when IAA was removed (One-way ANOVA Bonferroni's multiple comparison test: WT v kcc-3 = 0.0824, WT v kcc-3; AP =0.2855, kcc-3 v kcc-3; AP = 0.0008). **(D-E)** Variability of Ca^{2+} responses to isoamyl alcohol in WT (D) and AP chimera in *kcc-3* mutant animals (E). Light traces are single trials and bold lines are the average of all trials. **(F)** KCC-3 localization is a two-step process. First, N-terminal sequences can guide KCC proteins to basolateral membranes. Second, C-terminal sequences can determine apical vs. microdomain localization. Cilia also play a role in guiding KCC-3 from broad apical membranes to localized microdomain membranes.

SUPPLEMENTAL MATERIALS FOR

Neuron cilia constrain glial regulators to microdomains around distal neurons

Sneha Ray[1, 2], Pralaksha Gurung,[2] Sean Manning[1], Alexandra Kravchuk[1, 3], Aakanksha Singhvi[1, 4,*]

Correspondence and reagent requests to: asinghvi@fredhutch.org

This PDF file includes:

Materials and Methods

Figures. S1 to S8

Supplementary Materials Reference List

EXPERIMENTAL PROCEDURES

C. elegans methods

C. elegans were cultured as previously described (Brenner, 1974; Stiernagle, 2006). Bristol N2 strain was used as wild type. Animals were raised at 20ºC (unless noted) for at least one week without starvation. L4 larval animals were picked to fresh plates and assayed 24 hours later, unless otherwise noted. Germ-line transformations by micro-injection to generate unstable extra-chromosomal array transgenes were carried out using standard protocols (Mello, Kramer, Stinchcomb, & Ambros, 1991). Integration of extra-chromosomal arrays was performed using UV. All transgenic arrays were generated with 30 ng/µl P_{mig-24}:Venus, 15 ng/uL $P_{unc-122}$:GFP or 20 ng/µL $P_{unc-122}$:RFP as co-injection markers (Abraham, Lu, & Shaham, 2007; Armenti, Lohmer, Sherwood, & Nance, 2014; Miyabayashi, Palfreyman, Sluder, Slack, & Sengupta, 1999). Information on all strains and reagents is available by request.

Strains

Strains were sourced from (a) the CGC, funded by NIH Office of Research Infrastructure Programs (P40 OD010440), (b) the International C. elegans Gene Knockout Consortium (C. elegans Gene Knockout Facility at the Oklahoma Medical Research Foundation, funded by the National Institutes of Health; and the C. elegans Reverse Genetics Core Facility at the University of British Columbia, funded by the Canadian Institute for Health Research, Genome Canada, Genome BC, the Michael Smith Foundation, and the National Institutes of Health) and (c) National BioResource Project (NBRP), Japan.

Plasmids

P_{AMsh}:KCC-3:worm-mScarlet and P_{AMsh}:CFP:SL2:KCC-3:worm-mScarlet: Codon-optimized worm mScarlet was synthesized by Genewiz with flanking AgeI/EcoRI digestion sites and cloned into pAB44 using AgeI/EcoRI to make pSR1/2 (pF53:worm-mScarlet). *mScarlet* and the *unc-54* 3'UTR was cloned into pAS272 (P_{AMsh}:KCC-3:mcherry) using Age1/Apa1 from pSR1/2 to make pSR5/6 (P_{AMsh}:KCC-3:mScarlet [out of frame]). Site-directed mutagenesis was used to add TATG in front of mScarlet in pSR5/6 to make pSR7/8 (P_{AMsh} :KCC-3:mScarlet [in frame]).

CFP was PCR amplified from pIL43 (gift from Max Heiman) with flanking FseI/XbaI sites and inserted into pAS548 (pSM:SL2:mCherry) to make pSR9/10 (pSM:CFP:SL2:mCherry). CFP-SL2 was then PCR amplified from pSR9/10 and inserted into pSR7 (P_{AMsh}:KCC-3:mScarlet) using FseI/AscI to make pSR11/12 (P_{AMsh} :CFP:SL2:KCC-3:mScarlet).

KCC-1/KCC-2: cDNA for *C. elegans* KCC-1 and KCC-2 were PCR amplified in one (KCC-2) or two (KCC-1) segments from a mixed stage cDNA library and cloned into pSR7 using BamH1/EcoRI (KCC-1) or BamH1/SalI (KCC-2) to generate pSR17 (P_{AMsh}:KCC-1:mScarlet) and pSR61/62 (P_{AMsh}:KCC-2:mScarlet).

DYF-11 rescue constructs: All promoters were PCR amplified from gDNA of mixed stage animals and inserted into pAN1 (P_{DYF-11}:DYF-11:GFP) using either SphI/SalI or Gibson assembly. Promoters cloned: P_{GPA-3} (5.4 kb upstream start codon), P_{TAX-4} (3.1 kb upstream start codon), P_{FLP-19} (3.6 kb upstream start codon), P_{ODR-1} (2.4 kb upstream start codon), $P_{R102.2}$ (602 bp upstream start codon), P_{CEH-36} (3kb upstream start codon), and P_{ODR-4} (2.3 kb upstream start codon).

Laser Ablation

Laser ablation was done on the photoactivation system on the Deltavision Elite RoHS wide-field microscope. L1 animals were picked and mounted on an agar pad on a glass microscope slide. One AFD neuron was focused with a 100x objective plus digital zoom. The neuron was blasted with a 405 laser at 100% for 2s to kill the neuron. Animals were rescued off the agar pad and allowed to recover on an NGM plate. AFD cell death was assessed the following day for lack of GFP fluorescence in AFD. Animals were scored for KCC-3 localization one day later, in day 1 adults.

KCC-2/KCC-3 Chimera Generation

We used a PCR fusion based approach to create KCC-2/KCC-3 chimera proteins (Hobert, 2018). Briefly, 2 or more segments of KCC-2 or KCC-3 were PCR amplified with nested primers. The 3' primer for every segment but the last included a 24bp overhang to the following segment. In the first PCR, all KCC segments are amplified independently. In the second PCR, nested primers fuse the independent segments to create one contiguous KCC chimeric protein. This product is then inserted into pSR7 using BamH1/Sal1 sites to create the final plasmid.

***dyf-11* Rescue Experiments**

All rescue constructs were injected into ASJ583 (*dyf-11(mn392);* dnaIs10 [P_{AMsh}:KCC-3:mScarlet]). For blinded scoring, both extra-chromosomal array-positive and negative animals were assessed for KCC-3 localization first and then for presence of the rescue construct.

Statistical Methods

All data and statistics were graphed and analyzed using Prism9. Proportional data is presented as the proportional sum across multiple days of data collection ± 95% confidence interval. Two-Sided Fisher's Exact tests were performed to compare across genotypes.

Microscopy, Image Processing and Analysis

Worms were immobilized with 40mM sodium azide. Images were collected on a Deltavision Elite RoHS wide-field deconvolution system, 40x/1.3 NA oil-immersion or OLY 100×/1.40 NA oil-immersion objective and a DV Elite CMOS Camera. Some images were also captured on a VisiTech iSIM super resolution microscope. Image processing was done in FIJI ImageJ.

Behavioral Assays

All chemotaxis behavioral assays as previously described (Bargmann, Hartwieg, & Horvitz, 1993). Briefly, animals are placed at the black dot, 1 µL odorant diluted in ethanol is placed at +, and 1 µL ethanol is placed at – (Figure 5G). 1 µL of 1M sodium azide is also placed at both + and – points to anesthetize animals. Animals are allowed to explore on the plate for 1hr. All assays performed on day 1 adult animals. Statistical analysis was performed with unpaired t-test (Graphpad).

Calcium imaging

Calcium imaging was conducted in microfluidic chambers (Chronis, Zimmer, & Bargmann, 2007). Imaging was performed at 7 Hz on a Leica DMi8 inverted microscope with a 63x/1.40 NA oil immersion objective and an Andor iXon Life 888 EMCCD camera, using Leica LAS-X software. L4 animals were picked 24 hours prior to imaging and left in 20°C overnight. Animals were

immobilized using 1 mM levamisole prior to being loaded into the imaging chamber. Animals were presented with alternating S-Basal buffer and 0.01% isoamyl alcohol diluted in S-basal buffer. Image analysis was performed using ImageJ. ΔF/F was calculated by $(F-F_0)/F_0$, where F_0 was designated by the average fluorescent intensity prior to odor presentation (t=1s - t=10s).

Figure S1

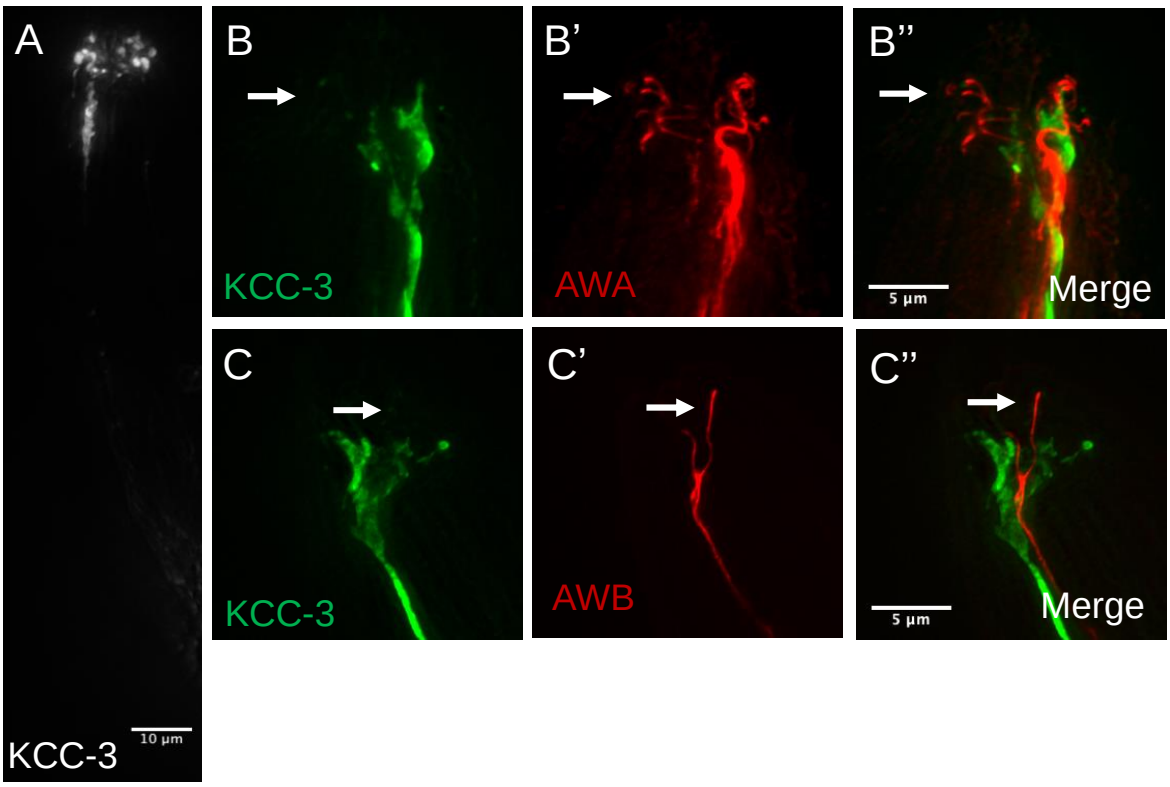

Figure S1. KCC-3 localizes to an apical region specifically around AFD-NRE

(A) Fluorescence image of KCC-3 translational reporter in day 1 adults. **(B-B'')** Fluorescent images of KCC-3 (B, pseudo-colored green), AWA neuron (B', pseudo-colored red), and merge (B") showing that KCC-3 does not preferentially localize to AWA NREs (white arrow; 8/8 animals). **(C-C'')** Fluorescent images of KCC-3 (C, pseudo-colored green), AWB neuron (C', pseudo-colored red), and merge (C") showing that KCC-3 does not localize to AWB NREs (white arrow; 4/4 animals). Scale bar, 5µm.

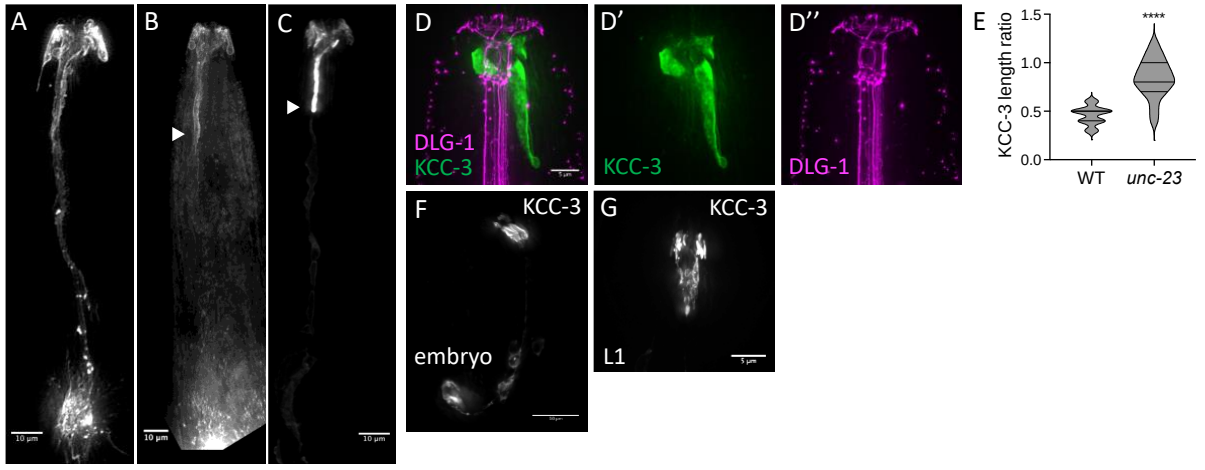

Figure S2. KCC-3 localizes to a glial apical microdomain

(A-C) Fluorescent images of AMsh membranes tagged with BasoRed (A), ApiGreen (B), and a PH-PLC apical marker (C). **(D-D'')** Fluorescent image overlay (D) of KCC-3 (D') and the junctional DLG-1 (D'') marker (7/7 animals). **(E)** Quantification of KCC-3 length expressed as ratio over animal length from nosetip to the first pharyngeal bulb. **** $p < 0.0001$ (Unpaired t-test. **(F-G)** Fluorescent images showing apical localization and GAB boundary (white arrow) of KCC-3 in a translational reporter in 3-fold stage embryos (G) and L1 larvae (H).

Figure S3

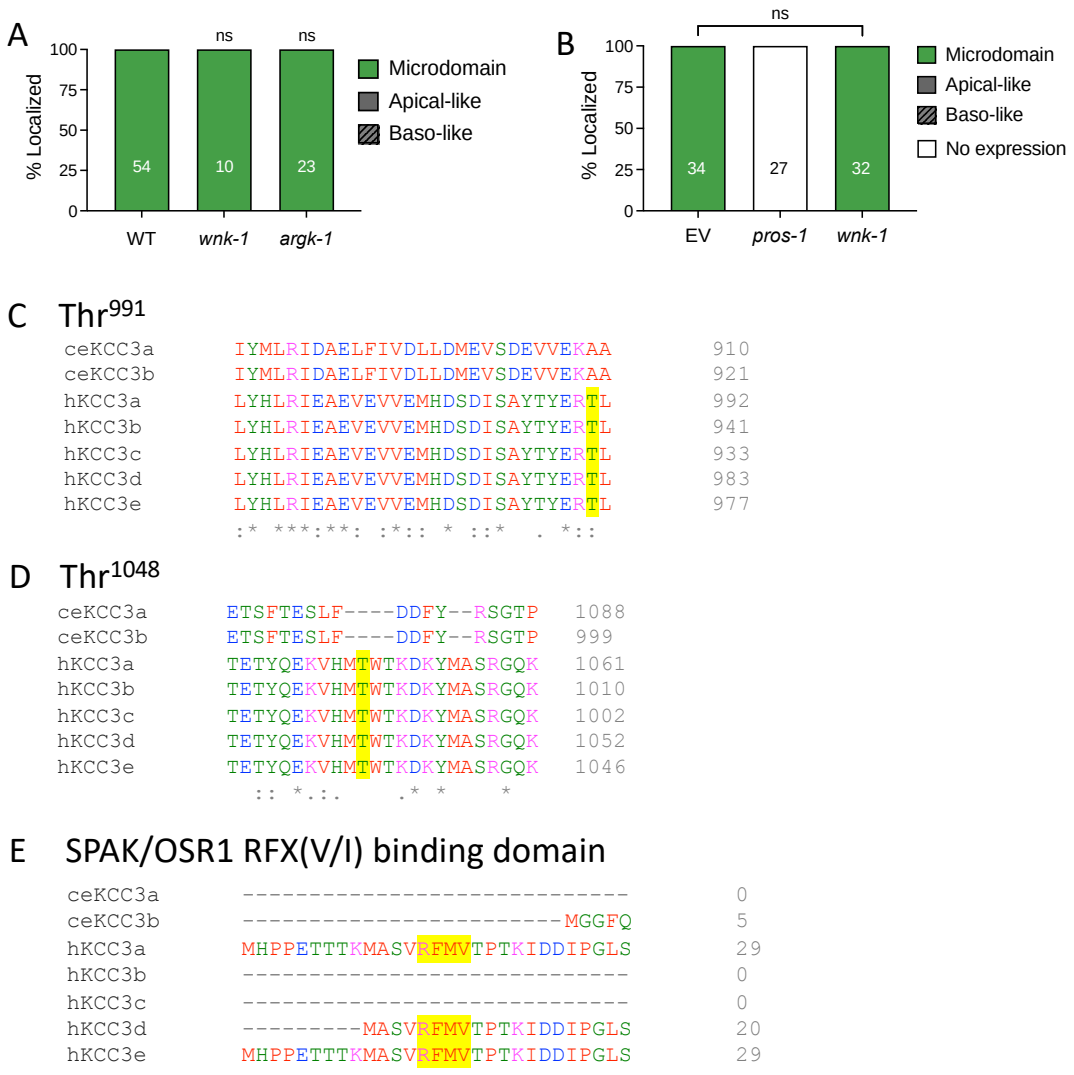

Figure S3. Glial KCC-3 microdomain does not require canonical regulators

(A) Quantification of KCC-3 localization in *wnk-1* and *argk-1* loss of function mutants. **(B)** Quantification of KCC-3 localization after RNAi for *wnk-1*, with *pros-1* RNAi as a positive control. **(C-E)** WNK/SPAK phosphorylation sites (C-D) and RFX(V/I) binding domain (E) in human and *C. elegans* KCC-3. These human KCC-3 sites are not conserved in *C. elegans* KCC-3.

A

Category	Features
Basolateral	• GAB absent (entire glial cell); outer membrane
Apical	• GAB present; expression in AMsh “wings
Micro-domain	• GAB present; restricted expression
Other	• GAB absent (entire glial cell); inner membranes

B

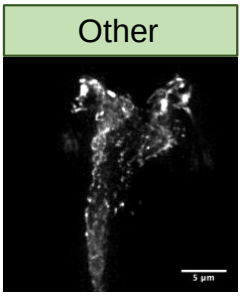

C

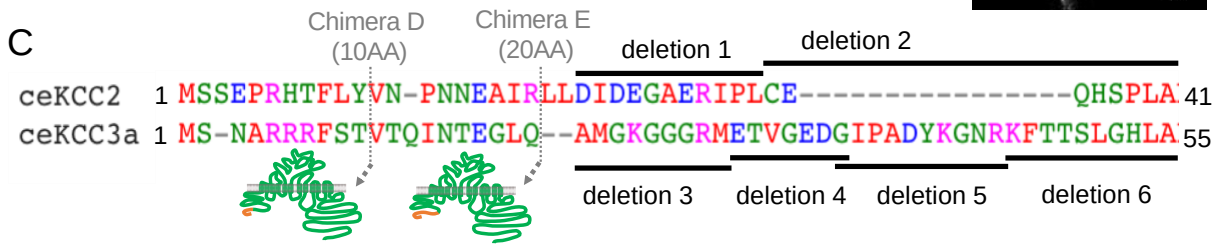

D

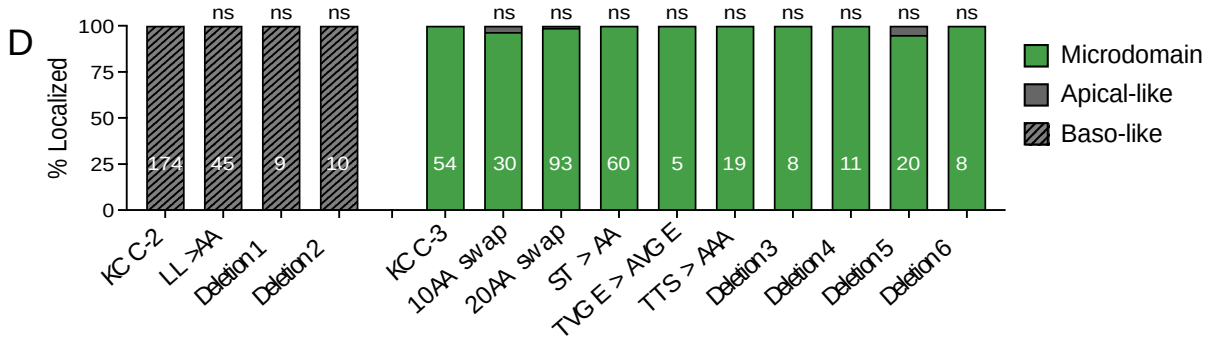

E

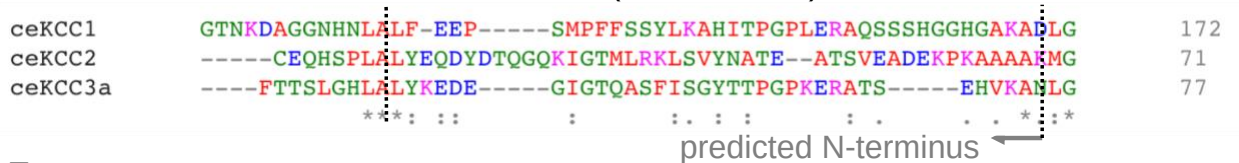

F

G

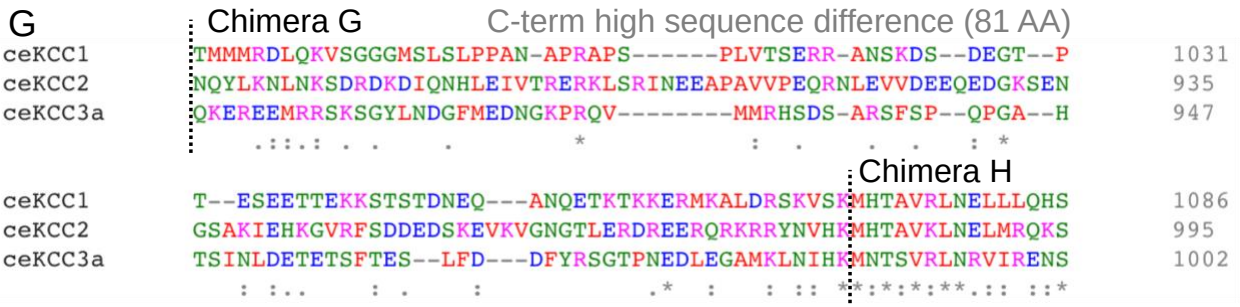

Figure S4: Glial KCC-3 localizes in a two-step process through two protein regions

(A) Description of categories to delineate KCC localization patterns. **(B)** Fluorescent image of KCC chimera localization pattern categorized as "other". **(C-D)** Description (C) and quantification of localization (D) of additional chimeras (10AA swap, 20AA swap), point mutations (LL>AA, ST>AA, TVGE>AVGE, TTS>AAA), and short deletions of KCC-2 and KCC-3. Dotted lines are where KCC-2 and KCC-3 were swapped to create the 10AA and 20AA chimeras, with chimera schematics under the sequence alignment. Point mutations are highlighted, and deletions are denoted by a black bar above or below the sequence that was deleted. The graph (D) is divided into KCC-2 mutations and deletions first and then KCC-3 based chimeras, mutations, and deletions. **(E-G)** Aligned KCC-1, KCC-2, and KCC-3 sequences at the N-terminal (E), mid-protein (F) and C-terminal regions (G). Dotted lines are where KCC-2 and KCC-3 sequences were swapped to create the chimeras used in the study. Grey box in B denotes region of high sequence dissimilarity at the C-terminal. Fisher's exact test.

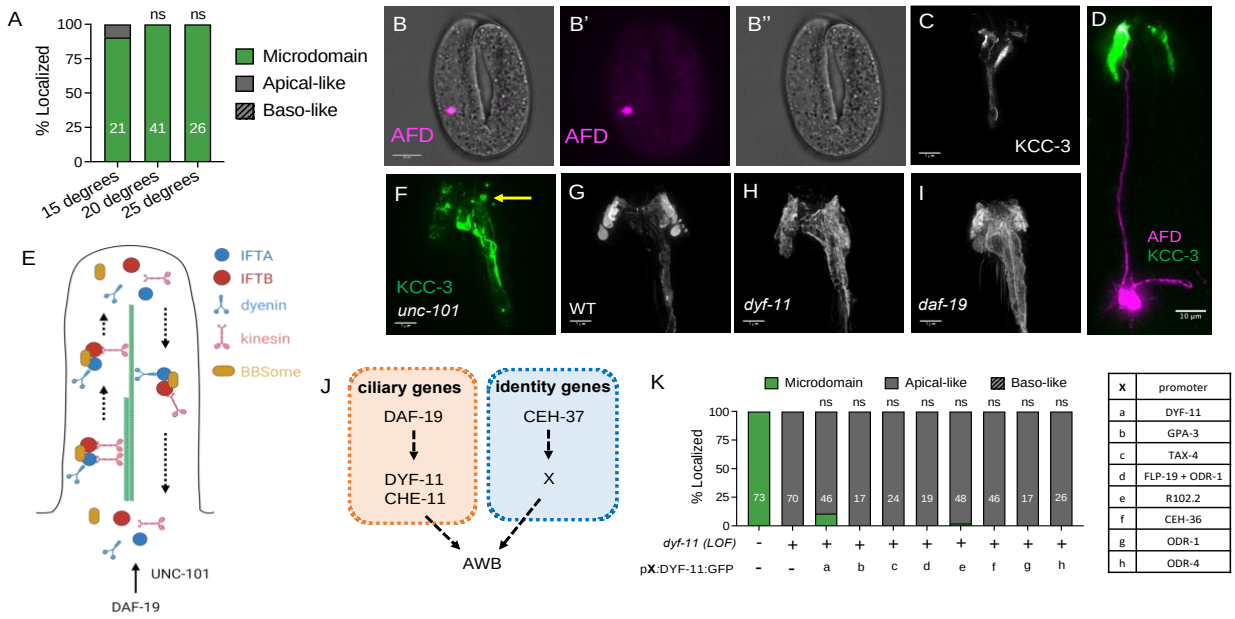

Figure S5: Glial KCC-3 localization is regulated by distal non-AFD-NRE cilia

(A) Quantification of KCC-3 localization in Day 1 adults raised at 15°C, 20°C, and 25°C. **(B-B'')** Merge (B) images of P_{SRTX-1} expression (B') in 3-fold embryo (B'', DIC). **(C)** Fluorescent image of KCC-3 expression in Day 1 animals after AFD laser ablation in L1 larvae. **(D)** Fluorescent image of KCC-3 and AFD neuron in Day 1 animals, with AFD ablated on one side. KCC-3 localizes apically to a micro-domain. **(E)** Schematic of intraflagellar transport (IFT) in *C. elegans*. **(F)** Fluorescent image of KCC-3 localization in *unc-101* mutants. Yellow arrow points to regions lacking AFD enrichment. **(G-I)** Fluorescent images of cytosolic CFP in AMsh glia in WT (G), *dyf-11* mutants (H), and *daf-19* mutants (I). **(J)** Schematic of amphid NRE development, with AWB as an example. Ciliary genes, such as *daf-19*, interact with identity genes, such as *ceh-37*, for the development of unique NRE shape and function. **(K)** Quantification of control non-extrachromosomal arrays animals in DYF-11 experiments.

Figure S6

Ray et al.

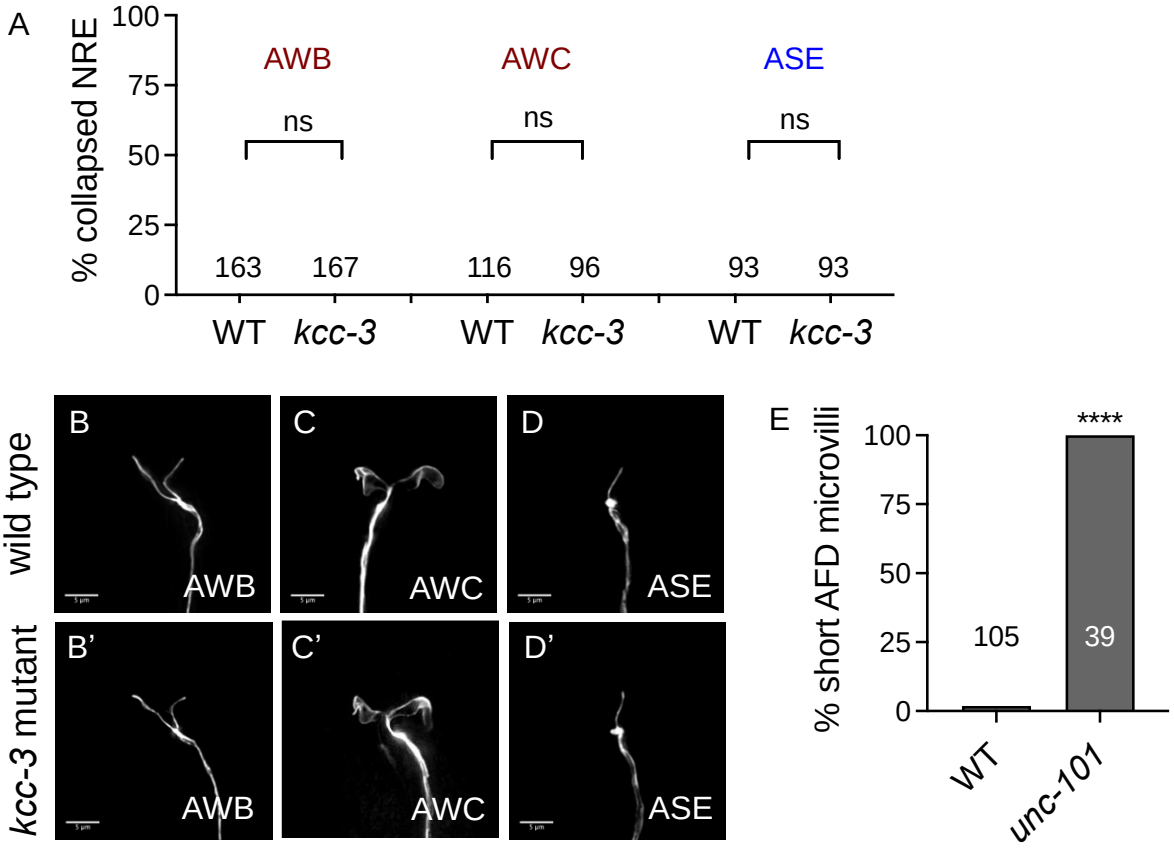

Figure S6. KCC-3 does not regulate non-AFD NRE shape

(A) Quantification of AWB, AWC, and ASE collapsed shape in WT and *kcc-3(ok228)* animals. **(B-B')** Fluorescent images of AWB in WT (B) and *kcc-3* mutant (B') animals. **(C-C')** Fluorescent images of AWC in WT (C) and *kcc-3* mutant (C') animals. **(D-D')** Fluorescent images of ASE in WT (D) and *kcc-3* mutant (D') animals. **(E)** Quantification of AFD collapsed shape in WT and *unc-101* animals. All scale bars 5um.

A

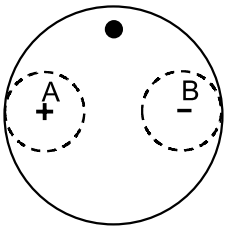

$$CI = \frac{A-B}{Total\ worms}$$

$$CI_{mod} = \frac{A-B}{A+B}$$

B

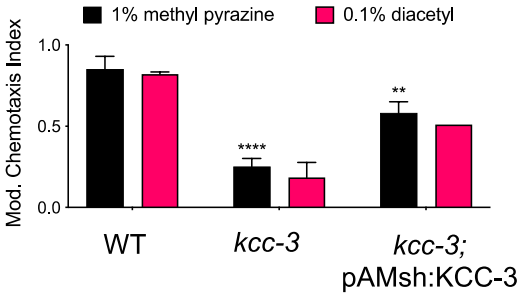

C

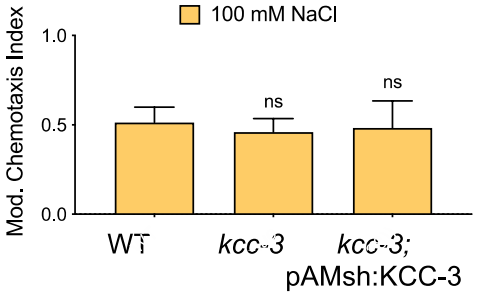

D

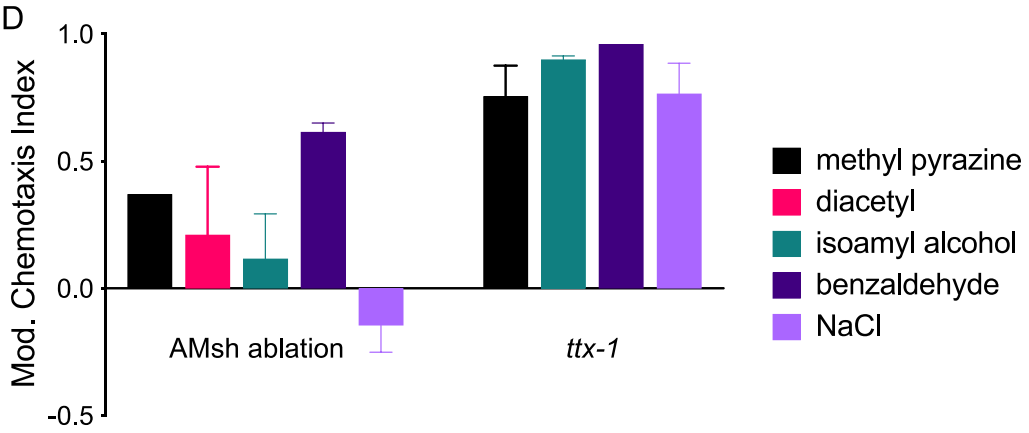

E

Neuron	Chemoattractant	N2	*dyf-11*	*kcc-3*
AWA	1% methyl pyrazine	0.43	0.2	0.15
AWC	1% isoamyl alcohol	0.48	0.21	0.18
ASE	100mM NaCl	0.6	0	0.54

Figure S7. KCC-3 regulates non-AFD NRE behavior

(A) Schematic of chemotaxis assays, including equation for chemotaxis index (CI) and modified chemotaxis index (CI_{mod}). **(B)** Chemotaxis index quantifications for AWA-sensed odorants 1% methyl pyrazine and 0.1% diacetyl. (**C)** Chemotaxis index quantifications for ASE-sensed tastant 100mM NaCl. AMsh ablated animals and *ttx-1* mutant animals for odorants and tastant tested in Figure 5. **(D)** Chemotaxis index quantifications for animals with AMsh glia ablation and *ttx-1* mutants. **(E)** Chemotaxis index quantification of *dyf-11* cilia mutants to 1% methyl pyrazine, 1% isoamyl alcohol, and 100mM NaCl. Same day CI values of WT and *kcc-3(ok228)* mutants included for comparison.

REAGENTS

A. Mutants

LG1: *tax-2(p691), unc-101(m1), che-1(p678, che-14(ok193)*

LG2: *kcc-3(ok228), daf-19(m86), oig-8(ot818)*

LG3: *lit-1(ns132)*

LG4: *osm-3(p802), gcy-8(ns335)*

LG5: *osm-6(p811), ttx-1(p767), che-11(e1810), che-12(e1812), unc-23(e25), bbs-8(nx77), sma-1(e30)*

LGX: *dyf-11(mn392), odr-7(ky4), ceh-36(ky646), ceh-37(ok642), daf-6(e1377)*

B. Integrated transgenes

Strain	Chromosome	Genotype	Reference
dnaIs10	V	$P_{F53F4.13}$*:KCC-3:mScarlet*	This study
dnaIs15	IV	$P_{F53F4.13}$*:CFP:SL2KCC-3:mScarlet*	This study
nsIs228	I	P_{SRTX-1}*:GFP*	(Singhvi et al., 2016)
ntIs1	V	P_{GCY-5}*:GFP*	(Sarin et al., 2007)
kyIs37	II	P_{ODR-10}*:GFP*	(P. Sengupta, Chou, & Bargmann, 1996)
kyIs140	I	P_{STR-2}*:GFP*	(Troemel, Sagasti, & Bargmann, 1999)
kyIs104	X	P_{STR-1}*:GFP*	(Troemel, Kimmel, & Bargmann, 1997)
oyIs87	III	$P_{GPA-4delta6}$*:myr:GFP*	(Maurya & Sengupta, 2021)
dnaIs19		$P_{F53F4.13}$*:SAX-7deltacyt:sfGFP*	(Martin et al., 2022)

hmnIs30		P_{GCY-5}*:AJM-1:YFP*	Gift from Max Heiman
xnIs17		P_{DLG-1}*:DLG-1:GFP*	(Firestein & Rongo, 2001)

C. Extra-chromosomal arrays

Strain	**Genotype**	**Reference**
nsEx2606	$P_{TO2B11.3}$*:GFP:LIT-1*	(Oikonomou et al., 2011)
nsEx4131	P_{VAP-1}*:VAP-1:sfGFP*	Gift from Shai Shaham
nsEx5658	P_{KCC-3}*:KCC-3:GFP* (recombineered fosmid)	(Singhvi et al., 2016)
nsEx4394	$P_{SRTX-1B}$*:DYF-11:GFP*	

C. Extrachromosomal transgenes and plasmids generated in this study

***** denotes plasmids made outside of the study, which were injected to make stable extra-chromosomal arrays

Extra-chromosomal array (dnaEx) number	**Plasmid**	**Genotype**
26, 312, 313	pSR7	$P_{F53F4.13}$*:KCC-3:mScarlet*
52, 53, 54, 55, 56, 68	pSR11	$P_{F53F4.13}$*:CFP:SL2KCC-3:mScarlet*
222, 223, 224	pCM11*	$P_{F53F4.13}$*:SAX-7:mApple*
256, 258, 320	pCM11* + Recombineered fosmid	$P_{F53F4.13}$*:SAX-7:mApple;* P_{KCC-3}*:KCC-3:GFP*
515, 543, 544	pOO1	$P_{F53F4.13}$*:PH-PLCdelta:GFP*
77, 78, 79	pJF48*	P_{SRTX-1}*:EGL-1*
220, 221, 228	pAN1	P_{DYF-11}*:DYF-11:GFP*

333, 337, 338	pSR57	P_{GPA-3}*:DYF-11:GFP*
317, 318, 319	pSR53	P_{TAX-4}*:DYF-11:GFP*
204, 207, 208	pSR35	P_{ODR-1}*:DYF-11:GFP*
334, 335, 336	pSR35 + pSR56	P_{ODR-1}*:DYF-11:GFP;* P_{FLP-19}*:DYF-11:GFP*
450, 453, 488	pSR85	$P_{R102.2}$*:DYF-11:GFP*
326, 327, 328	pSR52	P_{ODR-4}*:DYF-11:GFP*
418	pSR77 + pSR79 + pSR82	P_{CEH-36}*:DYF-11:GFP* P_{ODR-10}*:DYF-11:GFP* $P_{R13H4.1}$*:DYF-11:GFP*
84	pSR17	$P_{F53F4.13}$*:KCC-1a:mScarlet*
75, 76	pSR15	$P_{F53F4.13}$*:KCC-2a:mScarlet*
153	pSR24	$P_{F53F4.13}$*:Chimera A:mScarlet*
188, 189, 193	pSR27	$P_{F53F4.13}$*:Chimera B:mScarlet*
194, 206	pSR33/34	$P_{F53F4.13}$*:Chimera C:mScarlet*
314, 315, 316	pSR43	$P_{F53F4.13}$*:Chimera D:mScarlet*
325, 351, 352	pSR45	$P_{F53F4.13}$*:Chimera E:mScarlet*
167, 454, 462, 484	pSR25	$P_{F53F4.13}$*:Chimera F:mScarlet*
410, 411, 417	pSR83	$P_{F53F4.13}$*:Chimera G:mScarlet*
445, 446, 447	pSR87	$P_{F53F4.13}$*:Chimera H:mScarlet*
252, 257, 302	pSR39	$P_{F53F4.13}$*:KCC-2 LL>AA:mScarlet*
332, 342, 381	pSR61	$P_{F53F4.13}$*:KCC-3 TTS>AAA:mScarlet*
253, 254, 255	pSR41	$P_{F53F4.13}$*:KCC-3 ST>AA:mScarlet*
339, 340, 341	pSR59	$P_{F53F4.13}$*:KCC-3 TVGE>AVGE:mScarlet*
384, 385, 386	pSR69	$P_{F53F4.13}$*:KCC-2 deletion 1:mScarlet*

412, 413, 415	pSR71	*$P_{F53F4.13}$:KCC-2 deletion 2:mScarlet*
428, 430	pSR66	*$P_{F53F4.13}$:KCC-3 deletion 3:mScarlet*
407, 427, 429	pSR73	*$P_{F53F4.13}$:KCC-3 deletion 4:mScarlet*
383, 387, 388	pSR67	*$P_{F53F4.13}$:KCC-3 deletion 5:mScarlet*
408, 409, 425, 426	pSR75	*$P_{F53F4.13}$:KCC-3 deletion 6:mScarlet*
5, 6	pSR7 + pCF27*	*$P_{F53F4.13}$:KCC-3:mScarlet;* *P_{VAP-1}:VAP-1:sfGFP*
514, 517, 524	pPG5/6	*P_{HLH-17}:KCC-3:mScarlet*

RAW DATA

Figure 2K	Strain	Condition	Microdomain	Apical-like	Baso-like	Total
	ASJ30 (dnaEx6)	L2/L3	10	0	0	10
	ASJ30 (dnaEx6)	L4	19	0	0	19
	ASJ30 (dnaEx6)	Day 1	41	0	0	41
	ASJ30 (dnaEx6)	Day 10	12	9	0	21

Figure S2E	WT			*unc-23*		
	KCC-3 length (um)	Length to 1st pharangeal bulb	Ratio	KCC-3 length (um)	Length to 1st pharangeal bulb (um)	Ratio
	27	56	0.5	44	49	0.9
	33	57	0.6	53	54	1.0
	22	58	0.4	43	49	0.9
	33	64	0.5	51	47	1.1
	20	64	0.3	33	50	0.7
	25	64	0.4	18	48	0.4
	30	61	0.5	45	50	0.9
				42	56	0.8
				51	49	1.0
				32	48	0.7
				39	49	0.8
				46	46	1.0
				37	46	0.8
				35	44	0.8
				34	48	0.7
				31	54	0.6
				56	47	1.2
				51	58	0.9
				40	48	0.8
				54	49	1.1
				25	47	0.5

Figure 3G	Strain	Microdomain	Apical-like	Baso-like	Total		
	ASJ286 (dnaIs10 V)	73	0	0	62		
	ASJ467 (dnaIs10 V; che-14(ok193) I)	50	12	0	62		
	ASJ424 (dnaIs10 V; nsIs228 I; daf-6 (e1377) X)	70	22	0	92		
	ASJ468 (dnaIs10 V; nsIs228 I; lit-1 (ns132) III)	18	7	0	25		
	ASJ373 (dnaIs10 V; nsIs228 I; snx-1 (ns133) X)	68	0	0	68		
Figure 3H	Strain	Normal	Globular	Total			
	OS7635 (VAP-1:GFP)	25	0	25			
	ASJ1195 (VAP-1:GFP; kcc-3 (ok228) II)	25	8	33			
Figure S3A	Strain	Microdomain	Apical-like	Baso-like	Total		
	ASJ463 (dnaIs15 IV)	54	0	0	54		
	ASJ1214 (dnaIs10 V; wnk-1 (tm487)/nTI IV	10	0	0	10		
	ASJ511 (dnaIs15 IV; argk-1(ok2973) V)	82	0	0	82		
Figure S3B	Strain	RNAi	Microdomain	Apical-like	Baso-like	No expression	Total
	ASJ306 (dnaIs10; nsIs228 I)	EV	34	0	0	0	34
		pros-1	0	0	0	27	27
		wnk-1	32	0	0	0	32

Figure 4C	Strain	Microdomain	Apical-like	Other	Baso-like	Total (n)
	ASJ286 (dnaIs10[pF53:KCC-3:mSc])	54	0	0	0	19
	ASJ317 (dnaEx84[pF53:KCC-1:mSc])	0	0	0	92	92
	ASJ278/279 (dnaEx75/76[pF53:KCC-2-2:mSc])	0	0	0	174	174
Figure 4J	Strain	Microdomain	Apical-like	Other	Baso-like	Total (n)
	ASJ1133 (dnaEx454; nsIs228 I)	11	42	0	0	53
	ASj1024 (dnaEx454; nsIs228 I; kcc-3(ok228) II)	20	21	3	0	44
	ASJ931 (dnaEx410)	55	24	0	0	79
	ASJ1185 (dnaEx410; nsIs228 I; kcc-3(ok228) II)	41	6	0	0	47
Figure 4K	Strain	Microdomain	Apical-like	Other	Baso-like	Total (n)
	ASJ286 (dnaIs10[pF53:KCC-3:mSc])	54	0	0	0	19
	ASJ278/279 (dnaEx75/76[pF53:KCC-2-2:mSc])	0	0	0	174	174
	ASJ469 (dnaEx153[Chimera A])	0	0	0	86	86
	ASJ632 (dnaEx193[Chimera B])	0	0	0	27	27
	ASJ671 (dnaEx206[Chimera C])	0	0	14	0	14
	ASJ800	0	1	33	0	34
	ASJ1133 (dnaEx454; nsIs228 I)	11	42	0	0	53
	ASJ931 (dnaEx410)	55	24	0	0	79
	ASJ1015 (dnaEX446)	0	2	37	0	39
Figure S54D	Strain	Microdomain	Apical-like	Other	Baso-like	Total (n)
	ASJ278/279 (dnaEx75/76[pF53:KCC-2-2:mSc])	0	0	0	174	174
	ASJ744/754/764 (dnaEx252/257/302[p53:KCC2 LL>AA:mSc])	0	0	0	45	45
	ASJ878 (dnaEx386[p53:KCC2 del 1:mSc])	0	0	0	9	9
	ASJ934 (dnaEx413[p53:KCC2 del 2:mSc])	0	0	0	10	10
	ASJ286 (dnaIs10[pF53:KCC-3:mSc])	54	0	0	0	19
	ASJ792/793/794 (dnaEx314/315/316[pF53:KCC2 10AA:mSc])	29	1	0	0	30
	ASJ803/834/835 (dnaEx325/351/352[pF53:KCC2 20AA:mSc])	92	1	0	0	93
	ASJ745/746 (dnaEx253/254[p53:KCC3 ST>AA:mSc])	60	0	0	0	60
	ASJ820 (dnaEx339[p53:KCC3 CK:mSc])	5	0	0	0	5
	ASJ813 (dnaEx332[p53:KCC3 TTS>AAA:mSc])	19	0	0	0	19
	ASJ970 (dnaEx430[p53:KCC3 del 3:mSc])	8	0	0	0	8
	ASJ928 (dnaEx407[p53:KCC3 del 4:mSc])	11	0	0	0	11
	ASJ879/880 (dnaEx387/388[p53:KCC3 del 5:mSc])	19	1	0	0	20
	ASJ960 (dnaEx425[p53:KCC3 del 6:mSc])	8	0	0	0	8

Figure 5B	Strain	Microdomain	Apical-like	Baso-like	Total	
	ASJ30 (dnaEx6)	41	0	0	41	
	ASJ128 (dnaEx6; ttx-1(p767) IV)	84	3	0	87	
	ASJ583 (dnaIs10 V; dyf-11 (mn392) X)	0	30	0	30	
	ASJ129 (dnaEx6; tax-2(p691) I)	61	1	0	62	
	ASJ136 (dnaEx6; gcy-8(ns335) IV)	41	3	0	44	
Figure 5E	Strain	Condition	Microdomain	Apical-like	Baso-like	Total
	ASJ309 (dnaEx79; nsIs228 I; dnaIs10 V)	Mock	8	0	0	8
		Ablated	8	0	0	8
	ASJ306 (nsIs228 I; dnaIs10 V)	Mock	12	0	0	12
		Ablated	12	0	0	12
Figure 5F	Strain	Microdomain	Apical-like	Baso-like	Total	
	ASJ463 (dnaIs15 IV) 2X OUT	54	0	0	54	
	ASJ1074 (dnaIs15 IV; daf-19 (m86) II; daf-12 (sa204) X)	8	30	0	38	
	ASJ1075 (dnaIs15 IV; unc-101 (m1) I)	8	28	0	36	
	ASJ1098 (dnaIs15 IV; che-11 (e1810) V)	0	20	0	20	
	ASJ676 (dnaIs15 IV; osm-6(p811) V)	10	15	0	25	
	ASJ1111 (dnaIs15 IV; bbs-8 (nx77) V)	5	13	0	18	
	ASJ1105 (dnaIs10 V; osm-3 (p802) IV)	5	18	0	23	
	ASJ1094 (dnaIs15 IV; che-12 (e1812) V)	16	1	0	17	
	ASJ1102 (dnaIs15 IV; oig-8 (ot818) II)	9	4	0	13	
Figure 5G	Strain	Condition	Microdomain	Apical-like	Baso-like	Total
	ASJ134 (dnaEx28)		44	0	0	45
	ASJ277 (dnaEx28; che-1 (p678) I		23	1	0	24
	ASJ277 (dnaEx28; ceh-37 (ok642) X		45	1	0	46
	ASJ277 (dnaEx28; odr-7 (ky4) X		82	1	1	84
	ASJ308 (dnaEx28; ceh-36 (ky646) X		83	3	0	86
	ASJ824 (oyIs87 III; dnaIs15 IV)	Mock	2	0	0	2
		Ablated	2	0	0	2
	ASJ787 (kyIs104 X; dnaIs10 V)	Mock	6	0	0	6
		Ablated	6	0	0	6
	ASJ304 (kyIs140 I; dnaIs10 V)	Mock	13	0	0	13
		Ablated	13	0	0	13
Figure 4H/S4K	Strain	Condition	Microdomain	Apical-like	Baso-like	Total
	ASJ286 (dnaIs10 V)	DV	73	0	0	73
	ASJ583 (dnaIs10 V; dyf-11 (mn392) X)	DV	0	30	0	30
	ASJ691 (dnaEx221[pDYF-11:DYF-11:GFP])	ex-array	35	22	0	57
		non-ex	5	41	0	46
	ASJ1019/1023 (dnaEx450/453[pR102.2:DYF-11:GFP])	ex-array	29	28	0	57
		non-ex	1	47	0	48
	ASJ818/819 (dnaEx337/338[pGPA-3:DYF-11:GFP])	ex-array	26	6	0	32
		non-ex	0	17	0	17
	ASJ795/796 (dnaEx317/318[pTAX-4:DYF-11:GFP])	ex-array	15	13	0	28
		non-ex	0	24	0	24
	ASJ815/817 (dnaEx334/336[pFLP-19+pODR-1:DYF-11:GFP])	ex-array	12	13	0	25
		non-ex	0	19	0	19
	ASJ943 (dnaEx418[pR13H4.1+pCEH-36+pODR-10:DYF-11:GFP])	ex-array	32	29	0	61
		non-ex	0	46	0	46
	ASJ672/673 (dnaEx207/208[pODR-1:DYF-11:GFP])	ex-array	8	21	0	29
		non-ex	0	27	0	27
	ASJ804/805(dnaEx326/327[pODR-4:DYF-11:GFP])	ex-array	0	11	0	11
		non-ex	0	5	0	5
	ASJ583 (dnaIs10 V; dyf-11 (mn392) X)	compound	18	79	0	97
	ASJ701 (nsEx4394[pSRTXB:DYF-11:GFP])	compound	4	28	0	32
Figure S4A	Strain	Condition	Microdomain	Apical-like	Baso-like	Total
	ASJ30 (dnaEx6)	20 degrees	41	0	0	41
	ASJ30 (dnaEx6)	15 degrees	19	2	0	21
	ASJ30 (dnaEx6)	25 degrees	26	0	0	26

Figure S6A	Strain	Wildtype	Collapsed	Total			
	CX3553 (lin-15B&lin-15A(n765) kyIs104[str-1p::GFP] X)	163	**0**	163			
	ASJ237 (lin-15B&lin-15A(n765) kyIs104[str-1p::GFP] X); kcc-3(ok228) II)	167	0	167			
	OH3192 (ntIs1 [gcy-5p:GFP + lin-15 (+)] V)	93	**0**	93			
	ASJ229 (ntIs1 [gcy-5p:GFP + lin-15 (+)] V; kcc-3(ok228) II)	93	0	93			
	CX3695 (kyIs140 I)	116	**0**	116			
	OS3909 (kyIs140 I; kcc-3(ok228) II)	96	0	96			
Figure 6E	Isoamyl alcohol	Modified Chemotaxis Index					
	Strain\Date	2/24/21	3/25/21	4/30/21	5/7/21	5/14/21	Average
	N2	0.71	0.89	0.89	0.67	0.7	0.772
	OS9081 (nsIs228 I; kcc-3(ok228) II)	0.27	0.2	0.62	0.39	-0.05	0.286
	ASJ341 (nsIs228 I; kcc-3(ok228) II; dnaIs10 V		0.64	0.83		0.81	0.76
	OS1932 (nsIs109)		0.32		0.01	0.02	0.11666667
	ASJ114 (ttx-1(p767))				0.91	0.89	0.9
	Benzaldehyde	Modified Chemotaxis Index					
	Strain\Date	4/30/21	5/14/21	5/20/21	Average		
	N2	0.95	0.96	0.98	0.96333333		
	OS9081 (nsIs228 I; kcc-3(ok228) II)	0.47	0.48	0.69	0.54666667		
	ASJ341 (nsIs228 I; kcc-3(ok228) II; dnaIs10 V	0.92	0.98	0.89	0.93		
	OS1932 (nsIs109)		0.64	0.59	0.615		
	ASJ114 (ttx-1(p767))			0.96	0.96		
Figure 6F	Isoamyl alcohol	Chemotaxis Index					
	Strain\Date	4/4/23	5/3/23	5/9/23	5/11/23	Average	
	PY10421 (oyIs87 III)	0.87	0.92		0.95	0.91333333	
	LX1024 (kcc-3 (ok228) II)		0.41	0.53	0.5	0.48	
	ASJ1177 (oyIs87 III; dnaEx454 [Chimera G])	0.89	0.96	0.84		0.89666667	
	ASJ1218 (oyIs87 III; dnaEx454 [Chimera G]; kcc-3 (ok228) II)		0.58	0.63		0.605	

Figure S7B	1% methyl pyrazine	Modified Chemotaxis Index				
	Strain\Date	3/25/21	4/30/21	5/7/21	Average	
	N2	0.76	0.88	0.91	0.85	
	OS9081 (nsIs228 I; kcc-3(ok228) II)	0.31	0.22	0.22	0.25	
	ASJ341 (nsIs228 I; kcc-3(ok228) II; dnaIs10 V	0.53	0.66	0.55	0.58	
	OS1932 (nsIs109)	0.37		0.37	0.37	
	ASJ114 (ttx-1(p767))		0.67	0.84	0.755	
	0.1% Diacetyl	Modified Chemotaxis Index				
	Strain\Date	5/14/21	5/20/21	Average		
	N2	0.81	0.83	0.82		
	OS9081 (nsIs228 I; kcc-3(ok228) II)	0.12	0.25	0.185		
	ASJ341 (nsIs228 I; kcc-3(ok228) II; dnaIs10 V		0.51	0.51		
	OS1932 (nsIs109)	0.4	0.02	0.21		
Figure S7C	100 mM NaCl	Modified Chemotaxis Index				
	Strain\Date	3/11/21	3/25/21	4/30/21	5/7/21	Average
	N2	0.6	0.51	0.43		0.51333333
	OS9081 (nsIs228 I; kcc-3(ok228) II)	0.54	0.39	0.45		0.46
	ASJ341 (nsIs228 I; kcc-3(ok228) II; dnaIs10 V	0.47	0.64	0.34		0.48333333
	OS1932 (nsIs109)	-0.07	-0.22			-0.145
	ASJ114 (ttx-1(p767))			0.68	0.85	0.765
Figure S7D	Included in other behavior data					

Chapter 4

MISCELLANEOUS EXPERIMENTS

This chapter contains smaller experiments done during my graduate years that have not yet fit into a larger story. For each, I describe the rationale, methods, results, and interpretation.

RNAi screen for modulators of AFD shape

Our previous work shows that the cation chloride cotransporter (CCC) KCC-3 acts in the AMsh glia to modulate the shape of the AFD thermosensory neuron (Singhvi et al., 2016). CCCs often work with other members of its own family, as well as other ion channels and transporters to modulate cell volume (Figure 1A) (Payne, Rivera, Voipio, & Kaila, 2003). CCCs are also modulated by various kinases (Figure 1A) (Alessi et al., 2014). Here, I aimed to determine whether other ion transporters, channels, or kinases work with KCC-3 to affect AFD shape using an RNAi screen. Briefly, I bleach synchronized young animals that have their AFD neurons labeled with GFP, and then raised them on RNAi bacteria. I then assessed AFD for WT, messy, and collapsed shape in Day 1 adults. I used an empty vector control to control for the effect of the RNAi itself, and PROS-1 RNAi, which significantly shortens AFD NRE shape (Wallace et al., 2016), and KCC-3 RNAi as positive controls. In total, I assessed 24 different RNAi constructs (Figure 1B). 2 of these, DELM-1 and NKCC-1, showed a significant effect on AFD shape compared to empty vector controls (Figure 1C). I subsequently assessed putative null alleles of these genes, but failed to see an effect of either *delm-1* or *nkcc-1* on AFD shape (Figure 1D-E). To understand the discrepancy between the RNAi and mutant alleles, I sequenced the RNAi clones. DELM-1 sequenced properly; however, the NKCC-1 clone sequenced to the uncharacterized C42D4.2 protein. This suggests that C42D4.2, rather than NKCC-1, affects AFD

shape. That DELM-1 RNAi and the mutant *delm-1* allele had differing effects on AFD shape is perplexing. One possibility is that off-target effects of the DELM-1 RNAi caused AFD shape defects, and that genes sequencially similar to DELM-1, but not DELM-1 itself, affects AFD shape.

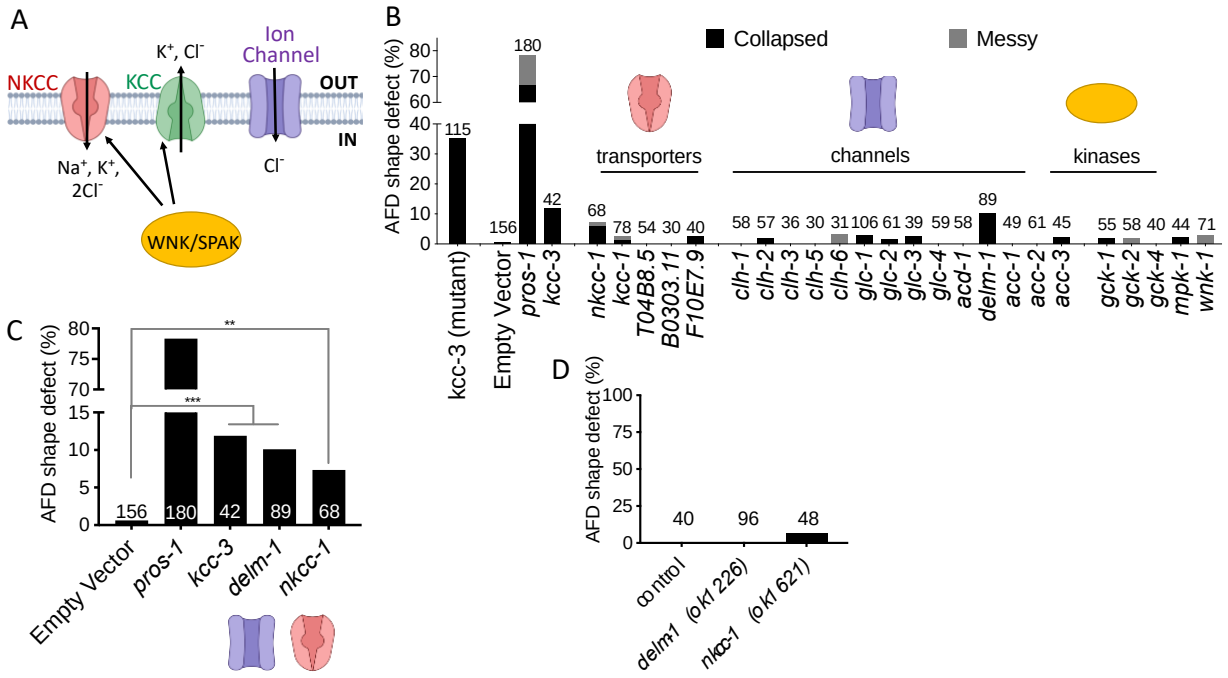

FIGURE 1: RNAi screen of ion transporters, channels, and kinases for AFD shape defect

(A) Schematic of how ion transporters, channels, and kinases work together to modulate cell volume. **(B)** RNAi screen of 24 candidate genes. **(C)** Two potential hits, *delm-1* and *nkcc-1*, along with controls empty vector, *pros-1*, and *kcc-3*. **(D)** Mutations in *delm-1* and *nkcc-1* failed to show significant AFD microvilli defects compared to WT animals. ** $p < 0.01$, *** $p < 0.001$, Fisher's exact test.

RNAi of WNK-1 on AFD shape

WNK-1 is known to affect CCCs in other systems (Alessi et al., 2014). We asked if WNK-1 regulates AMsh glial KCC-3 through activation, inhibition, or neither, using AFD shape as a metric (Figure 2A). To assess if WNK-1 activates KCC-3, we asked if WNK-1 RNAi shortens AFD shape in wildtype animals (Figure 2B). To assess if WNK-1 inhibits KCC-3, we asked if WNK-1 RNAi rescues AFD shape in a *pde-1* mutant background, in which animals have short AFD NREs (Figure 2C). We found that that AFD shape did not differ in either of these experiments compared to empty vector controls. While initially surprising, we subsequently noted that *C. elegans* KCC-3 does not have canonical WNK-1 binding or phosphorylation sites (Chapter 3, Figure S3C-E) and does not affect localization (Chapter 3, Figure S3A). Together this suggests that WNK-1 does not regulate AMsh KCC-3. Future work can focus on identifying novel modulators of KCC-3 and AFD shape.

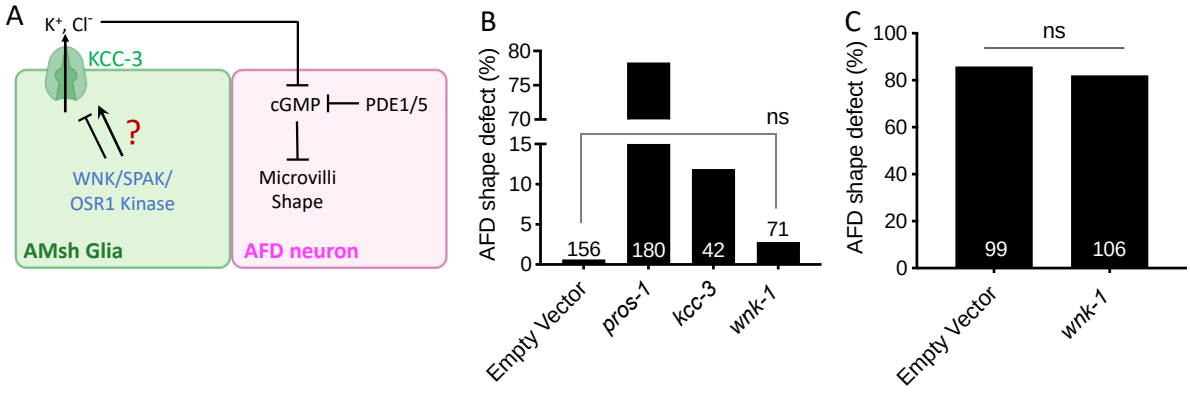

FIGURE 2: RNAi of WNK-1 on AFD shape

(A) Schematic of KCC-3 regulation of AFD microvilli shape. **(B)** RNAi of WNK-1 in WT animals. **(C)** RNAi of WNK-1 in *pde-1* mutant animals.

AFD shape in kcc-3 *mutants using different AFD markers*

Our previous work showed that *kcc-3* mutants have defects in AFD NRE shape (Singhvi et al., 2016). To verify that changes in AFD shape is not due to the particular marker used, I assessed AFD shape in *kcc-3* mutants using various AFD markers made in the lab. The original work was done using a cytosolic AFD GFP marker expressed under the P_{srtx-1} promoter (nsIs228), which shows expression in both AFD neurons and AWCR. P_{srtx-1} was subsequently promoter-bashed to make a $P_{srtx-1b}$ promoter that only expresses in the AFD neurons. Under the $P_{srtx-1b}$ promoter, we express both a cytosolic GFP marker (nsIs373) and a fusion SRTX-1:GFP protein (nsIs645), which only labels AFD NRE microvilli. I assessed AFD shape in both wildtype and *kcc-3* mutant animals in all three of these strains. Interestingly, AFD shows about a 50% reduction in NRE shape defects in *kcc-3* mutants with either cytosolic (nsIs373) or fusion (nsIs645) GFP markers expressed under the $P_{srtx-1b}$ promoter compared to the P_{srtx-1} promoter (Figure 3A). This suggests that the larger P_{srtx-1} promoter (1261 bp) may contribute to AFD shape defects compared to the $P_{srtx-1b}$ promoter (493 bp). Alternatively, the integration process of nsIs228 may have introduced a closely linked mutation that affects AFD shape. Regardless, studying this data closely may reveal additional mechanisms of AFD NRE shape regulation.

Engulfment in kcc-3 *mutants*

We previously found that AMsh glial engulfment modulates AFD NRE shape (Raiders et al., 2021). We wondered whether short microvilli seen in *kcc-3* mutants arise from changes in AMsh glial engulfment. Here, I used the AFD-specific GCY-8 GFP-labeled fosmid to assess the level of engulfment in *kcc-3* mutant animals. Briefly, as established previously in the lab (Raiders et al., 2021), I binned the number of GFP+ puncta in the AMsh cell body of wildtype

and *kcc-3* mutant animals into four categories: normal (10+), moderate (5-9), scant (1-4), and none (0). I assessed engulfment in Day1 animals of both genotypes, and in L4 animals of just *kcc-3* mutant animals. Compared to wildtype controls, *kcc-3* mutants show significantly less engulfment in Day 1 animals (Figure 3B). Engulfment in *kcc-3* mutants is also similar for Day 1 and L4 animals (Figure 3B). We conclude that, in L4 larvae and early adults, increased pruning by AMsh glia does not drive short microvilli in *kcc-3* mutants. However, this does not preclude a role for increased pruning on AFD NRE shape in *kcc-3* mutants earlier in development. Further, the decreased pruning in L4 larvae and Day 1 adults may be an effect of shorter microvilli to engulf in *kcc-3* mutants.

KCC-3 localization in miscellaneous mutants

I have tested additional mutants for their effect on KCC-3 localization. The *efn-1* ephrin ligand and *vab-1* ephrin receptor were previously identified in the lab to disrupt AFD shape. As such, I wondered if putative null alleles of these genes affect KCC-3 localization, with downstream effects on AFD NRE shape. I found that KCC-3 localizes to an apical microdomain in these animals, similar to wildtype controls, suggesting that the ephrin system does not guide KCC-3 localization (Figure 3C). *fig-1* is a thrombospondin-like extracellular protein secreted by AMsh glia that affects dye-filling, a glia-dependent property of some *C. elegans* neurons to uptake lipophilic dyes, and behavior mediated by some amphid neurons (Bacaj, Tevlin, Lu, & Shaham, 2009). Interestingly, I found that *fig-1* drastically affects KCC-3 localization. The *ns305* point mutation leaves apical-like localization intact, but spreads KCC-3 beyond its microdomain. The larger *tm2079* mutation, however, abolishes apical-like or microdomain KCC-3 localization. This suggests that the FIG-1 AMsh protein guides KCC-3 to a microdomain and future work can

focus on further understanding the interaction between FIG-1 and KCC-3. In addition, future work could assess whether FIG-1 also guides localization of other AMsh proteins as well. *sma-1* is an ortholog of beta(H)-spectrin that affects AMsh glial shape and apical-domain polarity (Martin, Bent, & Singhvi, 2022). I find that KCC-3 microdomain localization remains intact in *sma-1* putative null animals, suggesting that, while spectrins play a role in broad AMsh polarity, they are not involved in localizing proteins to a smaller microdomain.

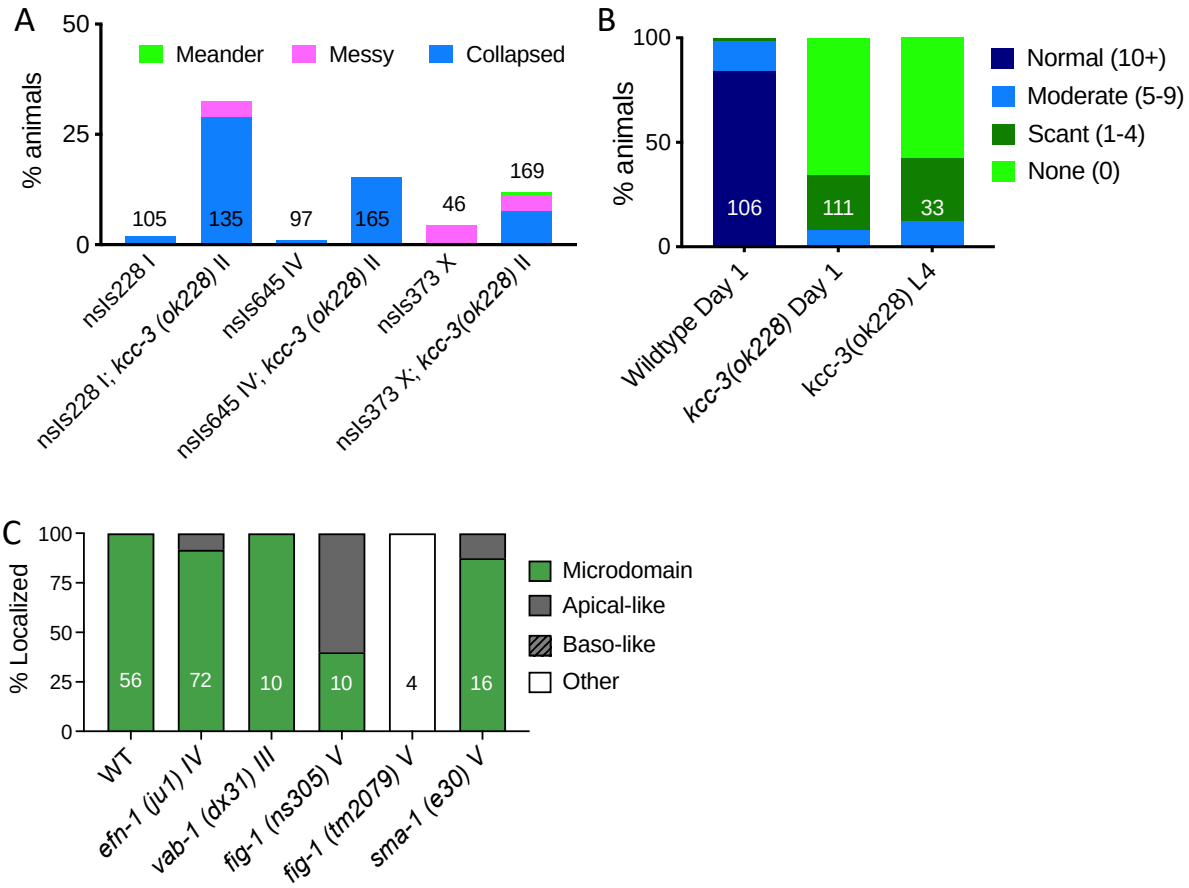

FIGURE 3: Miscellaneous quantification

(A) Assessment of neuron shape in *kcc-3 (ok228)* mutants using different AFD markers. **(B)** Quantification of engulfment puncta seen in WT and *kcc-3* mutant animals, at stages L4 and Day1. **(C)** KCC-3 localization quantification of additional miscellaneous mutants.

Localization of AMsh KCC-3 to AFD cilia

My thesis work shows that KCC-3 does not localize to the ciliated NREs of non-AFD neurons (Chapter 3). AFD too has a pseudo-ciliated process (Doroquez, Berciu, Anderson, Sengupta, & Nicastro, 2014). To determine whether KCC-3 localizes to the AFD cilia, I assessed colocalization between fluorescently labeled AMsh KCC-3 and DYF-11:GFP expressed under the $P_{srtx\text{-}1b}$ promoter, which labels the cilia of only AFD neurons. I found that AMsh KCC-3 does localize around AFD cilia (Figure 4A-A"). This suggests that the cilia of AFD is distinct from those of other amphid neurons. This distinction is intriguing, and may allow for a way to identify the ciliary signal that localizes KCC-3. For example, future work could compare cilia-related genes between AFD and other amphid neurons using RNA sequencing approaches. The resulting dataset could then guide a candidate screen of cilia genes on KCC-3 localization.

Expression of an AMsh golgi marker

Aakanksha had previously made a Golgi marker (MANS:mCherry) expressed under the T02B11.3 AMsh promoter. When imaging this strain, I noted that Golgi in the anterior glia has a glial apical boundary (GAB) (Figure 4B), similar to KCC-3 and other apical markers. It would be interesting to assess whether Golgi and other members of the endosomal system regulate GAB in the future.

Dual images of AMsh basolateral markers and non-AFD amphid neurons

I wanted to investigate whether other amphid neurons are apically or basolaterally localized. I made strains colabeling AWC and the AMsh basolateral marker (Figure 4C-C") and AWA and the AMsh basolateral marker (Figure 4D-D") showing that the NREs of these neurons

do not localize to basolateral membranes. Future work can colabel these neurons with apical membrane markers to confirm that they localize to apical membranes.

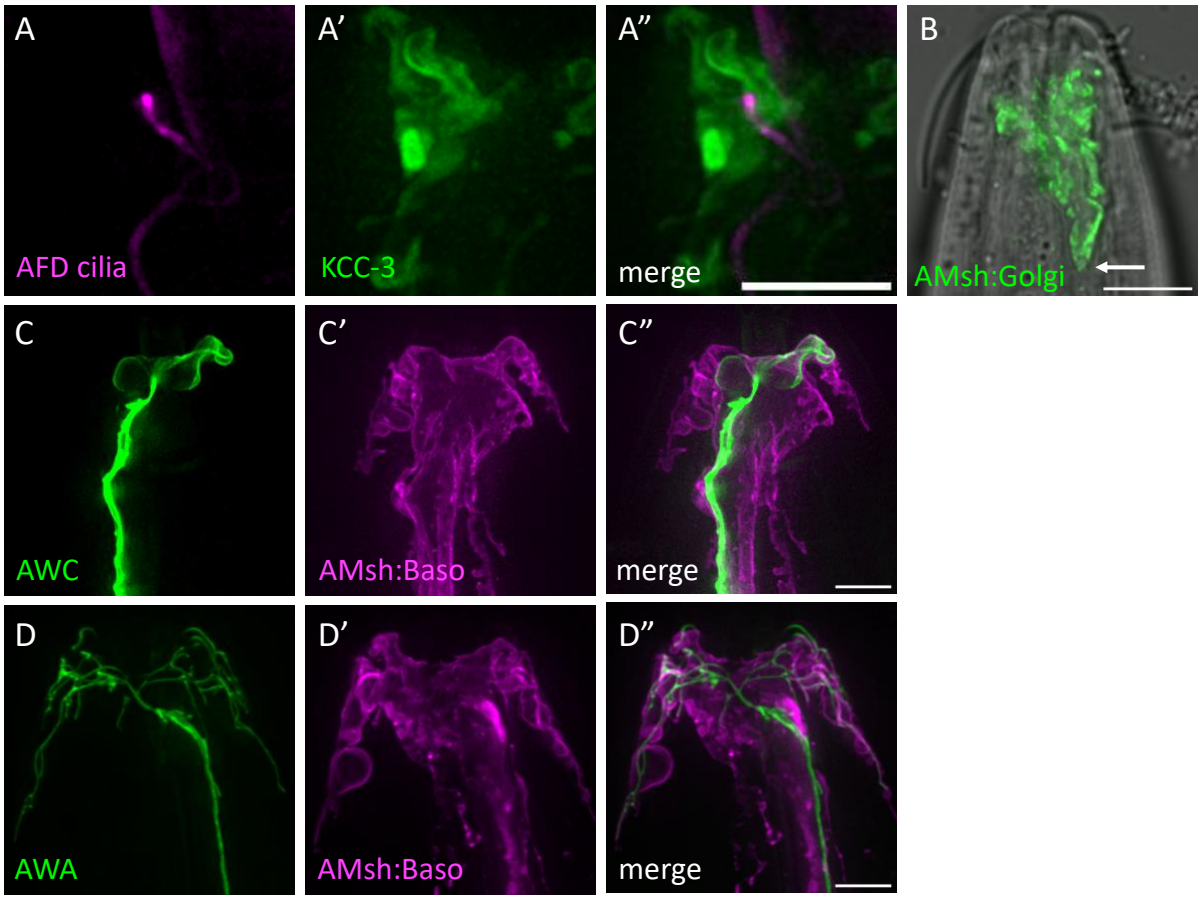

FIGURE 4: Miscellaneous images

(A-A") Localization of AMsh KCC-3 to AFD cilia. **(B)** Expression of a Golgi marker under an AMsh promoter. White arrow points to the GAB. **(C-C")** Expression of a AWC marker and AMsh:basolateral marker. **(D-D")** Expression of a AWC marker and AMsh:basolateral marker. All scale bars 5um.

Chapter 5

DISCUSSION

This thesis has focused on understanding the specificity of glia-neuron interactions, using the cation chloride transporter KCC-3 in *C. elegans* AMsh glia as a model. In Chapter 2, I share a publication that collates our current knowledge on how peripheral glia use ionic regulation to regulate sensation, with emphasis on scholarly gaps. In Chapter 3, I discussed my work on how the *C. elegans* AMsh glia localizes KCC-3 to a microdomain around just AFD NREs. My dissertation work makes the following contributions to my scientific field:

(1) The first description of a glial molecule (KCC-3) that localizes to just one associated neuron (AFD). KCC-3 does not localize to an anatomical feature of AMsh glia, such as the amphid channel, making this an unique case of glia-neuron specificity.

(2) Identification of a novel mode of polarity in glial cells, the glial apical boundary (GAB), disparate from classic apical-basolateral polarity.

(3) Cilia of non-AFD neurons direct KCC-3 localization to a microdomain.

(4) Structure-function analysis of KCC proteins, including identification of a novel N-terminal basolateral targeting sequence of KCC-2, and a two-part localization sequences for the microdomain localization of KCC-3. The latter involves a central sequence that guides KCC-3 to apical-like adneuronal membrane, and a C-terminal sequences that guides KCC-3 to a microdomain.

(5) The microdomain-localized KCC-3 affects neurons contained within the microdomain and neurons outside of the microdomain.

In this discussion, I expand on these findings and contextualize them with current knowledge in the field. I further discuss pressing questions, future experimental directions, and implications of these findings in the broader scientific world.

The glial apical boundary (GAB)

Along with others (Low et al., 2019; Martin, Bent, & Singhvi, 2022), I found that markers that express in an apical domain in canonical epithelia also localize to an unique domain in AMsh glia. However, this domain is not bounded by junctional proteins, as apical proteins are in epithelia (Rodriguez-Boulan & Macara, 2014). This suggests that the polarity attained by the GAB is distinct from that of classic tight junction mediated polarity. This further suggests that AMsh glia have two simultaneous modes of polarization happening in one cell, tight junction-mediated polarity established by AJM-1 and a novel mode of polarity at the GAB. This is reminiscent of how some sensory neurons have both apical-basolateral polarity and axon-somatodendritic polarity, or how epithelia exhibit both apical-basal polarity and planar cell polarity. To the former, sensory neurons such as mammalian olfactory receptor neurons and photoreceptor cells have sensory endings that form tight junctions with the epithelia they protrude through, suggesting apical-basal polarity, while also having an axonal segment which is distinct from the somatodendritic compartment (Liang, 2020; Mehalow et al., 2003). To the latter, epithelia have apical-basolateral polarity, and PCP that occurs orthogonally to the apical-basolateral axis (Rodriguez-Boulan & Macara, 2014). Thus, multiple modes of polarity can occur in one cell.

How is the GAB is regulated and organized? In neurons, the dendrosomatic and axonal domains are kept separate and distinct by the axon initial segment (AIS). The AIS is comprised

of scaffolding proteins, with ankyrinG as a central component, bound to actin/spectrins on one side and microtubules on the other (Hedstrom, Ogawa, & Rasband, 2008; Leterrier, 2018). While I have not looked at colocalized expression of the beta-spectrin SMA-1 and KCC-3, SMA-1 expression appears anterior to the GAB (Martin et al., 2022), suggesting that spectrins may not underlie GAB regulation. Future work could screen through known scaffolding proteins (PDZ or SH domain proteins), actin/microtubule binding proteins (FERM domain proteins or microtubule-associated proteins), and other spectrins, first for expression in glia and then for localization to the GAB domain. Both localization to and maintenance of the AIS requires endocytosis to remove proteins from where they do not belong (Eichel et al., 2022). Future work can also examine the localization of endosomal pathway components in relation to the GAB and ask how KCC-3 or the apical PH-PLC marker act when endosomal pathway components are disrupted. This can provide a basic understanding of how the GAB is regulated. Curiously, Golgi markers express in the anterior glia, with a stop similar to where the GAB is (Chapter 4, Figure 4B). It would be interesting to investigate closely how these organelles, along with the ER, localize in the anterior glia, and whether the localization of these organelles is what determines the GAB.

Another question is whether other *C. elegans* glia have a structure like GAB. I found that other C elegans glia, such as the CEPsh and PHsh glia, also localize KCC-3 to an anterior microdomain. Future work could look at how apical markers, such as truncated SAX-7 and PH-PLC, or tight junction markers, such as AJM-1 and DLG-1, localize in these other glia. If these glia also show localization of apical markers without tight junction demarcation, this may suggest that GAB is a fundamental feature of *C. elegans* glia. If so, future work can assess

whether GAB across glia are regulated using similar or distinct mechanism and can help elucidate glial heterogeneity.

The AMsh glia makes apical junctional complexes with sensory neurons, similar to sustentacular cells in the olfactory/vomeronasal systems in vertebrates or Muller glia in the retina (Heiman, 2022). Based on our findings, it may be interesting to assess whether these cells have other forms of polarity similar to the GAB. Polarity in other glial cells is also understudied. In the developed brain, astrocytes and oligodendrocytes form multiple irregular processes that contact other cell types and how these branches form and are polarized towards other cells is unknown. As these cells do not form classic apical junctions, our findings about an alternate form of polarization with GAB may guide our understanding of polarization in other cell types as well. The ease of screens and genetic manipulation in *C. elegans* can further streamline our understanding of broad glial polarity rules by studying AMsh GAB.

KCC proteins and their localization

Despite their disease relevance, not much is known about how KCC proteins localize. Localization of chloride ion regulators like proteins in the cation chloride cotransporter (CCC) family or CFTR is crucial for proper ion homeostasis of cells (Chamma, Chevy, Poncer, & Lévi, 2012). Further, defects in chloride ion regulation is associated with hearing loss, seizures, retinal degeneration, and cystic fibrosis (Kahle et al., 2015; Liou, 2019; Ray & Singhvi, 2021). In my thesis work, I found that KCC-2 localizes basolaterally in AMsh glia, and that the first 41AA of the KCC-2 N-terminus can direct KCC-3 to basolateral membranes. I further found that swapping the first 20 AA of KCC-3 with KCC-2 leaves the chimera with apical microdomain localization patterns, suggesting that 21-41 AA of KCC-2 drive basolateral localization. This 19

AA does not have obvious similarities with the 91 AA sequence of full-length SAX-7 that directs basolateral localization (Lillis, Zaccardi, & Heiman, 2022). This sequence also does not have conserved tyrosine-based basolateral targeting motifs, and mutation of a dileucine motif does not disrupt KCC-2 localization. This suggests that KCC-2 may be guided to basolateral-like AMsh glial membranes using a novel pathway. Additionally, this suggests that AMsh glia may have multiple modes of localizing proteins to its basolateral-like abneuronal membranes. A final future experiment could involve deleting the 21-41AA of KCC-2 to assess sufficiency of this site in directing KCC-2 basolateral localization.

I additionally found that a KCC-3 sequence between 390-915 AA localizes KCC-3 to apical-like adneuronal membranes, and that a proximal C-terminal sequence between 910-1002 AA localizes KCC-3 to an apical microdomain. Further, microdomain localization requires prior apical membrane localization. The 390-915 AA region of KCC-3 includes 4 glycosylation sites, which could drive adneuronal membrane localization. Similarly, the 910-1002 AA region of KCC-3 includes myristolation sites, which could drive microdomain localization. Future work could involve generation of additional chimeras and site-directed mutagenesis to identify shorter localization motifs, which could also inform localization mechanisms. Curiously, *C. elegans* KCC-3 does not have any of the homologous regulatory phosphorylation or kinase binding sites seen in human or rodent KCC-3 (this study; Blaesse, Airaksinen, Rivera, & Kaila, 2009). Thus, we could also use a proximity ligation assay to identify novel KCC regulators. Briefly, I can tag the C-terminal of KCC-3 with the biotin ligase enzyme TurboID, raise animals on biotin-rich bacteria, lyse animals and capture biotinylated proteins on streptavidin-coated beads, and run biotinylated proteins through mass spectroscopy to identify tagged proteins. This method has been successfully performed on intact *C. elegans* (Sanchez & Feldman, 2021), and tagging the

C-terminus will preferentially biotinylate proteins that are important for microdomain localization.

KCCs show polarized and microdomain localization in other systems. KCC-3 localizes to the microvilli of Schwann cells in mice, and on membranes of Deiter's and inner phalangeal cells facing hair cells (Sun, Lin, Tzeng, Delpire, & Shen, 2010; Zdebik, Wangemann, & Jentsch, 2009). Future experiments can ask if mutation of homologous regions of the KCC-3 C-terminal also disrupts localization in these systems. As KCC localization is understudied, this could provide valuable information about KCC regulation across systems.

Neuron cilia guide KCC-3 to a microdomain

In my thesis, I discovered that the neuron cilia constrain KCC-3 to a microdomain around AFD. I found that the IFT process, with anterograde IFTA-mediated transport and retrograde IFTB-mediated transport, are both crucial for KCC-3 localization. However, IFT controls all known aspects of cilia development and function, and the exact ciliary mechanism remains unknown.

In cilia mutants, KCC-3 localizes beyond its AFD microdomain and into the wings of AMsh glia. When both KCC-3 and an apical membrane marker is labeled in AMsh glia in *dyf-11* cilia mutants, KCC-3 colocalizes with the apical membrane marker near AFD. However, KCC-3 localizes in globules within the apical membrane marker in the AMsh glia wings. When KCC-3 is expressed with a cytoplasmic glial marker, these also do not colocalize. Thus, I hypothesize that KCC-3 may be stuck in vacuoles or vesicles in the AMsh wings in cilia mutants. This can be assessed in the future by co-labelling KCC-3 with different markers in the endosomal system, such as those for the ER, Golgi, RAB-5+ early endosomes, RAB-7+ late endosomes, and RAB-

11+ recycling endosomes. Interestingly, previous work found that a lack of neuron cilia causes branching outpockets of the amphid channel and disrupted channel protein localization (Perens & Shaham, 2005). In particular, VAP-1:GFP vacuoles accumulate within the sheath glia in *daf-19* cilia mutants. Thus, one hypothesis is that neuronal cilia interact with the glial endosomal system to localize microdomain proteins. This may involve cilia directing vesicles of microdomain proteins to the lysosomal degradation pathway or recycling endosomes, when found outside its microdomain. The cilia may also guide sorting of vesicles to their appropriate final destination.

There are many molecular mechanisms by which cilia could direct glial KCC-3 microdomain localization. *tax-2* mutants show normal KCC-3 localization, suggesting that neuron activity, driven primarily by cilia in *C. elegans*, does not guide KCC-3 localization. To bolster this finding, we could assess KCC-3 localization in additional neuron activity mutants, such as *tax-4, osm-9,* and *ocr-2,* and after chemogenetic manipulation of neuron activity using histamine-gated cation and chloride channels (Martin et al., 2022; Venkatachalam & Montell, 2007). Mutant cilia still produce extracellular vesicles (EVs) that are subsequently endocytosed by AMsh glia (Razzauti & Laurent, 2021); however the content of these EVs are reportedly distinct in cilia mutants compared to wildtype animals (Piali Sengupta, personal communication). Thus, altered EV content could contribute to KCC-3 mislocalization in cilia mutants. To test this, we could test how KCC-3 localizes in mutants for known cargo in ciliary EV, such as tetraspanin-6/7 (Razzauti & Laurent, 2021). A remaining possibility is that a ciliary protein could physically disrupt KCC-3 localizing to their membranes, either directly or indirectly through another glial protein. I found that multiple sets of amphid cilia could rescue KCC-3 localization in *dyf-11* mutants. As such, the ciliary signal could be one that is

ubiquitously expressed by amphid cilia. Alternatively, as all non-AFD ciliary NREs are exposed to an interconnected extracellular space, another possibility is that the ciliary signal is a secreted molecule.

There are a few unbiased ways to identify the ciliary signal involved in KCC-3 localization, if the above limited experiments fail. First, future work could involve a forward genetic screen in WT animals with AMsh KCC-3 labeled, identifying mutants that look like KCC-3 in *dyf-11* or other cilia mutants. However, a caveat of this method is that it will likely identify genes involved in general cilia regulatory processes. A dye-fill assay, wherein animals with defective cilia fail to uptake fluorescent dyes, can be used to screen through general cilia defects. Alternatively, we could perform bulk RNAseq of $P_{ODR\text{-}1}$:DYF-11, $P_{R102.2}$:DYF-11, and *dyf-11* mutant animals, and look for genes that both rescues have in common that are distinct from the mutant animals. This way we could screen out neuron specific genes, while still enriching for ciliary genes. We could then select against general IFT proteins and perform a reverse genetic RNAi screen of putative ciliary cargo genes, enriching for membrane and secreted proteins.

Many neurons have a primary cilium, often on their cell bodies. A single astrocyte can enwrap 4-6 neuron cell bodies (Chung, Welsh, Barres, & Stevens, 2015), suggesting that they may encounter multiple cilia of different neurons. How neuronal cilia in other systems affect glia is not known. However, as cilia are signaling hubs (Green & Mykytyn, 2014), it would not be surprising that neuron cilia affect glial properties in other systems as well.

How does KCC-3 modulate non-adjacent neurons?

KCC-3 affects the shape and function of AFD NREs, which it localizes to. Interestingly, I found that KCC-3 also regulates behavior, but not shape, mediated by neurons outside of its microdomain. How does a glial molecule affect a neuron it does not localize to?

There are a few potential mechanisms that could lead to this phenotype. One possibility is that lack of KCC-3 affects glial organization of microdomains, which could then affect the function of non-contacting neurons. Evidence from my thesis suggests that AMsh glial microdomains affect one another. Mutations in proteins that localize to the channel microdomain, such as LIT-1, CHE-14, and DAF-6, cause KCC-3 mislocalization. *kcc-3* mutants additionally alter VAP-1 expression patterns. Thus, lack of KCC-3 may disorder neighboring microdomains, including those around wing neurons. Another possibility is that lack of KCC-3 affects glial physiology. To test this, future work could assess calcium signals in AMsh glia in WT and *kcc-3* mutant animals and assess if there is a difference in calcium levels in basal conditions or in response to stimuli. Finally, as KCC-3 is a transporter, a lack of KCC-3 may affect global ionic homeostasis of AMsh glia, which can subsequently affect glial cell size. The extracellular space between AMsh glia and amphid neurons, especially wing neurons, is thought to be quite short (Perkins, Hedgecock, Thomson, & Culotti, 1986). Thus, any changes to ionic balance or glial cell size may be enough to affect wing neuron function, while not enough to disrupt shape. Channel neurons, with more extracellular space around their NREs (Perkins et al., 1986), may be less sensitive to changes to glial ionic homeostasis. Future work can assess electron micrographs of WT and *kcc-3* mutant animals to discern whether there are quantifiable differences in AMsh glial size.

Glia-neuron specificity in other systems

My thesis work has fueled my curiosity about glia-neuron specificity in other systems. One thing I would love to investigate is whether glia in other systems have asymmetric distribution of synaptogenic or transporter proteins in their NRE-adjacent processes. This can be assessed through immunohistochemistry or immunocytochemistry assays in astrocytes, retinal pigment epithelia (RPE), or taste buds from tissue samples or culture models. In addition, as astrocytes have RNA in their PAPs, future work could involve *in situ* hybridization to identify heterogeneity in these NRE-adjacent glial RNAs. Finally, it would be interesting to assess if RPE cells disproportionately engulf rod or cone NREs. One way to assess this is to label cone and rod photoreceptors using different fluorescent cytoplasmic or membrane probes, and then measure the prevalence of these fluorescent proteins in RPE cells. All of these endeavors would inform us qualitatively of glia-neuron specificity, but understanding the mechanistic underpinnings of any glial asymmetry would be difficult to gather in any of the above systems.

Conclusion

I spent my graduate years trying to understand glia-neuron specificity, using the *C. elegans* AMsh glial KCC-3 as a model. Overall, this effort has proven fruitful, and has uncovered a novel mode of glial polarity, a role of cilia in glia-neuron specificity, and structure-function analysis of KCC proteins. Further, this thesis has produced an even greater number of remaining questions, including mechanisms of GAB polarity, ciliary control of glial KCC-3, and how KCC-3 controls function of distal neurons. In all, my hope is that this thesis fuels future experimental endeavors in the realm of glia-neuron interactions in *C. elegans* and beyond.

APPENDIX

This appendix includes raw data for all experiments contained in Chapter 4. Tables 1 and 2 correspond to Chapter 4 Figure 1. Tables 1 and 3 correspond to Chapter 4 Figure 2. Tables 4-6 correspond to Chapter 4 Figure 3.

Table 1: RNAi screen of transporters, channels, and kinases for defective AFD shape (nsIs228)

Kcc-3 Related RNAi Screen					
Summary: L1 RNAi screen for factors that may work with KCC-3 to affect AFD morphology.					
Doing screen on nsIs228 and scoring day 1 adults for collapsed AFD.					
Exp #	Date	RNAi bacteria	AFD collapsed (#)	AFD messy (#)	n = animals
1	4/18/18	GFP	0	0	5
		pros-1 (positive control)	1	0	1
		kcc-3 (positive control)	0	0	5
		kcc-1	1	1	48
		mpk-1	0	0	2
		wnk-1	0	1	7
2	4/20/18	pros-1 (positive control)	20	12	48
		kcc-3 (positive control)	2	0	10
		nkcc-1	4	1	17
		mpk-1	1	0	42
		wnk-1	0	1	37
3	4/25/18	empty vector (negative control)	0	0	56
		pros-1 (positive control)	20	5	28
		acd-1	0	0	58
		T04b8.5	0	1	55
		clh-2	1	0	57
		gck-2	0	2	59
		gck-1	1	0	55
		clh-6	0	1	31
4	5/2/18	GFP	1	0	31
		pros-1 (positive control)	15	2	23
		glc-2	1	0	61
		acc-1	0	0	49
		delm-1	3	0	62
		clh-3	0	0	36
		clh-5	0	0	31
		B0303.11	0	0	30
6	5/11/18	empty vector (negative control)	0	0	40
		pros-1 (positive control)	21	0	27
		glc-4	0	0	59
		acc-2	0	0	61
		clh-1	0	0	58
7	5/18/18	empty vector (negative control)	0	0	39
		pros-1 (positive control)	26	0	28
		kcc-3 (positive control)	3	0	27
		nkcc-1	0	0	51
		kcc-1	0	0	30
		wnk-1	0	0	27
		delm-1	6	0	27
8	5/23/18	empty vector (negative control)	1	0	31
		pros-1 (positive control)	20	2	28
		F10E7.9	1	0	40
		gck-4	0	0	40
		acc-3	1	0	45
		glc-3	1	0	39
		glc-1	3	0	41

Table 2: RNAi screen of transporters, channels, and kinases for defective AFD shape (nsIs645)

Repeated L1 RNAi for AFD morphology using nsIs645. ALL BLINDED!						
Exp #	Date	RNAi bacteria	AFD collapsed (#)	AFD messy (#)	AFD Short (#)	n = animals
1	9/24/18	empty vector (negative control)	0	0	0	66
		pros-1 (positive control)	20	30	4	68
		glc-1	0	0	0	59
2	10/12/18	empty vector (negative control)	0	0	0	27
		pros-1 (positive control)	9	7	0	27
		glc-1	0	0	0	34

Table 3: RNAi screen of WNK-1 in a *pde-1/5* mutant background

***pde-1/5* mutant WNK-1 RNAi**						
Summary: L1 WNK-1 RNAi on OS8638 [nsIs373; *pde-1(nj57) pde-5(nj49)I*].						
Does WNK-1 knockdown rescue AFD microvilli defects in *pde-1/5* mutant backgrounds.						
Essentially seeing if WNK-1 plays a role in determining AFD shape.						
Exp #	Date	RNAi bacteria	AFD collapsed (#)	AFD messy (#)	AFD short mv (#)	n = animals
1 (non-blinded)	9/24/18	empty vector	19	10	0	32
		wnk-1	21	6	0	34
1 (blinded)		empty vector	32	1	0	38
		wnk-1	38	2	2	46
Exp #	Date	RNAi bacteria	Countable mv (#)	Blebby (#)	Intermediate/collapsing (#)	n = animals
2	10/12/18	empty vector	6	16	7	29
		wnk-1	8	10	8	26

Table 4: AFD shape of *kcc-3* mutants with varied AFD markers

Neuron Shape scores					
All raised at 20 deg, 2 gen not starved and scored at Day 1 unless noted					
All sig compared to bolded control at top of section, unless noted					
Strain	Wildtype	Collapsed	Messy	Meander	Total
OS4565 (nsIs228 I)	103	2	0	0	105
OS9081 (nsIs228 I; kcc-3(ok228) II)	91	39	5	0	135
OS10884 (nsIs645 IV)	96	1	0	0	97
ASJ191 (nsIs645 IV; kcc-3(ok228) II)	143	22	0	0	165
OS7270 (nsIs373 X)	44	0	2	0	46
ASJ228 (nsIs373 X; kcc-3(ok228) II)	149	13	6	1	169

Table 5: Engulfment of WT and *kcc-3* mutant animals

Engulfment Scoring									
Date	Starved?	Strain	Temperature Raised	Age	10+	5-9	1-4	0	comments
1/14/20	no	483	20 degrees	Day 1	31	5	0	0	tiny bit contamination
2/27/20					30	5	0	0	
3/12/20					28	5	2	0	
1/14/20	no	483; kcc-3	20 degrees	Day 1	0	5	21	46	
1/16/20					0	4	8	27	
3/17/20	no	483; kcc-3	20 degrees	L4	0	4	10	19	

Table 6: KCC-3 localization of miscellaneous mutants

KCC-3 localization scores					
All raised at 20C, scored at day 1 adults, not starved at least 1 wk unless noted					
(only those on score sheets counted)					
Strain	Subapical	Apical	Basolateral	Other	Total (n)
ASJ463 (dnaIs15 IV) 2X OUT	54	0	0	0	54
ASJ358 (dnaIs10 V; nsIs228 I; efn-1(ju1) IV	66	6	0	0	72
ASJ368 (dnaIs10 V; nsIs228 I; vab-1 (dx31) II)	10	0	0	0	10
ASJ1103 (dnaIs15 IV; fig-1 (ns305) V)	4	6	0	0	10
ASJ1103 (dnaIs15 IV; fig-1 (ns305) V)	0	0	0	4	4
ASJ1068 (dnaIs15 IV; sma-1 (e30) V)	14	2	0	0	16

REFERENCES

Chapter 1

Agarwal, A., Wu, P. H., Hughes, E. G., Fukaya, M., Tischfield, M. A., Langseth, A. J., … Bergles, D. E. (2017). Transient Opening of the Mitochondrial Permeability Transition Pore Induces Microdomain Calcium Transients in Astrocyte Processes. *Neuron*, *93*(3), 587-605.e7. https://doi.org/10.1016/j.neuron.2016.12.034

Alessi, D. R., Zhang, J., Khanna, A., Hochdörfer, T., Shang, Y., & Kahle, K. T. (2014). The WNK-SPAK/OSR1 pathway: Master regulator of cation-chloride cotransporters. *Science Signaling*, *7*(334), 1–11. https://doi.org/10.1126/scisignal.2005365

Allen, N. J., & Eroglu, C. (2017). Cell Biology of Astrocyte-Synapse Interactions. *Neuron*, *96*(3), 697–708. https://doi.org/10.1016/j.neuron.2017.09.056

Bacaj, T., Tevlin, M., Lu, Y., & Shaham, S. (2009). Glia Are Essential for Sensory Organ Function in C. elegans. *Science*, *6*(5902), 247–253. https://doi.org/10.1111/j.1743-6109.2008.01122.x.Endothelial

Barres, B. A. (2008). Perspective The Mystery and Magic of Glia : A Perspective on Their Roles in Health and Disease. *Neuron*, *60*(3), 430–440. https://doi.org/10.1016/j.neuron.2008.10.013

Boettger, T., Rust, M. B., Maier, H., Seidenbecher, T., Schweizer, M., Keating, D. J., … Jentsch, T. J. (2003). Loss of K-Cl co-transporter KCC3 causes deafness, neurodegeneration and reduced seizure threshold. *EMBO Journal*, *22*(20), 5422–5434. https://doi.org/10.1093/emboj/cdg519

Chi, X., Li, X., Chen, Y., Zhang, Y., Su, Q., & Zhou, Q. (2020). Cryo-EM structures of the full-

length human KCC2 and KCC3 cation-chloride cotransporters. *Cell Research 2020 31:4*, *31*(4), 482–484. https://doi.org/10.1038/S41422-020-00437-X

Chou, F. S., Li, R., & Wang, P. S. (2018). Molecular components and polarity of radial glial cells during cerebral cortex development. *Cellular and Molecular Life Sciences : CMLS*, *75*(6), 1027–1041. https://doi.org/10.1007/S00018-017-2680-0

Chung, W. S., Welsh, C. A., Barres, B. A., & Stevens, B. (2015). Do glia drive synaptic and cognitive impairment in disease? *Nature Neuroscience*, *18*(11), 1539–1545. https://doi.org/10.1038/nn.4142

de los Heros, P., Alessi, D. R., Gourlay, R., Campbell, D. G., Deak, M., Macartney, T. J., … Zhang, J. (2014). The WNK-regulated SPAK/OSR1 kinases directly phosphorylate and inhibit the K^+–Cl^- co-transporters. *Biochemical Journal*, *458*(3), 559–573. https://doi.org/10.1042/BJ20131478

Díaz-Castro, B., Robel, S., & Mishra, A. (2023). Astrocyte Endfeet in Brain Function and Pathology: Open Questions, *7*. https://doi.org/10.1146/annurev-neuro-091922

Ding, G., Zou, W., Zhang, H., Xue, Y., Cai, Y., Huang, G., … Kang, L. (2015). In Vivo tactile stimulation-evoked responses in Caenorhabditis elegans amphid sheath glia. *PLoS ONE*, *10*(2). https://doi.org/10.1371/journal.pone.0117114

Ding, J., & Delpire, E. (2014). Deletion of KCC3 in parvalbumin neurons leads to locomotor deficit in a conditional mouse model of peripheral neuropathy associated with agenesis of the corpus callosum. *Behavioural Brain Research*, *274*, 128–136. https://doi.org/10.1016/J.BBR.2014.08.005

Djukic, B., Casper, K. B., Philpot, B. D., Chin, L. S., & McCarthy, K. D. (2007). Conditional Knock-Out of Kir4.1 Leads to Glial Membrane Depolarization, Inhibition of Potassium and

Glutamate Uptake, and Enhanced Short-Term Synaptic Potentiation. *Journal of Neuroscience, 27*(42), 11354–11365. https://doi.org/10.1523/JNEUROSCI.0723-07.2007

Duan, D., Zhang, H., Yue, X., Fan, Y., Xue, Y., Shao, J., … Kang, L. (2020). Sensory Glia Detect Repulsive Odorants and Drive Olfactory Adaptation. *Neuron, 108*(4), 707-721.e8. https://doi.org/10.1016/j.neuron.2020.08.026

Duncan, G. J., Simkins, T. J., & Emery, B. (2021). Neuron-Oligodendrocyte Interactions in the Structure and Integrity of Axons. *Frontiers in Cell and Developmental Biology, 9*. https://doi.org/10.3389/FCELL.2021.653101

Etienne-Manneville, S. (2008). Polarity proteins in glial cell functions. *Current Opinion in Neurobiology*, *18*(5), 488–494. https://doi.org/10.1016/J.CONB.2008.09.014

Eulenburg, V., & Gomeza, J. (2010). Neurotransmitter transporters expressed in glial cells as regulators of synapse function. *Brain Research Reviews*, *63*(1–2), 103–112. https://doi.org/10.1016/J.BRAINRESREV.2010.01.003

Falin, R. A., Miyazaki, H., & Strange, K. (2011). C. elegans STK39/SPAK ortholog-mediated inhibition of ClC anion channel activity is regulated by WNK-independent ERK kinase signaling. *American Journal of Physiology - Cell Physiology*, *300*(3). https://doi.org/10.1152/ajpcell.00343.2010

Garneau, A. P., Marcoux, A. A., Frenette-Cotton, R., Mac-Way, F., Lavoie, J. L., & Isenring, P. (2017, November 7). Molecular insights into the normal operation, regulation, and multisystemic roles of K+-Cl– cotransporter 3 (KCC3). *American Journal of Physiology - Cell Physiology*. American Physiological Society. https://doi.org/10.1152/ajpcell.00106.2017

Howard, H. C., Mount, D. B., Rochefort, D., Byun, N., Dupré, N., Lu, J., … Rouleau, G. A.

(2002). The K-Cl cotransporter KCC3 is mutant in a severe peripheral neuropathy associated with agenesis of the corpus callosum. *Nature Genetics*, *32*(3), 384–392. https://doi.org/10.1038/ng1002

Jäkel, S., & Dimou, L. (2017). Glial Cells and Their Function in the Adult Brain: A Journey through the History of Their Ablation. *Frontiers in Cellular Neuroscience*, *11*(February), 1–17. https://doi.org/10.3389/fncel.2017.00024

Kahle, K. T., Khanna, A. R., Alper, S. L., Adragna, N. C., Lauf, P. K., Sun, D., & Delpire, E. (2015). K-Cl cotransporters, cell volume homeostasis, and neurological disease. *Trends in Molecular Medicine*, *21*(8), 513–523. https://doi.org/10.1016/j.molmed.2015.05.008

Kaila, K., Price, T. J., Payne, J. A., Puskarjov, M., & Voipio, J. (2014). Cation-chloride cotransporters in neuronal development, plasticity and disease. *Nature Reviews Neuroscience*, *15*(10), 637–654. https://doi.org/10.1038/nrn3819

Khakh, B. S., & Sofroniew, M. V. (2015). Diversity of astrocyte functions and phenotypes in neural circuits. *Nature Neuroscience*, *18*(7), 942–952. https://doi.org/10.1038/nn.4043

Lavialle, M., Aumann, G., Anlauf, E., Pröls, F., Arpin, M., & Derouiche, A. (2011). Structural plasticity of perisynaptic astrocyte processes involves ezrin and metabotropic glutamate receptors. *Proceedings of the National Academy of Sciences of the United States of America*, *108*(31), 12915–12919. https://doi.org/10.1073/PNAS.1100957108/-/DCSUPPLEMENTAL/SM03.AVI

Le Salin-Cantegrel, Adè, Shekarabi, M., Bastien Holbert, S., Dion, P., Rochefort, D., Laganiè Re, J., … Rouleau, G. A. (2008). HMSN/ACC truncation mutations disrupt brain-type creatine kinase-dependant activation of K+/Cl-co-transporter 3. *Human Molecular Genetics*, *17*(17), 2703–2711. https://doi.org/10.1093/hmg/ddn172

Martin, C. G., Bent, J. S., & Singhvi, A. (2022). Epithelia delimits glial apical polarity against mechanical shear to maintain glia-neuron - architecture. *BioRxiv*, 2022.12.26.521704. https://doi.org/10.1101/2022.12.26.521704

Oikonomou, G., Perens, E. A., Lu, Y., Watanabe, S., Jorgensen, E. M., & Shaham, S. (2011). Opposing Activities of LIT-1/NLK and DAF-6/Patched-Related Direct Sensory Compartment Morphogenesis in C. elegans. *PLoS Biology*, *9*(8), e1001121. https://doi.org/10.1371/journal.pbio.1001121

Pearson, M. M., Lu, J., Mount, D. B., & Delpire, E. (2001). Localization of the K(+)-Cl(-) cotransporter, KCC3, in the central and peripheral nervous systems: expression in the choroid plexus, large neurons and white matter tracts. *Neuroscience*, *103*(2), 481–491. https://doi.org/10.1016/S0306-4522(00)00567-4

Perens, E. A., & Shaham, S. (2005). C. elegans daf-6 encodes a patched-related protein required for lumen formation. *Developmental Cell*, *8*(6), 893–906. https://doi.org/10.1016/j.devcel.2005.03.009

Pogodalla, N., Kranenburg, H., Rey, S., Rodrigues, S., Cardona, A., & Klämbt, C. (2021). Drosophila ßHeavy-Spectrin is required in polarized ensheathing glia that form a diffusion-barrier around the neuropil. *Nature Communications*, *12*(1). https://doi.org/10.1038/S41467-021-26462-X

Purice, M. D., Quitevis, E. J. A., Manning, R. S., Severs, L. J., Tran, N.-T., Sorrentino, V., … Singhvi, A. (2023). Molecular heterogeneity of C. elegans glia across sexes. *BioRxiv*, 2023.03.21.533668. https://doi.org/10.1101/2023.03.21.533668

Raiders, S., Black, E. C., Bae, A., MacFarlane, S., Klein, M., Shaham, S., & Singhvi, A. (2021). Glia actively sculpt sensory neurons by controlled phagocytosis to tune animal behavior.

ELife, *10*. https://doi.org/10.7554/eLife.63532

Ray, S., & Singhvi, A. (2021). Charging Up the Periphery: Glial Ionic Regulation in Sensory Perception. *Frontiers in Cell and Developmental Biology*, *9*, 1989. https://doi.org/10.3389/FCELL.2021.687732/BIBTEX

Ridet, J. L., Malhotra, S. K., Privat, A., & Gage, F. H. (1997). Reactive astrocytes: cellular and molecular cues to biological function. *Trends in Neurosciences*, *20*(12), 570–577. https://doi.org/10.1016/S0166-2236(97)01139-9

Rodriguez, Y. A., Roebber, J. K., Dvoryanchikov, G., Makhoul, V., Roper, S. D., & Chaudhari, N. (2021). "Tripartite Synapses" in Taste Buds: A Role for Type I Glial-like Taste Cells. *Journal of Neuroscience*, *41*(48), 9860–9871. https://doi.org/10.1523/JNEUROSCI.1444-21.2021

Sakers, K., Lake, A. M., Khazanchi, R., Ouwenga, R., Vasek, M. J., Dani, A., & Dougherty, J. D. (2017). Astrocytes locally translate transcripts in their peripheral processes. *Proceedings of the National Academy of Sciences of the United States of America*, *114*(19), E3830–E3838. https://doi.org/10.1073/pnas.1617782114

Salin-Cantegrel, Adèle, Rivière, J. B., Shekarabi, M., Rasheed, S., DaCal, S., Laganière, J., … Rouleau, G. A. (2011). Transit defect of potassium-chloride co-transporter 3 is a major pathogenic mechanism in hereditary motor and sensory neuropathy with agenesis of the corpus callosum. *Journal of Biological Chemistry*, *286*(32), 28456–28465. https://doi.org/10.1074/jbc.M111.226894

Shekarabi, M., Moldrich, R. X., Rasheed, S., Salin-Cantegrel, A., Laganiere, J., Rochefort, D., … Rouleau, G. A. (2012). Loss of Neuronal Potassium/Chloride Cotransporter 3 (KCC3) Is Responsible for the Degenerative Phenotype in a Conditional Mouse Model of Hereditary

Motor and Sensory Neuropathy Associated with Agenesis of the Corpus Callosum. *Journal of Neuroscience*, *32*(11), 3865–3876. https://doi.org/10.1523/JNEUROSCI.3679-11.2012

Singhvi, A., Liu, B., Friedman, C. J., Fong, J., Lu, Y., Huang, X. Y., & Shaham, S. (2016). A Glial K/Cl Transporter Controls Neuronal Receptive Ending Shape by Chloride Inhibition of an rGC. *Cell*, *165*(4), 936–948. https://doi.org/10.1016/j.cell.2016.03.026

Singhvi, A., & Shaham, S. (2019). Glia-Neuron Interactions in *Caenorhabditis elegans*. *Annual Review of Neuroscience*, *42*(1), 149–168. https://doi.org/10.1146/annurev-neuro-070918-050314

Singhvi, A., Shaham, S., & Rapti, G. (2023). Glia development and function in the nervous system of Caenorhabditis elegans. *Cold Spring Harbor Perspectives in Biology*, *(in press)*.

Song, S., Luo, L., Sun, B., & Sun, D. (2020). Roles of glial ion transporters in brain diseases. *Glia*, *68*(3), 472–494. https://doi.org/10.1002/glia.23699

Sun, Y. T., Lin, T. S., Tzeng, S. F., Delpire, E., & Shen, M. R. (2010). Deficiency of electroneutral K+-Cl- cotransporter 3 causes a disruption in impulse propagation along peripheral nerves. *Glia*, *58*(13), 1544–1552. https://doi.org/10.1002/glia.21028

Tanis, J. E., Bellemer, A., Moresco, J. J., Forbush, B., & Koelle, M. R. (2009). The Potassium Chloride Cotransporter KCC-2 Coordinates Development of Inhibitory Neurotransmission and Synapse Structure in Caenorhabditis elegans. *Journal of Neuroscience*, *29*(32), 9943–9954. https://doi.org/10.1523/JNEUROSCI.1989-09.2009

Tricaud, N. (2018). Myelinating schwann cell polarity and mechanically-driven myelin sheath elongation. *Frontiers in Cellular Neuroscience*, *11*, 414. https://doi.org/10.3389/FNCEL.2017.00414/BIBTEX

Tworig, J. M., & Feller, M. B. (2022). Müller Glia in Retinal Development: From Specification

to Circuit Integration. *Frontiers in Neural Circuits*, *15*. https://doi.org/10.3389/FNCIR.2021.815923

Wan, G., Corfas, G., & Stone, J. S. (2013). Inner ear supporting cells: Rethinking the silent majority. *Seminars in Cell and Developmental Biology*. Elsevier Ltd. https://doi.org/10.1016/j.semcdb.2013.03.009

Wilton, D. K., Dissing-Olesen, L., & Stevens, B. (2019). Neuron-Glia Signaling in Synapse Elimination. *Annual Review of Neuroscience*, *42*(1), 107–127. https://doi.org/10.1146/annurev-neuro-070918-050306

Yang, S. M., Michel, K., Jokhi, V., Nedivi, E., & Arlotta, P. (2020). Neuron-class specific responses govern adaptive myelin remodeling in the neocortex. *Science (New York, N.Y.)*, *370*(6523). https://doi.org/10.1126/SCIENCE.ABD2109

Zhang, J., Bhuiyan, M. I. H., Zhang, T., Karimy, J. K., Wu, Z., Fiesler, V. M., … Deng, X. (2020). Modulation of brain cation-Cl− cotransport via the SPAK kinase inhibitor ZT-1a. *Nature Communications 2020 11:1*, *11*(1), 1–17. https://doi.org/10.1038/S41467-019-13851-6

Chapter 2

Abraira, Victoria E., and David D. Ginty. 2013. “The Sensory Neurons of Touch.” *Neuron* 79 (4): 618–39. https://doi.org/10.1016/J.NEURON.2013.07.051.

Allen, Nicola J., and Cagla Eroglu. 2017. “Cell Biology of Astrocyte-Synapse Interactions.” *Neuron* 96 (3): 697–708. https://doi.org/10.1016/j.neuron.2017.09.056.

Alonso-González, Paula, Roberto Cabo, Isabel San José, Angel Gago, Iván C. Suazo, Olivia García-Suárez, Juan Cobo, and José A. Vega. 2017. “Human Digital Meissner Corpuscles Display Immunoreactivity for the Multifunctional Ion Channels Trpc6 and Trpv4.” *The*

Anatomical Record 300 (6): 1022–31. https://doi.org/10.1002/AR.23522.

Anselmi, Fabio, Victor H. Hernandez, Giulia Crispino, Anke Seydel, Saida Ortolanoa, Stephen D. Roper, Nicoletta Kessaris, et al. 2008. "ATP Release through Connexin Hemichannels and Gap Junction Transfer of Second Messengers Propagate Ca2+ Signals across the Inner Ear." *Proceedings of the National Academy of Sciences of the United States of America* 105 (48): 18770–75. https://doi.org/10.1073/pnas.0800793105.

Bacaj, Taulant, Maya Tevlin, Yun Lu, and Shai Shaham. 2008. "Glia Are Essential for Sensory Organ Function in C. Elegans." *Science* 322 (5902): 744–47. https://doi.org/10.1126/science.1163074.

Bartel, Dianna L., Susan L. Sullivan, Élise G. Lavoie, Jean Sévigny, and Thomas E. Finger. 2006. "Nucleoside Triphosphate Diphosphohydrolase-2 Is the Ecto-ATPase of Type I Cells in Taste Buds." *The Journal of Comparative Neurology* 497 (1): 1–12. https://doi.org/10.1002/cne.20954.

Ben-Shahar, Yehuda. 2011. "Sensory Functions for Degenerin/Epithelial Sodium Channels (DEG/ENaC)." In *Advances in Genetics*, 76:1–26. NIH Public Access. https://doi.org/10.1016/B978-0-12-386481-9.00001-8.

Boettger, Thomas, Marco B. Rust, Hannes Maier, Thomas Seidenbecher, Michaela Schweizer, Damien J. Keating, Jörg Faulhaber, et al. 2003. "Loss of K-Cl Co-Transporter KCC3 Causes Deafness, Neurodegeneration and Reduced Seizure Threshold." *EMBO Journal* 22 (20): 5422–34. https://doi.org/10.1093/emboj/cdg519.

Bösl, Michael R., Valentin Stein, Christian Hübner, Anselm A. Zdebik, Sven Eric Jordt, Amal K. Mukhopadhyay, Michail S. Davidoff, Adolf Friedrich Holstein, and Thomas J. Jentsch. 2001. "Male Germ Cells and Photoreceptors, Both Dependent on Close Cell-Cell

Interactions, Degenerate upon ClC-2 Cl- Channel Disruption." *EMBO Journal* 20 (6): 1289–99. https://doi.org/10.1093/emboj/20.6.1289.

Buck, Linda B. 2004. "Olfactory Receptors and Odor Coding in Mammals." *Nutrition Reviews* 62 (11 Pt 2): S184–88. https://doi.org/10.1111/j.1753-4887.2004.tb00097.x.

Calavia, M. G., J. A. Montaño, O. García-Suárez, J. Feito, M. A. Guervós, A. Germanà, M. Del Valle, P. Pérez-Piñera, J. Cobo, and J. A. Vega. 2010. "Differential Localization of Acid-Sensing Ion Channels 1 and 2 in Human Cutaneus Pacinian Corpuscles." *Cellular and Molecular Neurobiology* 30 (6): 841–48. https://doi.org/10.1007/s10571-010-9511-2.

Charlton-Perkins, Mark A., Edward D. Sendler, Elke K. Buschbeck, and Tiffany A. Cook. 2017. "Multifunctional Glial Support by Semper Cells in the Drosophila Retina." *PLoS Genetics* 13 (5): e1006782. https://doi.org/10.1371/journal.pgen.1006782.

Chen, C. Russell, Carolina Kachramanoglou, Daqing Li, Peter Andrews, and David Choi. 2014. "Anatomy and Cellular Constituents of the Human Olfactory Mucosa: A Review." *Journal of Neurological Surgery, Part B: Skull Base*. Thieme Medical Publishers, Inc. https://doi.org/10.1055/s-0033-1361837.

Chotard, Carole, and Iris Salecker. 2004. "Neurons and Glia: Team Players in Axon Guidance." *Trends in Neurosciences*. Elsevier. https://doi.org/10.1016/j.tins.2004.09.001.

CHOTARD, CAROLE, and IRIS SALECKER. 2007. "Glial Cell Development and Function in the Drosophila Visual System." *Neuron Glia Biology* 3 (1): 17. https://doi.org/10.1017/s1740925x07000592.

Christopherson, Karen S., Erik M. Ullian, Caleb C.A. Stokes, Christine E. Mullowney, Johannes W. Hell, Azin Agah, Jack Lawler, Deane F. Mosher, Paul Bornstein, and Ben A. Barres. 2005. "Thrombospondins Are Astrocyte-Secreted Proteins That Promote CNS

Synaptogenesis." *Cell* 120 (3): 421–33. https://doi.org/10.1016/j.cell.2004.12.020.

Chung, Won Suk, Laura E. Clarke, Gordon X. Wang, Benjamin K. Stafford, Alexander Sher, Chandrani Chakraborty, Julia Joung, et al. 2013. "Astrocytes Mediate Synapse Elimination through MEGF10 and MERTK Pathways." *Nature* 504 (7480): 394–400. https://doi.org/10.1038/nature12776.

Cobo, Ramón, Jorge García-Piqueras, Juan Cobo, and José A. Vega. 2021. "The Human Cutaneous Sensory Corpuscles: An Update." *Journal of Clinical Medicine* 10 (2): 227. https://doi.org/10.3390/jcm10020227.

Cohen-Salmon, Martine, Thomas Ott, Vincent Michel, Jean Pierre Hardelin, Isabelle Perfettini, Michel Eybalin, Tao Wu, et al. 2002. "Targeted Ablation of Connexin26 in the Inner Ear Epithelial Gap Junction Network Causes Hearing Impairment and Cell Death." *Current Biology* 12 (13): 1106–11. https://doi.org/10.1016/S0960-9822(02)00904-1.

Coles, Jonathan A. 1989. "Functions of Glial Cells in the Retina of the Honeybee Drone." *Glia* 2 (1): 1–9. https://doi.org/10.1002/glia.440020102.

Corey, David P. 2009. "Cell Biology of Mechanotransduction in Inner-Ear Hair Cells." *F1000 Biology Reports* 1 (July): 58. https://doi.org/10.3410/b1-58.

Doty, Richard L. 2012. "Olfaction in Parkinson's Disease and Related Disorders." *Neurobiology of Disease*. NIH Public Access. https://doi.org/10.1016/j.nbd.2011.10.026.

Dvoryanchikov, Gennady, Michael S. Sinclair, Isabel Perea-Martinez, Tong Wang, and Nirupa Chaudhari. 2009. "Inward Rectifier Channel, ROMK, Is Localized to the Apical Tips of Glial-like Cells in Mouse Taste Buds." *The Journal of Comparative Neurology* 517 (1): 1–14. https://doi.org/10.1002/cne.22152.

Eberl, Daniel F., and Grace Boekhoff-Falk. 2007. "Development of Johnston's Organ in

Drosophila." *International Journal of Developmental Biology*. NIH Public Access. https://doi.org/10.1387/ijdb.072364de.

Elsaesser, Rebecca, and Jacques Paysan. 2007. "The Sense of Smell, Its Signalling Pathways, and the Dichotomy of Cilia and Microvilli in Olfactory Sensory Cells." *BMC Neuroscience*. BMC Neurosci. https://doi.org/10.1186/1471-2202-8-S3-S1.

Garneau, Alexandre P, Andrée-Anne Marcoux, Rachelle Frenette-Cotton, Fabrice Mac-Way, Julie L Lavoie, and Paul Isenring. 2017. "Molecular Insights into the Normal Operation, Regulation and Multisystemic Roles of K^+-Cl^- Cotransporter 3 (KCC3)." *American Journal of Physiology - Cell Physiology* 3: ajpcell.00106.2017. https://doi.org/10.1152/ajpcell.00106.2017.

Ghiaroni, Valeria, Francesca Fieni, Roberto Tirindelli, Pierangelo Pietra, and Albertino Bigiani. 2003. "Ion Conductances in Supporting Cells Isolated From the Mouse Vomeronasal Organ." *Journal of Neurophysiology* 89 (1): 118–27. https://doi.org/10.1152/jn.00545.2002.

Grant, J., C. Matthewman, and L. Bianchi. 2015. "A Novel Mechanism of PH Buffering in C. Elegans Glia: Bicarbonate Transport via the Voltage-Gated ClC Cl- Channel CLH-1." *Journal of Neuroscience* 35 (50): 16377–97. https://doi.org/10.1523/JNEUROSCI.3237-15.2015.

Gründer, Stefan, Andrea Müller, and J. Peter Ruppersberg. 2001. "Developmental and Cellular Expression Pattern of Epithelial Sodium Channel α, β and γ Subunits in the Inner Ear of the Rat." *European Journal of Neuroscience* 13 (4): 641–48. https://doi.org/10.1046/j.1460-9568.2001.01426.x.

Guipponi, Michel, Grégoire Vuagniaux, Marie Wattenhofer, Kazunori Shibuya, Maria Vazquez, Loretta Dougherty, Nathalie Scamuffa, et al. 2002. "The Transmembrane Serine Protease

(TMPRSS3) Mutated in Deafness DFNB8/10 Activates the Epithelial Sodium Channel (ENaC) in Vitro." *Human Molecular Genetics* 11 (23): 2829–36. https://doi.org/10.1093/hmg/11.23.2829.

Hama, Kiyoshi, and Kogaku Saito. 1977. "Fine Structure of the Afferent Synapse of the Hair Cells in the Saccular Macula of the Goldfish, with Special Reference to the Anastomosing Tubules." *Journal of Neurocytology* 6 (4): 361–73. https://doi.org/10.1007/BF01178223.

Han, Lu, Ying Wang, Rachele Sangaletti, Giulia D'Urso, Yun Lu, Shai Shaham, and Laura Bianchi. 2013. "Two Novel DEG/ENaC Channel Subunits Expressed in Glia Are Needed for Nose-Touch Sensitivity in Caenorhabditis Elegans." *Journal of Neuroscience* 33 (3): 936–49. https://doi.org/10.1523/JNEUROSCI.2749-12.2013.

Hartenstein, Volker. 1988. "Development of Drosophila Larval Sensory Organs: Spatiotemporal Pattern of Sensory Neurones, Peripheral Axonal Pathways and Sensilla Differentiation." *Development*. Vol. 102.

Hegg, Colleen Cosgrove, Mavis Irwin, and Mary T. Lucero. 2009. "Calcium Store-Mediated Signaling in Sustentacular Cells of the Mouse Olfactory Epithelium." *GLIA* 57 (6): 634–44. https://doi.org/10.1002/glia.20792.

Heydel, Jean-Marie, Alexandra Coelho, Nicolas Thiebaud, Arièle Legendre, Anne-Marie Le Bon, Philippe Faure, Fabrice Neiers, Yves Artur, Jérôme Golebiowski, and Loïc Briand. 2013. "Odorant-Binding Proteins and Xenobiotic Metabolizing Enzymes: Implications in Olfactory Perireceptor Events." *The Anatomical Record* 296 (9): 1333–45. https://doi.org/10.1002/ar.22735.

Hilu-Dadia, Reut, and Estee Kurant. 2020. "Glial Phagocytosis in Developing and Mature Drosophila CNS: Tight Regulation for a Healthy Brain." *Current Opinion in Immunology*.

Elsevier Ltd. https://doi.org/10.1016/j.coi.2019.11.010.

Hitomi, Yasumasa, Akiko Suzuki, Yoshiro Kawano, Kayoko Nozawa-Inoue, Makoto Inoue, and Takeyasu Maeda. 2009. "Immunohistochemical Detection of ENaCβ in the Terminal Schwann Cells Associated with the Periodontal Ruffini Endings of the Rat Incisor." *Biomedical Research* 30 (2): 113–19. https://doi.org/10.2220/biomedres.30.113.

Huang, Huachen, Shanshan Song, Suneel Banerjee, Tong Jiang, Jinwei Zhang, Kristopher T. Kahle, Dandan Sun, and Zhongling Zhang. 2019. "The WNK-SPAK/OSR1 Kinases and the Cation-Chloride Cotransporters as Therapeutic Targets for Neurological Diseases." *Aging and Disease*. International Society on Aging and Disease. https://doi.org/10.14336/AD.2018.0928.

Jin, Sheng Chih, Charuta G. Furey, Xue Zeng, August Allocco, Carol Nelson-Williams, Weilai Dong, Jason K. Karimy, et al. 2019. "*SLC12A* Ion Transporter Mutations in Sporadic and Familial Human Congenital Hydrocephalus." *Molecular Genetics & Genomic Medicine* 7 (9): 892. https://doi.org/10.1002/mgg3.892.

Kapoor, Niren, William Lee, Edlira Clark, Rafal Bartoszewski, Carmel M. McNicholas, Cecelia B. Latham, Zsuzsanna Bebok, et al. 2011. "Interaction of ASIC1 and ENaC Subunits in Human Glioma Cells and Rat Astrocytes." *American Journal of Physiology - Cell Physiology* 300 (6). https://doi.org/10.1152/ajpcell.00199.2010.

Kikuchi, Toshihiko, Joe C. Adams, David L. Paul, and Robert S. Kimura. 1994. "Gap Junction Systems in the Rat Vestibular Labyrinth: Immunohistochemical and Ultrastructural Analysis." *Acta Oto-Laryngologica* 114 (3): 520–28. https://doi.org/10.3109/00016489409126097.

Kim, Sung Huhn, and Daniel C. Marcus. 2011. "Regulation of Sodium Transport in the Inner

Ear." *Hearing Research*. Hear Res. https://doi.org/10.1016/j.heares.2011.05.003.

Kitajiri, Shin Ichiro, and Tatsuya Katsuno. 2016. "Tricellular Tight Junctions in the Inner Ear." *BioMed Research International*. Hindawi Limited. https://doi.org/10.1155/2016/6137541.

Larter, Nikki K., Jennifer S. Sun, and John R. Carlson. 2016. "Organization and Function of Drosophila Odorant Binding Proteins." *ELife* 5 (NOVEMBER2016). https://doi.org/10.7554/eLife.20242.

Lawton, D. Maxwell, David N. Furness, Bernd Lindemann, and Carole M. Hackney. 2000. "Localization of the Glutamate-Aspartate Transporter, GLAST, in Rat Taste Buds." *European Journal of Neuroscience* 12 (9): 3163–71. https://doi.org/10.1046/j.1460-9568.2000.00207.x.

MacDonald, Jennifer M., Margaret G. Beach, Ermelinda Porpiglia, Amy E. Sheehan, Ryan J. Watts, and Marc R. Freeman. 2006. "The Drosophila Cell Corpse Engulfment Receptor Draper Mediates Glial Clearance of Severed Axons." *Neuron* 50 (6): 869–81. https://doi.org/10.1016/j.neuron.2006.04.028.

Marco, Elysa J., Leighton B.N. Hinkley, Susanna S. Hill, and Srikantan S. Nagarajan. 2011. "Sensory Processing in Autism: A Review of Neurophysiologic Findings." *Pediatric Research* 69 (5 PART 2): 48R. https://doi.org/10.1203/PDR.0b013e3182130c54.

Medler, Kathryn F., Robert F. Margolskee, and Sue C. Kinnamon. 2003. "Electrophysiological Characterization of Voltage-Gated Currents in Defined Taste Cell Types of Mice." *Journal of Neuroscience* 23 (7): 2608–17. https://doi.org/10.1523/jneurosci.23-07-02608.2003.

Montaño, J. A., M. G. Calavia, O. García-Suárez, J. A. Suarez-Quintanilla, A. Gálvez, P. Pérez-Piñera, J. Cobo, and J. A. Vega. 2009. "The Expression of ENa+C and ASIC2 Proteins in Pacinian Corpuscles Is Differently Regulated by TrkB and Its Ligands BDNF and NT-4."

Neuroscience Letters 463 (2): 114–18. https://doi.org/10.1016/j.neulet.2009.07.073.

Nadol, Joseph B., Michael J. Mulroy, Daniel A. Goodenough, and Thomas F. Weiss. 1976. "Tight and Gap Junctions in a Vertebrate Inner Ear." *American Journal of Anatomy* 147 (3): 281–301. https://doi.org/10.1002/aja.1001470304.

Newman, Eric A., and Kathleen R. Zahs. 1998. "Modulation of Neuronal Activity by Glial Cells in the Retina." *Journal of Neuroscience* 18 (11): 4022–28. https://doi.org/10.1523/jneurosci.18-11-04022.1998.

Nicolson, Teresa. 2017. "The Genetics of Hair-Cell Function in Zebrafish." *Journal of Neurogenetics* 31 (3): 102. https://doi.org/10.1080/01677063.2017.1342246.

Olsen, Michelle L., Baljit S. Khakh, Serguei N. Skatchkov, Min Zhou, C. Justin Lee, and Nathalie Rouach. 2015. "New Insights on Astrocyte Ion Channels: Critical for Homeostasis and Neuron-Glia Signaling." *Journal of Neuroscience* 35 (41): 13827–35. https://doi.org/10.1523/JNEUROSCI.2603-15.2015.

Pawson, Lorraine, Norma B. Slepecky, and Stanley J. Bolanowski. 2000. "Immunocytochemical Identification of Proteins within the Pacinian Corpuscle." *Somatosensory and Motor Research* 17 (2): 159–70. https://doi.org/10.1080/08990220050020571.

Perkins, Lizabeth A., Edward M. Hedgecock, J. Nichol Thomson, and Joseph G. Culotti. 1986. "Mutant Sensory Cilia in the Nematode Caenorhabditis Elegans." *Developmental Biology* 117 (2): 456–87. https://doi.org/10.1016/0012-1606(86)90314-3.

Pinto-Teixeira, Filipe, Oriol Viader-Llargués, Elen Torres-Mejía, Melissa Turan, Estela González-Gualda, Laura Pola-Morell, and Hernań Lopez-Schier. 2015. "Inexhaustible Hair-Cell Regeneration in Young and Aged Zebrafish." *Biology Open* 4 (7): 903–9. https://doi.org/10.1242/bio.012112.

Raiders, Stephan, Erik Calvin Black, Andrea Bae, Stephen MacFarlane, Mason Klein, Shai Shaham, and Aakanksha Singhvi. 2021. “Glia Actively Sculpt Sensory Neurons by Controlled Phagocytosis to Tune Animal Behavior.” *ELife* 10 (March). https://doi.org/10.7554/eLife.63532.

Raiders, Stephan, Taeho Han, Nicole Scott-Hewitt, Sarah Kucenas, Deborah Lew, Mary A. Logan, and Aakanksha Singhvi. 2021. “Engulfed by Glia: Glial Pruning in Development, Function, and Injury across Species.” *The Journal of Neuroscience*, January, JN-SY-1660-20. https://doi.org/10.1523/JNEUROSCI.1660-20.2020.

Reichenbach, Andreas, and Andreas Bringmann. 2020. “Glia of the Human Retina.” *GLIA* 68 (4): 768–96. https://doi.org/10.1002/glia.23727.

Reichenbach, Tobias, and A. J. Hudspeth. 2014. “The Physics of Hearing: Fluid Mechanics and the Active Process of the Inner Ear.” *Reports on Progress in Physics* 77 (7). https://doi.org/10.1088/0034-4885/77/7/076601.

Riazuddin, Saima, Zubair M. Ahmed, Alan S. Fanning, Ayala Lagziel, Shin Ichiro Kitajiri, Khushnooda Ramzan, Shaheen N. Khan, et al. 2006. “Tricellulin Is a Tight-Junction Protein Necessary for Hearing.” *American Journal of Human Genetics* 79 (6): 1040–51. https://doi.org/10.1086/510022.

Romanov, Roman A., and Stanislav S. Kolesnikov. 2006. “Electrophysiologically Identified Subpopulations of Taste Bud Cells.” *Neuroscience Letters* 395 (3): 249–54. https://doi.org/10.1016/j.neulet.2005.10.085.

Roper, Stephen D., and Nirupa Chaudhari. 2017. “Taste Buds: Cells, Signals and Synapses.” *Nature Reviews Neuroscience*. Nature Publishing Group. https://doi.org/10.1038/nrn.2017.68.

Seifert, Gerald, Christian Henneberger, and Christian Steinhäuser. 2018. “Diversity of Astrocyte Potassium Channels: An Update.” *Brain Research Bulletin*. Elsevier Inc. https://doi.org/10.1016/j.brainresbull.2016.12.002.

Seyfarth, Ernst August, Esmond J. Sanders, and Andrew S. French. 1995. “Sodium Channel Distribution in a Spider Mechanosensory Organ.” *Brain Research* 683 (1): 93–101. https://doi.org/10.1016/0006-8993(95)00317-J.

Shaham, Shai. 2010. “Chemosensory Organs as Models of Neuronal Synapses.” *Nature Reviews Neuroscience*. Nature Publishing Group. https://doi.org/10.1038/nrn2740.

Shekarabi, M., R. X. Moldrich, S. Rasheed, A. Salin-Cantegrel, J. Laganiere, D. Rochefort, P. Hince, et al. 2012. “Loss of Neuronal Potassium/Chloride Cotransporter 3 (KCC3) Is Responsible for the Degenerative Phenotype in a Conditional Mouse Model of Hereditary Motor and Sensory Neuropathy Associated with Agenesis of the Corpus Callosum.” *Journal of Neuroscience* 32 (11): 3865–76. https://doi.org/10.1523/JNEUROSCI.3679-11.2012.

Simard, M., and M. Nedergaard. 2004. “The Neurobiology of Glia in the Context of Water and Ion Homeostasis.” *Neuroscience* 129 (4): 877–96. https://doi.org/10.1016/j.neuroscience.2004.09.053.

Singhvi, Aakanksha, Bingqian Liu, Christine J. Friedman, Jennifer Fong, Yun Lu, Xin Yun Huang, and Shai Shaham. 2016. “A Glial K/Cl Transporter Controls Neuronal Receptive Ending Shape by Chloride Inhibition of an RGC.” *Cell* 165 (4): 936–48. https://doi.org/10.1016/j.cell.2016.03.026.

Singhvi, Aakanksha, and Shai Shaham. 2019. “Glia-Neuron Interactions in *Caenorhabditis Elegans*.” *Annual Review of Neuroscience* 42 (1): 149–68. https://doi.org/10.1146/annurev-

neuro-070918-050314.

Song, Shanshan, Lanxin Luo, Baoshan Sun, and Dandan Sun. 2020. “Roles of Glial Ion Transporters in Brain Diseases.” *Glia* 68 (3): 472–94. https://doi.org/10.1002/glia.23699.

Sparrow, J.R., D. Hicks, and C.P. Hamel. 2010. “The Retinal Pigment Epithelium in Health and Disease.” *Current Molecular Medicine* 10 (9): 802–23. https://doi.org/10.2174/156652410793937813.

Spicer, Samuel S., and Bradley A. Schulte. 1998. “Evidence for a Medial K+ Recycling Pathway from Inner Hair Cells.” *Hearing Research* 118 (1–2): 1–12. https://doi.org/10.1016/S0378-5955(98)00006-9.

Stephenson, Ryan, Astkhik Mangasarian, Gail Ishiyama, Kumiko Hosokawa, Seiji Hosokawa, Akira Ishiyama, and Ivan A. Lopez. 2021. “Immunohistochemical Location of Na+, K+-ATPase A1 Subunit in the Human Inner Ear.” *Hearing Research* 400 (February): 108113. https://doi.org/10.1016/j.heares.2020.108113.

Stong, Benjamin C., Qing Chang, Shoeb Ahmad, and Xi Lin. 2006. “A Novel Mechanism for Connexin 26 Mutation Linked Deafness: Cell Death Caused by Leaky Gap Junction Hemichannels.” *Laryngoscope* 116 (12): 2205–10. https://doi.org/10.1097/01.mlg.0000241944.77192.d2.

Strauss, Olaf. 2005. “The Retinal Pigment Epithelium in Visual Function.” *Physiological Reviews* 85: 845–81. https://doi.org/10.1152/physrev.00021.2004.

Sun, Xu, Dan Zhao, Yong Li Li, Ying Sun, Xu Hui Lei, Jia Ning Zhang, Ming Ming Wu, et al. 2013. “Regulation of ASIC1 by Ca2+/Calmodulin-Dependent Protein Kinase II in Human Glioblastoma Multiforme.” *Oncology Reports* 30 (6): 2852–58. https://doi.org/10.3892/or.2013.2777.

Tong, Xiaoping, Yan Ao, Guido C. Faas, Sinifunanya E. Nwaobi, Ji Xu, Martin D. Haustein, Mark A. Anderson, et al. 2014. “Astrocyte Kir4.1 Ion Channel Deficits Contribute to Neuronal Dysfunction in Huntington’s Disease Model Mice.” *Nature Neuroscience* 17 (5): 694–703. https://doi.org/10.1038/nn.3691.

Trotier, Didier. 1998. “Electrophysiological Properties of Frog Olfactory Supporting Cells.” *Chemical Senses* 23 (3): 363–69. https://doi.org/10.1093/chemse/23.3.363.

Trotier, Didier, and Patrick MacLeod. 1986. “Intracellular Recordings from Salamander Olfactory Supporting Cells.” *Brain Research* 374 (2): 205–11. https://doi.org/10.1016/0006-8993(86)90413-0.

Ugbode, Chris, Yuhan Hu, Benjamin Whalley, Chris Peers, Marcus Rattray, and Mark L. Dallas. 2017. “Astrocytic Transporters in Alzheimer’s Disease.” *Biochemical Journal*. Portland Press Ltd. https://doi.org/10.1042/BCJ20160505.

Vandenbeuch, Aurelie, Tod R. Clapp, and Sue C. Kinnamon. 2008. “Amiloride-Sensitive Channels in Type I Fungiform Taste Cells in Mouse.” *BMC Neuroscience* 9 (1): 1–13. https://doi.org/10.1186/1471-2202-9-1.

Verkhratsky, Alexei. 2019. “Astroglial Calcium Signaling in Aging and Alzheimer’s Disease.” *Cold Spring Harbor Perspectives in Biology* 11 (7). https://doi.org/10.1101/cshperspect.a035188.

Vogalis, Fivos, Colleen C. Hegg, and Mary T. Lucero. 2005. “Ionic Conductances in Sustentacular Cells of the Mouse Olfactory Epithelium.” *Journal of Physiology* 562 (3): 785–99. https://doi.org/10.1113/jphysiol.2004.079228.

Wan, Guoqiang, Gabriel Corfas, and Jennifer S. Stone. 2013. “Inner Ear Supporting Cells: Rethinking the Silent Majority.” *Seminars in Cell and Developmental Biology*. Elsevier Ltd.

https://doi.org/10.1016/j.semcdb.2013.03.009.

Wang, Y., G. D'Urso, and L. Bianchi. 2012. "Knockout of Glial Channel ACD-1 Exacerbates Sensory Deficits in a C. Elegans Mutant by Regulating Calcium Levels of Sensory Neurons." *Journal of Neurophysiology* 107 (1): 148–58. https://doi.org/10.1152/jn.00299.2011.

Wang, Ying, Alfonso Apicella, Sun Kyung Lee, Marina Ezcurra, Robert D. Slone, Maya Goldmit, William R. Schafer, Shai Shaham, Monica Driscoll, and Laura Bianchi. 2008. "A Glial DEG/ENaC Channel Functions with Neuronal Channel DEG-1 to Mediate Specific Sensory Functions in C. Elegans." *EMBO Journal* 27 (18): 2388–99. https://doi.org/10.1038/emboj.2008.161.

Ward, Samuel, Nichol Thomson, John G. White, and Sydney Brenner. 1975. "Electron Microscopical Reconstruction of the Anterior Sensory Anatomy of the Nematode Caenorhabditis Elegans." *Journal of Comparative Neurology* 160 (3): 313–37. https://doi.org/10.1002/cne.901600305.

Wilcox, Edward R., Quianna L. Burton, Sadaf Naz, Saima Riazuddin, Tenesha N. Smith, Barbara Ploplis, Inna Belyantseva, et al. 2001. "Mutations in the Gene Encoding Tight Junction Claudin-14 Cause Autosomal Recessive Deafness DFNB29." *Cell* 104 (1): 165–72. https://doi.org/10.1016/S0092-8674(01)00200-8.

Xiao, Qinghuan, H. Criss Hartzell, and Kuai Yu. 2010. "Bestrophins and Retinopathies." *Pflugers Archiv : European Journal of Physiology* 460 (2): 559. https://doi.org/10.1007/S00424-010-0821-5.

Yarmolinsky, David A., Charles S. Zuker, and Nicholas J.P. Ryba. 2009. "Common Sense about Taste: From Mammals to Insects." *Cell*. Cell. https://doi.org/10.1016/j.cell.2009.10.001.

Zdebik, Anselm A., Philine Wangemann, and Thomas J. Jentsch. 2009. “Potassium Ion Movement in the Inner Ear: Insights from Genetic Disease and Mouse Models.” *Physiology (Bethesda, Md.)* 24 (5): 307. https://doi.org/10.1152/PHYSIOL.00018.2009.

Zhang, Qiuxiang, Suna Li, Hiu Tung C. Wong, Xinyi J. He, Alisha Beirl, Ronald S. Petralia, Ya Xian Wang, and Katie S. Kindt. 2018. “Synaptically Silent Sensory Hair Cells in Zebrafish Are Recruited after Damage.” *Nature Communications* 9 (1): 1–16. https://doi.org/10.1038/s41467-018-03806-8.

Zhao, H. B., T. Kikuchi, A. Ngezahayo, and T. W. White. 2006. “Gap Junctions and Cochlear Homeostasis.” *Journal of Membrane Biology*. NIH Public Access. https://doi.org/10.1007/s00232-005-0832-x.

Zhao, Hong Bo, Ning Yu, and Carrie R. Fleming. 2005. “Gap Junctional Hemichannel-Mediated ATP Release and Hearing Controls in the Inner Ear.” *Proceedings of the National Academy of Sciences of the United States of America* 102 (51): 18724–29. https://doi.org/10.1073/pnas.0506481102.

Zhu, Yan, and Hong Bo Zhao. 2010. “ATP-Mediated Potassium Recycling in the Cochlear Supporting Cells.” *Purinergic Signalling* 6 (2): 221–29. https://doi.org/10.1007/s11302-010-9184-9.

Zidanic, M., and W. E. Brownell. 1990. “Fine Structure of the Intracochlear Potential Field. I. The Silent Current.” *Biophysical Journal* 57 (6): 1253–68. https://doi.org/10.1016/S0006-3495(90)82644-8.

Chapter 3 (main)

Agarwal, A., Wu, P. H., Hughes, E. G., Fukaya, M., Tischfield, M. A., Langseth, A. J., …

Bergles, D. E. (2017). Transient Opening of the Mitochondrial Permeability Transition Pore Induces Microdomain Calcium Transients in Astrocyte Processes. *Neuron*, *93*(3), 587-605.e7. https://doi.org/10.1016/j.neuron.2016.12.034

Alessi, D. R., Zhang, J., Khanna, A., Hochdörfer, T., Shang, Y., & Kahle, K. T. (2014). The WNK-SPAK/OSR1 pathway: Master regulator of cation-chloride cotransporters. *Science Signaling*, *7*(334), 1–11. https://doi.org/10.1126/scisignal.2005365

Allen, N. J., & Eroglu, C. (2017). Cell Biology of Astrocyte-Synapse Interactions. *Neuron*, *96*(3), 697–708. https://doi.org/10.1016/j.neuron.2017.09.056

Bacaj, T., Lu, Y., & Shaham, S. (2008). The Conserved Proteins CHE-12 and DYF-11 Are Required for Sensory Cilium Function in Caenorhabditis elegans. *Genetics*, *178*(2), 989. https://doi.org/10.1534/GENETICS.107.082453

Bacaj, T., Tevlin, M., Lu, Y., & Shaham, S. (2009). Glia Are Essential for Sensory Organ Function in C. elegans, *6*(5902), 247–253. https://doi.org/10.1111/j.1743-6109.2008.01122.x.Endothelial

Barres, B. A. (2008). Perspective The Mystery and Magic of Glia : A Perspective on Their Roles in Health and Disease. *Neuron*, *60*(3), 430–440. https://doi.org/10.1016/j.neuron.2008.10.013

Belin, S., Zuloaga, K. L., & Poitelon, Y. (2017). Influence of mechanical stimuli on schwann cell biology. *Frontiers in Cellular Neuroscience*, *11*, 347. https://doi.org/10.3389/FNCEL.2017.00347/BIBTEX

Blaesse, P., Airaksinen, M. S., Rivera, C., & Kaila, K. (2009). Cation-Chloride Cotransporters and Neuronal Function. *Neuron*, *61*(6), 820–838. https://doi.org/10.1016/j.neuron.2009.03.003

Boettger, T., Rust, M. B., Maier, H., Seidenbecher, T., Schweizer, M., Keating, D. J., … Jentsch, T. J. (2003). Loss of K-Cl co-transporter KCC3 causes deafness, neurodegeneration and reduced seizure threshold. *EMBO Journal*, *22*(20), 5422–5434. https://doi.org/10.1093/emboj/cdg519

Burgess, A., Shah, K., Hough, O., & Hynynen, K. (2016). C. elegans S6K Mutants Require a Creatine Kinase-Like Effector for Lifespan Extension, *15*(5), 477–491. https://doi.org/10.1586/14737175.2015.1028369.Focused

Chalasani, S. H., Chronis, N., Tsunozaki, M., Gray, J. M., Ramot, D., Goodman, M. B., & Bargmann, C. I. (2007). Dissecting a circuit for olfactory behaviour in Caenorhabditis elegans. *Nature 2007 450:7166*, *450*(7166), 63–70. https://doi.org/10.1038/nature06292

Chung, W. S., Welsh, C. A., Barres, B. A., & Stevens, B. (2015). Do glia drive synaptic and cognitive impairment in disease? *Nature Neuroscience*, *18*(11), 1539–1545. https://doi.org/10.1038/nn.4142

Coburn, C. M., & Bargmann, C. I. (1996). A putative cyclic nucleotide-gated channel is required for sensory development and function in C. elegans. *Neuron*, *17*(4), 695–706. https://doi.org/10.1016/S0896-6273(00)80201-9

Delpire, E., & Kahle, K. T. (2017). The KCC3 cotransporter as a therapeutic target for peripheral neuropathy. *Expert Opinion on Therapeutic Targets*, *21*(2), 113–116. https://doi.org/10.1080/14728222.2017.1275569

Ding, G., Zou, W., Zhang, H., Xue, Y., Cai, Y., Huang, G., … Kang, L. (2015). In Vivo tactile stimulation-evoked responses in Caenorhabditis elegans amphid sheath glia. *PLoS ONE*, *10*(2). https://doi.org/10.1371/journal.pone.0117114

Duan, D., Zhang, H., Yue, X., Fan, Y., Xue, Y., Shao, J., … Kang, L. (2020). Sensory Glia

Detect Repulsive Odorants and Drive Olfactory Adaptation. *Neuron*, *108*(4), 707-721.e8. https://doi.org/10.1016/j.neuron.2020.08.026

Dwyer, N. D., Adler, C. E., Crump, J. G., L'Etoile, N. D., & Bargmann, C. I. (2001). Polarized Dendritic Transport and the AP-1 μ1 Clathrin Adaptor UNC-101 Localize Odorant Receptors to Olfactory Cilia. *Neuron*, *31*(2), 277–287. https://doi.org/10.1016/S0896-6273(01)00361-0

Eroglu, Ç., Allen, N. J., Susman, M. W., O'Rourke, N. A., Park, C. Y., Özkan, E., … Barres, B. A. (2009). Gabapentin Receptor α2δ-1 Is a Neuronal Thrombospondin Receptor Responsible for Excitatory CNS Synaptogenesis. *Cell*, *139*(2), 380–392. https://doi.org/10.1016/j.cell.2009.09.025

Garneau, A. P., Marcoux, A.-A., Frenette-Cotton, R., Mac-Way, F., Lavoie, J. L., & Isenring, P. (2017). Molecular insights into the normal operation, regulation and multisystemic roles of K^+-Cl^- cotransporter 3 (KCC3). *American Journal of Physiology - Cell Physiology*, *3*, ajpcell.00106.2017. https://doi.org/10.1152/ajpcell.00106.2017

Goodman, M. B., & Sengupta, P. (2018). The extraordinary AFD thermosensor of C. elegans. *Pflugers Archiv : European Journal of Physiology*, *470*(5), 839. https://doi.org/10.1007/S00424-017-2089-5

Green, J. A., & Mykytyn, K. (2014). Neuronal Primary Cilia: An Underappreciated Signaling and Sensory Organelle in the Brain. *Neuropsychopharmacology*, *39*(1), 244. https://doi.org/10.1038/NPP.2013.203

Heiman, M. G., & Shaham, S. (2009). DEX-1 and DYF-7 Establish Sensory Dendrite Length by Anchoring Dendritic Tips during Cell Migration. *Cell*, *137*(2), 344–355. https://doi.org/10.1016/j.cell.2009.01.057

Hisamoto, N., Moriguchi, T., Urushiyama, S., Mitani, S., Shibuya, H., & Matsumoto, K. (2008). Caenorhabditis elegans WNK-STE20 pathway regulates tube formation by modulating ClC channel activity. *EMBO Reports*, *9*(1), 70–75. https://doi.org/10.1038/sj.embor.7401128

Howell, K., & Hobert, O. (2017). Morphological Diversity of C. elegans Sensory Cilia Instructed by the Differential Expression of an Immunoglobulin Domain Protein. *Current Biology : CB*, *27*(12), 1782-1790.e5. https://doi.org/10.1016/J.CUB.2017.05.006

Kaila, K., Price, T. J., Payne, J. A., Puskarjov, M., & Voipio, J. (2014). Cation-chloride cotransporters in neuronal development, plasticity and disease. *Nature Reviews Neuroscience*, *15*(10), 637–654. https://doi.org/10.1038/nrn3819

Khakh, B. S., & Sofroniew, M. V. (2015). Diversity of astrocyte functions and phenotypes in neural circuits. *Nature Neuroscience*, *18*(7), 942–952. https://doi.org/10.1038/nn.4043

Ki, S. M., Jeong, H. S., & Lee, J. E. (2021). Primary Cilia in Glial Cells: An Oasis in the Journey to Overcoming Neurodegenerative Diseases. *Frontiers in Neuroscience*, *15*, 1227. https://doi.org/10.3389/FNINS.2021.736888/BIBTEX

Kimura, K. D., Miyawaki, A., Matsumoto, K., & Mori, I. (2004). The C. elegans Thermosensory Neuron AFD Responds to Warming. *Current Biology*, *14*(14), 1291–1295. https://doi.org/10.1016/J.CUB.2004.06.060

Köppen, M., Simske, J. S., Sims, P. A., Firestein, B. L., Hall, D. H., Radice, A. D., … Hardin, J. D. (2001). Cooperative regulation of AJM-1 controls junctional integrity in Caenorhabditis elegans epithelia. *Nature Cell Biology*, *3*(11), 983–991. https://doi.org/10.1038/NCB1101-983

Kunitomo, H., & Iino, Y. (2008). Caenorhabditis elegans DYF-11, an orthologue of mammalian Traf3ip1/MIP-T3, is required for sensory cilia formation. *Genes to Cells*, *13*(1), 13–25.

https://doi.org/10.1111/j.1365-2443.2007.01147.x

Lanjuin, A., VanHoven, M. K., Bargmann, C. I., Thompson, J. K., & Sengupta, P. (2003). Otx/otd homeobox genes specify distinct sensory neuron identities in C. elegans. *Developmental Cell*, *5*(4), 621–633. https://doi.org/10.1016/s1534-5807(03)00293-4

Lechtreck, K. F. (2015). IFT-cargo interactions and protein transport in cilia. *Trends in Biochemical Sciences*, *40*(12), 765. https://doi.org/10.1016/J.TIBS.2015.09.003

Leterrier, C. (2018). The Axon Initial Segment: An Updated Viewpoint. *Journal of Neuroscience*, *38*(9), 2135–2145. https://doi.org/10.1523/JNEUROSCI.1922-17.2018

Low, I. I. C., Williams, C. R., Chong, M. K., Mclachlan, I. G., Wierbowski, B. M., Kolotuev, I., & Heiman, M. G. (2019). Morphogenesis of neurons and glia within an epithelium. https://doi.org/10.1242/dev.171124

Mahon, M. J. (2011). Apical membrane segregation of phosphatidylinositol-4,5-bisphosphate influences parathyroid hormone 1 receptor compartmental signaling and localization via direct regulation of ezrin in LLC-PK1 cells. *Cellular Signalling*, *23*(10), 1659. https://doi.org/10.1016/J.CELLSIG.2011.05.020

Martin, C. G., Bent, J. S., & Singhvi, A. (2022). Epithelia delimits glial apical polarity against mechanical shear to maintain glia-neuron - architecture. *BioRxiv*, 2022.12.26.521704. https://doi.org/10.1101/2022.12.26.521704

McMahon, L., Legouis, R., Vonesch, J. L., & Labouesse, M. (2001). Assembly of C. elegans apical junctions involves positioning and compaction by LET-413 and protein aggregation by the MAGUK protein DLG-1. *Journal of Cell Science*, *114*(12), 2265–2277. https://doi.org/10.1242/JCS.114.12.2265

Nehme, R., & Conradt, B. (2009). egl-1: a key activator of apoptotic cell death in C. elegans.

Oncogene 2009 27:1, *27*(1), S30–S40. https://doi.org/10.1038/onc.2009.41

Oikonomou, G., Perens, E. A., Lu, Y., & Shaham, S. (2012). Some, but not all, retromer components promote morphogenesis of C. elegans sensory compartments. *Developmental Biology*, *362*(1), 42–49. https://doi.org/10.1016/j.ydbio.2011.11.009

Oikonomou, G., Perens, E. A., Lu, Y., Watanabe, S., Jorgensen, E. M., & Shaham, S. (2011). Opposing Activities of LIT-1/NLK and DAF-6/Patched-Related Direct Sensory Compartment Morphogenesis in C. elegans. *PLoS Biology*, *9*(8), e1001121. https://doi.org/10.1371/journal.pbio.1001121

Oikonomou, G., & Shaham, S. (2011). The glia of caenorhabditis elegans. *Glia*, *59*(9), 1253–1263. https://doi.org/10.1002/glia.21084

Payne, J. A., Rivera, C., Voipio, J., & Kaila, K. (2003). Cation-chloride co-transporters in neuronal communication, development and trauma. *Trends in Neurosciences*, *26*(4), 199–206. https://doi.org/10.1016/S0166-2236(03)00068-7

Perens, E. A., & Shaham, S. (2005). C. elegans daf-6 encodes a patched-related protein required for lumen formation. *Developmental Cell*, *8*(6), 893–906. https://doi.org/10.1016/j.devcel.2005.03.009

Perkins, L. A., Hedgecock, E. M., Thomson, J. N., & Culotti, J. G. (1986). Mutant sensory cilia in the nematode Caenorhabditis elegans. *Developmental Biology*, *117*(2), 456–487. https://doi.org/10.1016/0012-1606(86)90314-3

Pogodalla, N., Kranenburg, H., Rey, S., Rodrigues, S., Cardona, A., & Klämbt, C. (2021). Drosophila ßHeavy-Spectrin is required in polarized ensheathing glia that form a diffusion-barrier around the neuropil. *Nature Communications*, *12*(1). https://doi.org/10.1038/S41467-021-26462-X

Purice, M. D., Quitevis, E. J. A., Manning, R. S., Severs, L. J., Tran, N.-T., Sorrentino, V., … Singhvi, A. (2023). Molecular heterogeneity of C. elegans glia across sexes. *BioRxiv*, 2023.03.21.533668. https://doi.org/10.1101/2023.03.21.533668

Raiders, S., Black, E. C., Bae, A., MacFarlane, S., Klein, M., Shaham, S., & Singhvi, A. (2021). Glia actively sculpt sensory neurons by controlled phagocytosis to tune animal behavior. *ELife*, *10*. https://doi.org/10.7554/eLife.63532

Raiders, S., Han, T., Scott-Hewitt, N., Kucenas, S., Lew, D., Logan, M. A., & Singhvi, A. (2021). Engulfed by Glia: Glial Pruning in Development, Function, and Injury across Species. *The Journal of Neuroscience*, JN-SY-1660-20. https://doi.org/10.1523/JNEUROSCI.1660-20.2020

Ray, S., & Singhvi, A. (2021). Charging Up the Periphery: Glial Ionic Regulation in Sensory Perception. *Frontiers in Cell and Developmental Biology*, *9*, 1989. https://doi.org/10.3389/FCELL.2021.687732/BIBTEX

Razzauti, A., & Laurent, P. (2021). Ectocytosis prevents accumulation of ciliary cargo in c. Elegans sensory neurons. *ELife*, *10*. https://doi.org/10.7554/ELIFE.67670

Rodriguez, Y. A., Roebber, J. K., Dvoryanchikov, G., Makhoul, V., Roper, S. D., & Chaudhari, N. (2021). "Tripartite Synapses" in Taste Buds: A Role for Type I Glial-like Taste Cells. *Journal of Neuroscience*, *41*(48), 9860–9871. https://doi.org/10.1523/JNEUROSCI.1444-21.2021

Salin-Cantegrel, A., Rivière, J. B., Shekarabi, M., Rasheed, S., DaCal, S., Laganière, J., … Rouleau, G. A. (2011). Transit defect of potassium-chloride co-transporter 3 is a major pathogenic mechanism in hereditary motor and sensory neuropathy with agenesis of the corpus callosum. *Journal of Biological Chemistry*, *286*(32), 28456–28465.

https://doi.org/10.1074/jbc.M111.226894

Satterlee, J. S., Sasakura, H., Kuhara, A., Berkeley, M., Mori, I., & Sengupta, P. (2001). Specification of thermosensory neuron fate in C. elegans requires ttx-1, a homolog of otd/Otx. *Neuron*, *31*(6), 943–956. https://doi.org/10.1016/S0896-6273(01)00431-7

Segbert, C., Johnson, K., Theres, C., Van Fürden, D., & Bossinger, O. (2004). Molecular and functional analysis of apical junction formation in the gut epithelium of Caenorhabditis elegans. *Developmental Biology*, *266*(1), 17–26. https://doi.org/10.1016/j.ydbio.2003.10.019

Sengupta, P. (2017). Cilia and sensory signaling: The journey from "animalcules" to human disease. *PLOS Biology*, *15*(4), e2002240. https://doi.org/10.1371/JOURNAL.PBIO.2002240

Sengupta, P., Colbert, H. A., & Bargmann, C. I. (1994). The C. elegans gene odr-7 encodes an olfactory-specific member of the nuclear receptor superfamily. *Cell*, *79*(6), 971–980. https://doi.org/10.1016/0092-8674(94)90028-0

Shekarabi, M., Moldrich, R. X., Rasheed, S., Salin-Cantegrel, A., Laganiere, J., Rochefort, D., … Rouleau, G. A. (2012). Loss of Neuronal Potassium/Chloride Cotransporter 3 (KCC3) Is Responsible for the Degenerative Phenotype in a Conditional Mouse Model of Hereditary Motor and Sensory Neuropathy Associated with Agenesis of the Corpus Callosum. *Journal of Neuroscience*, *32*(11), 3865–3876. https://doi.org/10.1523/JNEUROSCI.3679-11.2012

Shin, K., Fogg, V. C., & Margolis, B. (2006). Tight Junctions and Cell Polarity. *Https://Doi.Org/10.1146/Annurev.Cellbio.22.010305.104219*, *22*, 207–235. https://doi.org/10.1146/ANNUREV.CELLBIO.22.010305.104219

Simard, C. F., Bergeron, M. J., Frenette-Cotton, R., Carpentier, G. A., Pelchat, M. E., Caron, L.,

& Isenring, P. (2007). Homooligomeric and Heterooligomeric Associations between K+-Cl– Cotransporter Isoforms and between K+-Cl– and Na+-K+-Cl– Cotransporters. *Journal of Biological Chemistry*, *282*(25), 18083–18093. https://doi.org/10.1074/JBC.M607811200

Singhvi, A., Liu, B., Friedman, C. J., Fong, J., Lu, Y., Huang, X. Y., & Shaham, S. (2016). A Glial K/Cl Transporter Controls Neuronal Receptive Ending Shape by Chloride Inhibition of an rGC. *Cell*, *165*(4), 936–948. https://doi.org/10.1016/j.cell.2016.03.026

Singhvi, A., & Shaham, S. (2019). Glia-Neuron Interactions in *Caenorhabditis elegans*. *Annual Review of Neuroscience*, *42*(1), 149–168. https://doi.org/10.1146/annurev-neuro-070918-050314

Singhvi, A., Shaham, S., & Rapti, G. (2023). Glia development and function in the nervous system of Caenorhabditis elegans. *Cold Spring Harbor Perspectives in Biology*, *(in press)*.

Sparrow, J. R., Hicks, D., & Hamel, C. P. (2010). The Retinal Pigment Epithelium in Health and Disease. *Current Molecular Medicine*, *10*(9), 802–823. https://doi.org/10.2174/156652410793937813

Stogsdill, J. A., Ramirez, J., Liu, D., Kim, Y. H., Baldwin, K. T., Enustun, E., … Eroglu, C. (2017). Astrocytic neuroligins control astrocyte morphogenesis and synaptogenesis. *Nature*, *551*(7679), 192–197. https://doi.org/10.1038/nature24638

Sulston, J. E. (1983). Neuronal cell lineages in the nematode Caenorhabditis elegans. *Cold Spring Harbor Symposia on Quantitative Biology*, *48 Pt 2*, 443–452. https://doi.org/10.1101/sqb.1983.048.01.049

Sun, Y. T., Lin, T. S., Tzeng, S. F., Delpire, E., & Shen, M. R. (2010). Deficiency of electroneutral K+-Cl- cotransporter 3 causes a disruption in impulse propagation along peripheral nerves. *Glia*, *58*(13), 1544–1552. https://doi.org/10.1002/glia.21028

Swoboda, P., Adler, H. T., & Thomas, J. H. (2000). The RFX-type transcription factor DAF-19 regulates sensory neuron cilium formation in C. elegans. *Molecular Cell*, *5*(3), 411–421. https://doi.org/10.1016/S1097-2765(00)80436-0

Tanis, J. E., Bellemer, A., Moresco, J. J., Forbush, B., & Koelle, M. R. (2009). The Potassium Chloride Cotransporter KCC-2 Coordinates Development of Inhibitory Neurotransmission and Synapse Structure in Caenorhabditis elegans. *Journal of Neuroscience*, *29*(32), 9943–9954. https://doi.org/10.1523/JNEUROSCI.1989-09.2009

Uchida, O., Nakano, H., Koga, M., & Ohshima, Y. (2003, April). The C. elegans che-1 gene encodes a zinc finger transcription factor required for specification of the ASE chemosensory neurons. *Development*. Development. https://doi.org/10.1242/dev.00341

von Bartheld, C. S., Bahney, J., & Herculano-Houzel, S. (2016). The Search for True Numbers of Neurons and Glial Cells in the Human Brain: A Review of 150 Years of Cell Counting. *The Journal of Comparative Neurology*, *524*(18), 3865. https://doi.org/10.1002/CNE.24040

Wallace, S. W., Singhvi, A., Liang, Y., Lu, Y., Shaham, S., Wallace, S. W., … Shaham, S. (2016). PROS-1 / Prospero Is a Major Regulator of the Glia- Specific Secretome Controlling Sensory-Neuron Shape and Function in C . elegans Article PROS-1 / Prospero Is a Major Regulator of the Glia-Specific Secretome Controlling Sensory-Neuron Shape and Function. *CellReports*, *15*(3), 550–562. https://doi.org/10.1016/j.celrep.2016.03.051

Wang, Y., D'Urso, G., & Bianchi, L. (2012). Knockout of glial channel ACD-1 exacerbates sensory deficits in a C. elegans mutant by regulating calcium levels of sensory neurons. *Journal of Neurophysiology*, *107*(1), 148–158. https://doi.org/10.1152/jn.00299.2011

Wang, Ying, Apicella, A., Lee, S. K., Ezcurra, M., Slone, R. D., Goldmit, M., … Bianchi, L. (2008). A glial DEG/ENaC channel functions with neuronal channel DEG-1 to mediate

specific sensory functions in C. elegans. *EMBO Journal*, *27*(18), 2388–2399. https://doi.org/10.1038/emboj.2008.161

Ward, S., Thomson, N., White, J. G., & Brenner, S. (1975). Electron microscopical reconstruction of the anterior sensory anatomy of the nematode caenorhabditis elegans. *Journal of Comparative Neurology*, *160*(3), 313–337. https://doi.org/10.1002/cne.901600305

Yang, S. M., Michel, K., Jokhi, V., Nedivi, E., & Arlotta, P. (2020). Neuron-class specific responses govern adaptive myelin remodeling in the neocortex. *Science (New York, N.Y.)*, *370*(6523). https://doi.org/10.1126/SCIENCE.ABD2109

Yoshida, A., Nakano, S., Suzuki, T., Ihara, K., Higashiyama, T., & Mori, I. (2016). A glial K+/Cl-cotransporter modifies temperature-evoked dynamics in Caenorhabditis elegans sensory neurons. *Genes, Brain and Behavior*, *15*(4), 429–440. https://doi.org/10.1111/gbb.12260

Yu, X., Taylor, A. M., Nagai, J., Golshani, P., Evans, C. J., Coppola, G., & Khakh, B. S. (2018). Reducing Astrocyte Calcium Signaling In Vivo Alters Striatal Microcircuits and Causes Repetitive Behavior. *Neuron*, *99*, 1170-1187.e9. https://doi.org/10.1016/j.neuron.2018.08.015

Zhang, X., Liu, Y., Hong, X., Li, X., Meshul, C. K., Moore, C., … Tong, X. (2021). NG2 glia-derived GABA release tunes inhibitory synapses and contributes to stress-induced anxiety. *Nature Communications 2021 12:1*, *12*(1), 1–18. https://doi.org/10.1038/s41467-021-25956-y

Chapter 3 (supplement)

Abraham, M. C., Lu, Y., & Shaham, S. (2007). A morphologically conserved nonapoptotic program promotes linker cell death in Caenorhabditis elegans. *Developmental Cell*, *12*(1), 73–86. https://doi.org/10.1016/J.DEVCEL.2006.11.012

Armenti, S. T., Lohmer, L. L., Sherwood, D. R., & Nance, J. (2014). Repurposing an endogenous degradation system for rapid and targeted depletion of C. elegans proteins. *Development (Cambridge, England)*, *141*(23), 4640–4647. https://doi.org/10.1242/DEV.115048

Bargmann, C. I., Hartwieg, E., & Horvitz, H. R. (1993). Odorant-selective genes and neurons mediate olfaction in C. elegans. *Cell*, *74*(3), 515–527. https://doi.org/10.1016/0092-8674(93)80053-H

Brenner, S. (1974). The genetics of Caenorhabditis elegans. *Genetics*, *77*(1), 71–94. https://doi.org/10.1093/GENETICS/77.1.71

Chronis, N., Zimmer, M., & Bargmann, C. I. (2007). Microfluidics for in vivo imaging of neuronal and behavioral activity in Caenorhabditis elegans. *Nature Methods*, *4*(9), 727–731. https://doi.org/10.1038/NMETH1075

Firestein, B. L., & Rongo, C. (2001). DLG-1 is a MAGUK similar to SAP97 and is required for adherens junction formation. *Molecular Biology of the Cell*, *12*(11), 3465–3475. https://doi.org/10.1091/MBC.12.11.3465/ASSET/IMAGES/LARGE/MK1111663006.JPEG

Hobert, O. (2018). PCR Fusion-Based Approach to Create Reporter Gene Constructs for Expression Analysis in Transgenic C. elegans. *Https://Doi.Org/10.2144/02324bm01*, *32*(4), 728–730. https://doi.org/10.2144/02324BM01

Martin, C. G., Bent, J. S., & Singhvi, A. (2022). Epithelia delimits glial apical polarity against

mechanical shear to maintain glia-neuron - architecture. *BioRxiv*, 2022.12.26.521704. https://doi.org/10.1101/2022.12.26.521704

Maurya, A. K., & Sengupta, P. (2021). xbx-4, a homolog of the Joubert syndrome gene FAM149B1, acts via the CCRK and RCK kinase cascade to regulate cilia morphology. *Current Biology : CB*, *31*(24), 5642. https://doi.org/10.1016/J.CUB.2021.10.027

Mello, C. C., Kramer, J. M., Stinchcomb, D., & Ambros, V. (1991). Efficient gene transfer in C.elegans: extrachromosomal maintenance and integration of transforming sequences. *The EMBO Journal*, *10*(12), 3959–3970. https://doi.org/10.1002/J.1460-2075.1991.TB04966.X

Miyabayashi, T., Palfreyman, M. T., Sluder, A. E., Slack, F., & Sengupta, P. (1999). Expression and function of members of a divergent nuclear receptor family in Caenorhabditis elegans. *Developmental Biology*, *215*(2), 314–331. https://doi.org/10.1006/DBIO.1999.9470

Oikonomou, G., Perens, E. A., Lu, Y., Watanabe, S., Jorgensen, E. M., & Shaham, S. (2011). Opposing Activities of LIT-1/NLK and DAF-6/Patched-Related Direct Sensory Compartment Morphogenesis in C. elegans. *PLoS Biology*, *9*(8), e1001121. https://doi.org/10.1371/journal.pbio.1001121

Sarin, S., O'Meara, M. M., Flowers, E. B., Antonio, C., Poole, R. J., Didiano, D., … Hobert, O. (2007). Genetic Screens for Caenorhabditis elegans Mutants Defective in Left/Right Asymmetric Neuronal Fate Specification. *Genetics*, *176*(4), 2109. https://doi.org/10.1534/GENETICS.107.075648

Sengupta, P., Chou, J. H., & Bargmann, C. I. (1996). odr-10 Encodes a Seven Transmembrane Domain Olfactory Receptor Required for Responses to the Odorant Diacetyl. *Cell*, *84*(6), 899–909. https://doi.org/10.1016/S0092-8674(00)81068-5

Singhvi, A., Liu, B., Friedman, C. J., Fong, J., Lu, Y., Huang, X. Y., & Shaham, S. (2016). A

Glial K/Cl Transporter Controls Neuronal Receptive Ending Shape by Chloride Inhibition of an rGC. *Cell*, *165*(4), 936–948. https://doi.org/10.1016/j.cell.2016.03.026

Stiernagle, T. (2006). Maintenance of C. elegans. *WormBook : The Online Review of C. Elegans Biology*, 1–11. https://doi.org/10.1895/WORMBOOK.1.101.1

Troemel, E. R., Kimmel, B. E., & Bargmann, C. I. (1997). Reprogramming chemotaxis responses: Sensory neurons define olfactory preferences in C. elegans. *Cell*, *91*(2), 161–169. https://doi.org/10.1016/S0092-8674(00)80399-2

Troemel, E. R., Sagasti, A., & Bargmann, C. I. (1999). Lateral signaling mediated by axon contact and calcium entry regulates asymmetric odorant receptor expression in C. elegans. *Cell*, *99*(4), 387–398. https://doi.org/10.1016/S0092-8674(00)81525-1

Chapter 4

Alessi, D. R., Zhang, J., Khanna, A., Hochdörfer, T., Shang, Y., & Kahle, K. T. (2014). The WNK-SPAK/OSR1 pathway: Master regulator of cation-chloride cotransporters. *Science Signaling*, *7*(334), 1–11. https://doi.org/10.1126/scisignal.2005365

Bacaj, T., Tevlin, M., Lu, Y., & Shaham, S. (2009). Glia Are Essential for Sensory Organ Function in C. elegans. *Science*, *6*(5902), 247–253. https://doi.org/10.1111/j.1743-6109.2008.01122.x.Endothelial

Doroquez, D. B., Berciu, C., Anderson, J. R., Sengupta, P., & Nicastro, D. (2014). A high-resolution morphological and ultrastructural map of anterior sensory cilia and glia in Caenorhabditis elegans. *ELife*, *2014*(3), 1–35. https://doi.org/10.7554/eLife.01948

Martin, C. G., Bent, J. S., & Singhvi, A. (2022). Epithelia delimits glial apical polarity against mechanical shear to maintain glia-neuron - architecture. *BioRxiv*, 2022.12.26.521704.

https://doi.org/10.1101/2022.12.26.521704

Payne, J. A., Rivera, C., Voipio, J., & Kaila, K. (2003). Cation-chloride co-transporters in neuronal communication, development and trauma. *Trends in Neurosciences*, *26*(4), 199–206. https://doi.org/10.1016/S0166-2236(03)00068-7

Raiders, S., Black, E. C., Bae, A., MacFarlane, S., Klein, M., Shaham, S., & Singhvi, A. (2021). Glia actively sculpt sensory neurons by controlled phagocytosis to tune animal behavior. *ELife*, *10*. https://doi.org/10.7554/eLife.63532

Singhvi, A., Liu, B., Friedman, C. J., Fong, J., Lu, Y., Huang, X. Y., & Shaham, S. (2016). A Glial K/Cl Transporter Controls Neuronal Receptive Ending Shape by Chloride Inhibition of an rGC. *Cell*, *165*(4), 936–948. https://doi.org/10.1016/j.cell.2016.03.026

Wallace, S. W., Singhvi, A., Liang, Y., Lu, Y., Shaham, S., Wallace, S. W., … Shaham, S. (2016). PROS-1 / Prospero Is a Major Regulator of the Glia- Specific Secretome Controlling Sensory-Neuron Shape and Function in C . elegans. *CellReports*, *15*(3), 550–562. https://doi.org/10.1016/j.celrep.2016.03.051

Chapter 5

Blaesse, P., Airaksinen, M. S., Rivera, C., & Kaila, K. (2009). Cation-Chloride Cotransporters and Neuronal Function. *Neuron*, *61*(6), 820–838. https://doi.org/10.1016/j.neuron.2009.03.003

Chamma, I., Chevy, Q., Poncer, J. C., & Lévi, S. (2012). Role of the neuronal K-Cl co-transporter KCC2 in inhibitory and excitatory neurotransmission. *Frontiers in Cellular Neuroscience*, *6*(JANUARY). https://doi.org/10.3389/fncel.2012.00005

Chung, W. S., Welsh, C. A., Barres, B. A., & Stevens, B. (2015). Do glia drive synaptic and

cognitive impairment in disease? *Nature Neuroscience*, *18*(11), 1539–1545. https://doi.org/10.1038/nn.4142

Eichel, K., Uenaka, T., Belapurkar, V., Lu, R., Cheng, S., Pak, J. S., … Shen, K. (2022). Endocytosis in the axon initial segment maintains neuronal polarity. *Nature 2022 609:7925*, *609*(7925), 128–135. https://doi.org/10.1038/s41586-022-05074-5

Green, J. A., & Mykytyn, K. (2014). Neuronal Primary Cilia: An Underappreciated Signaling and Sensory Organelle in the Brain. *Neuropsychopharmacology*, *39*(1), 244. https://doi.org/10.1038/NPP.2013.203

Hedstrom, K. L., Ogawa, Y., & Rasband, M. N. (2008). AnkyrinG is required for maintenance of the axon initial segment and neuronal polarity. *The Journal of Cell Biology*, *183*(4), 635. https://doi.org/10.1083/JCB.200806112

Heiman, M. G. (2022). When is a neuron like an epithelial cell. *Developmental Biology*, *489*, 161–164. https://doi.org/10.1016/J.YDBIO.2022.06.012

Kahle, K. T., Khanna, A. R., Alper, S. L., Adragna, N. C., Lauf, P. K., Sun, D., & Delpire, E. (2015). K-Cl cotransporters, cell volume homeostasis, and neurological disease. *Trends in Molecular Medicine*, *21*(8), 513–523. https://doi.org/10.1016/j.molmed.2015.05.008

Leterrier, C. (2018). The Axon Initial Segment: An Updated Viewpoint. *Journal of Neuroscience*, *38*(9), 2135–2145. https://doi.org/10.1523/JNEUROSCI.1922-17.2018

Liang, F. (2020). Sustentacular cell enwrapment of olfactory receptor neuronal dendrites: An update. *Genes*, *11*(5). https://doi.org/10.3390/genes11050493

Lillis, M., Zaccardi, N. J., & Heiman, M. G. (2022). Axon-dendrite and apical-basolateral sorting in a single neuron. *Genetics*, *221*(1). https://doi.org/10.1093/GENETICS/IYAC036

Liou, T. G. (2019). The Clinical Biology of Cystic Fibrosis Transmembrane Regulator Protein:

Its Role and Function in Extrapulmonary Disease. *Chest*, *155*(3), 605. https://doi.org/10.1016/J.CHEST.2018.10.006

Low, I. I. C., Williams, C. R., Chong, M. K., Mclachlan, I. G., Wierbowski, B. M., Kolotuev, I., & Heiman, M. G. (2019). Morphogenesis of neurons and glia within an epithelium. https://doi.org/10.1242/dev.171124

Martin, C. G., Bent, J. S., & Singhvi, A. (2022). Epithelia delimits glial apical polarity against mechanical shear to maintain glia-neuron - architecture. *BioRxiv*, 2022.12.26.521704. https://doi.org/10.1101/2022.12.26.521704

Mehalow, A. K., Kameya, S., Smith, R. S., Hawes, N. L., Denegre, J. M., Young, J. A., … Nishina, P. M. (2003). CRB1 is essential for external limiting membrane integrity and photoreceptor morphogenesis in the mammalian retina. *Human Molecular Genetics*, *12*(17), 2179–2189. https://doi.org/10.1093/HMG/DDG232

Perens, E. A., & Shaham, S. (2005). C. elegans daf-6 encodes a patched-related protein required for lumen formation. *Developmental Cell*, *8*(6), 893–906. https://doi.org/10.1016/j.devcel.2005.03.009

Perkins, L. A., Hedgecock, E. M., Thomson, J. N., & Culotti, J. G. (1986). Mutant sensory cilia in the nematode Caenorhabditis elegans. *Developmental Biology*, *117*(2), 456–487. https://doi.org/10.1016/0012-1606(86)90314-3

Ray, S., & Singhvi, A. (2021). Charging Up the Periphery: Glial Ionic Regulation in Sensory Perception. *Frontiers in Cell and Developmental Biology*, *9*, 1989. https://doi.org/10.3389/FCELL.2021.687732/BIBTEX

Razzauti, A., & Laurent, P. (2021). Ectocytosis prevents accumulation of ciliary cargo in c. Elegans sensory neurons. *ELife*, *10*. https://doi.org/10.7554/ELIFE.67670

Rodriguez-Boulan, E., & Macara, I. G. (2014). Organization and execution of the epithelial polarity programme. *Nature Reviews Molecular Cell Biology*, *15*(4), 225–242. https://doi.org/10.1038/nrm3775

Sanchez, A. D., & Feldman, J. L. (2021). A proximity labeling protocol to probe proximity interactions in C. elegans. *STAR Protocols*, *2*(4), 100986. https://doi.org/10.1016/J.XPRO.2021.100986

Sun, Y. T., Lin, T. S., Tzeng, S. F., Delpire, E., & Shen, M. R. (2010). Deficiency of electroneutral K+-Cl- cotransporter 3 causes a disruption in impulse propagation along peripheral nerves. *Glia*, *58*(13), 1544–1552. https://doi.org/10.1002/glia.21028

Venkatachalam, K., & Montell, C. (2007). TRP channels. *Annu Rev Biochem.*, *76*, 387–417. https://doi.org/10.1146/annurev.biochem.75.103004.142819.TRP

Zdebik, A. A., Wangemann, P., & Jentsch, T. J. (2009). Potassium Ion Movement in the Inner Ear: Insights from Genetic Disease and Mouse Models. *Physiology (Bethesda, Md.)*, *24*(5), 307. https://doi.org/10.1152/PHYSIOL.00018.2009